PRODUCTION AND CHARACTERIZATION OF MAGHEMITE NANOPARTICLES

A THESIS SUBMITTED TO
THE GRADUATE SCHOOL OF NATURAL AND APPLIED SCIENCES
OF
MIDDLE EAST TECHNICAL UNIVERSITY

BY

ÖZGE ACARBAŞ BALTACI

IN PARTIAL FULFILLMENT OF THE REQUIREMENTS
FOR
THE DEGREE OF DOCTOR OF PHILOSOPHY
IN
METALLURGICAL AND MATERIALS ENGINEERING

SEPTEMBER 2010

Approval of the thesis:

PRODUCTION AND CHARACTERIZATION OF MAGHEMITE NANOPARTICLES

Submitted by **ÖZGE ACARBAŞ BALTACI** in partial fulfillment of the requirements for the degree of **Doctor of Philosophy in Metallurgical and Materials Engineering Department, Middle East Technical University** by,

Prof. Dr. Canan Özgen _____
Dean, Graduate School of **Natural and Applied Sciences**

Prof. Dr. Tayfur Öztürk _____
Head of Department, **Metallurgical and Materials Engineering**

Prof. Dr. Macit Özenbaş _____
Supervisor, **Metallurgical and Materials Engineering Dept., METU**

Prof. Dr. Mürvet Volkan _____
Co-Supervisor, **Chemistry Dept., METU**

Examining Committee Members:

Prof. Dr. Güngör Gündüz _____
Chemical Engineering Dept., METU

Prof. Dr. Macit Özenbaş _____
Metallurgical and Materials Engineering Dept., METU

Prof. Dr. Ali Kalkanlı _____
Metallurgical and Materials Engineering Dept., METU

Assoc. Prof. Dr. Mustafa Göktepe _____
Physics Dept., Balıkesir University

Assoc. Prof. Dr. Arcan Dericioğlu _____
Metallurgical and Materials Engineering Dept., METU

Date: 14 September 2010

I hereby declare that all information in this document has been obtained and presented accordance with the academic rules and ethical conduct. I also declare that, as required by these rules and conduct, I have fully cited and referenced all material and results that are not original to this work.

Name, Last name : Özge ACARBAŞ BALTACI

Signature :

ABSTRACT

PRODUCTION AND CHARACTERIZATION OF MAGHEMITE NANOPARTICLES

Acarbaş Baltacı, Özge

Ph. D., Department of Metallurgical and Materials Engineering

Supervisor: Prof. Dr. Macit Özenbaş

Co-Supervisor: Prof. Dr. Mürvet Volkan

September 2010, 153 pages

The aim of this study is to produce maghemite nanoparticles by using different production methods. To achieve this purpose Sol-Gel Processing and Microwave Synthesis methods were employed. Suitable characterization techniques like XRD, TEM, BET, and VSM were performed to control the properties of the synthesized particles whether they are suitable for certain applications.

In the sol-gel part of the study two different routes were employed to obtain maghemite nanoparticles. In the first route TEOS (tetraethoxysilane) was used as the precursor. Approximate particle sizes of these samples lie between 12.0-23.4 nm. From the magnetization measurements saturation magnetization (M_s) values are obtained between 4-12 emu/g. In the second route of the sol-gel method ethylene glycol and diethylene glycol were used as starting materials. M_s value was found as 28 emu/g for the ethylene glycol sample as the highest magnetization value due to having the highest amount of maghemite phase. The superparamagnetic behavior observed in these samples was tried to explain by curve fitting. Langevin and tangent hyperbolic functions were used to fit the magnetization curves. From the XRD study particle sizes of these samples lie in the 4.0-48.5 nm range and these results are consistent with the size distributions obtained from the TEM study.

In the last part of the study microwave method was used to produce maghemite nanoparticles. Most of the samples contain maghemite and hematite phases together and particle sizes were between 3-30 nm. M_s values of these microwave samples were lower than that of the sol-gel samples with a value about 3.0 emu/g.

Keywords: Maghemite, nanoparticle, superparamagnetism, sol-gel, microwave

ÖZ

MAGHEMİT NANOPARÇACIKLARIN ÜRETİMİ VE KARAKTERİZASYONU

Acarbaş Baltacı, Özge
Doktora, Metalurji ve Malzeme Mühendisliği Bölümü
Tez Yöneticisi: Prof. Dr. Macit Özenbaş
Ortak Tez Yöneticisi: Prof. Dr. Mürvet Volkan
September 2010, 153 pages

Bu çalışmanın amacı maghemit nanoparçacıklarını değişik üretim yöntemleri kullanarak üretebilmektir. Bu amaca ulaşabilmek için sol-jel ve mikrodalga sentezleme yöntemleri kullanılmıştır. Üretilen malzemelerin belli uygulama alanları için istenilen özelliklere sahip olup olmadıklarını denetlemek amacıyla XRD, TEM, BET ve VSM gibi uygun teknikler kullanılmıştır.

Çalışmanın sol-jel kısmında maghemit nanoparçacıklarını elde edebilmek için iki farklı yöntem uygulanmıştır. İlkinde başlangıç malzemesi olarak TEOS (tetraethoxysilane) kullanılmıştır. Bu şekilde elde edilen örneklerin tane boyutları yaklaşık 12.0-23.4 nm arasındadır. Manyetik ölçümlerden elde edilen doygun manyetizasyon (M_s) değerleri de 4-12 emu/g arasındadır. Çalışmanın ikinci kısmında etilen glikol ve dietilen glikol başlangıç malzemesi olarak kullanılmıştır. En yüksek M_s değeri 28 emu/g ile en fazla miktarda maghemit fazını barındıran etilen glikol örneğinde elde edilmiştir. Süperparamanyetik özellik gösteren bu örneklerin davranışları Langevin ve hiperbolik tanjant fonksiyonları kullanılarak açıklanmaya çalışılmıştır. XRD çalışmasından elde edilen tane boyutları yaklaşık 4.0-48.5 nm aralığındadır. TEM çalışmasından elde edilen tane boyut dağılımları da XRD sonuçlarını desteklemektedir.

Çalışmanın son kısmında maghemit nanoparçacıklarını üretmek için mikrodalga yöntemi kullanılmıştır. Hazırlanan çoğu örnekte maghemit ve hematit fazları birlikte bulunmaktadır. Yaklaşık tane boyutları 3-30 nm aralığındadır. Mikrodalga yöntemi ile elde edilen bu örneklerin M_s değerleri yaklaşık 3 emu/g civarında olup sol-jel yöntemiyle üretilen örneklere göre daha düşük değerde bulunmuştur.

Anahtar Sözcükler: Maghemit, nanoparçacık, süperparamanyetiklik, sol-jel, mikrodalga

To my family,

ACKNOWLEDGEMENTS

I would like to express my deepest gratitude to my supervisor Prof. Dr. Macit Özenbaş for his supervision, guidance, support and encouragement during the study of this thesis. I am grateful for sharing his experience and opinions throughout this period of work.

It is great pleasure to thank my co-supervisor Prof. Dr. Mürvet Volkan from Chemistry Department of METU.

I would also like to thank the examining committee members Prof. Dr. Güngör Gündüz from Chemical Engineering Department of METU and Assoc. Prof. Dr. Arcan Dericioğlu from Metallurgical and Materials Engineering Department of METU for their suggestions and comments during this study.

I would like to express my sincere thanks to Dr. Özgür Duygulu from TÜBİTAK-MAM for TEM analysis. I am also grateful to METU Central Laboratory for BET and TEM analysis, Kırıkkale and Anadolu Univesity for TEM analysis. I am also thankful to my colleague Mehmet Yıldırım from Metallurgical and Materials Engineering Department of METU for his helps on VSM study. I am also grateful to all the Department of Metallurgical and Materials Engineering staff.

I must also express my special thanks to my dear friends Ali Erdem Eken and Gökhan Kıdıl for their invaluable friendships and supports.

Words fail to express my eternal gratitude to my family who gave their endless love, support and guidance through my life. I am thankful to my mother Selime Acarbaş and my father Doğan Acarbaş. Their encouregement is the most important thing to

complete this study. I would like to specially thank to my husband Nihat Baltacı for his great love, neverending support and for being always there for me.

This thesis is dedicated to the precious memories of my grandmother Vasfiye Sürücü and my grandfather Mehmet Sürücü.

This thesis has been supported by the Scientific HR Development Program (ÖYP) at Middle East Technical University through the project BAP-08-11-DPT2002K120510.

TABLE OF CONTENTS

LIST OF TABLES

TABLES

LIST OF FIGURES

FIGURES

CHAPTER 1

INTRODUCTION

Nanotechnology is a new and growing field and it is related with the production and application areas of the nanomaterials and their properties resulted from their dimensions. Materials classified in this field are in the range between subnanometers to several hundred nanometers [1].

Metastable phases with different properties are produced with the help of the nanotechnology, for example materials having superconductivity and magnetism. Miniaturization is one of the important side of the nanotechnology. Computers, biosensors, nanorobots and nanoscaled electronics are some of the examples of miniaturization. These computers can be used to mimic the human brains, biosensors are used in the diagnosis and treatment of different diseases, and nanorobots are used in the human body to remove toxins from the body [2].

Nanotechnology covers the incorporation of different areas of science like physics, chemistry, materials science, molecular biology and pharmacology. This multidisciplinary property is resulting from several applications like electronics, optics, nanobiological systems and nanomedicine. Since there are different topics in nanotechnology like synthesis and processing of materials, their physical properties, nanodevice design and fabrication and design of the characterization tools for nanomaterials, multidisciplinary work is needed for nanotechnology [3].

Synthesis and processing of nanomaterials are important because their size, morphology, chemical composition and microstructure are important parameters in the applications [2].

Materials which consist of micrometer sized particles exhibit similar physical properties with their bulk form, on the other hand properties of materials with nanometer sized particles are quite different from the bulk form. For example nanometer sized crystals have lower melting points than their bulk form. Ferromagnetic and ferroelectric properties are changed when the size of the material decreases. Also conductivity and catalytic properties of the materials are related with the characteristic dimensions [2].

Drug delivery, micro-electromechanical systems (MEMS) and lab-on-a-chip are some of the examples that used in nanotechnology [1].

Various forms of materials can fall into the nanostructured materials class like nanoparticles, quantum dots, nanorods and nanowires, thin films, and bulk materials that consist of nanoscale building blocks. There are different techniques for the production of these materials. They are classified in four diffrent classes according to the growth media:

- Vapor phase growth: Laser reaction pyrolysis is used for nanoparticles, atomic layer deposition (ALD) is used for deposition of thin films.
- Liquid phase growth: Colloidal processing of nanoparticles and self assembly of monolayers.
- Solid phase formation: Fabrication of metallic particles in glass matrix.
- Hybrid growth: Vapor-liquid-solid (VLS) growth of nanowires.

According to the form of the products, production methods can be classifed in four different classes :

- Nanoparticles: Colloidal processing, flame combustion and phase segragation.

- Nanorods or nanowires: Template-based electroplating, solution-liquid-solid growth (SLS), and spontaneous anisotropic growth.
- Thin films: Molecular beam epitaxy (MBE) and atomic layer deposition (ALD).
- Nanostructured bulk materials: Photonic bandgap crystals by self-assembly of nanosized particles.

There are also different approaches to classify the fabrication techniques like top-down and bottom-up approaches, spontaneous and forced processes. Top-down and bottom-up approaches are two methods that are used to synthesize nanomaterials. If nanoparticles are produced with milling it can be said that top-down approach is used. On the other hand colloidal dispersion is an example of bottom-up approach. There is also a hybrid approach like lithography, since thin film growth by lithography can be considered as bottom-up, etching step is top-down method. Both approaches are quite important in nanotecnology and they have both advantages and disadvantages [1].

Most important disadvantage of the top-down method is the surface imperfections. There are impurities and structural defects on the nanowire surfaces that are produced by lithography. Since surface over volume ratio in nanomaterials is large, these defects are quite important [1].

In the bottom-up approach material is build-up from the bottom; atom-by-atom, molecule-by-molecule, or cluster-by-cluster. This approach plays an important role in the production of nanomaterials. Bottom-up approach finds wider usage than top-down approach since the tools are too big to deal with in the top-down approach [1].

Chemical industry widely uses the bottom-up approach in the production of salts and nitrates. Also single crystal growth and deposition of films in electronic industry generally use this approach [2].

Nanomaterials have more homogeneous chemical composition and less defects when they are produced by bottom-up approach. Because they are produced nearly in a thermodynamic equilibrium state with the help of the reduction of Gibbs free energy. On the other hand top-down approach introduces also internal stress to the material [2].

There are some challenges in the production of nanomaterials:

(1) Due to large surface area there is huge surface energy.
(2) To obtain materials with desired properties, size, size distribution, morphology, crystallinity, microstructure and chemical composition must be well controlled.
(3) Coarsening through Ostwald ripening and agglomeration must be prevented.

Dimensions of the nanoparticles are quite important since most of the physical characteristics are dependent on their dimensions. Generally production methods give us the broad size distribution of the nanoparticles and by controlling the reaction parameters like time, temperature and concentrations of the reactants, it is not always possible to obtain narrow size distribution easily. By using the surfactant stabilized solutions it can be possible to control the precipitation and obtain nanoparticles of specified size and dispersion degree [4].

Production and stabilization methods can not be considered separately from each other. Since nanoparticles, especially when they are smaller than 10 nm, have large surface energy, the selection of an inert medium is difficult and it affects the properties. Especially for magnetic nanoparticles it is more important since their modified surface exhibits different magnetic characteristics from their core. Despite this, generally production methods are not directly related to the stabilization methods [4].

Most of the production methods of nanoparticles are for magnetic particles. Size, shape and dispersity are the important parameters as said before because magnetic properties depends on the size of the particles. Also interactions of the nanoparticles should be prevented or at least decreased to a minimum degree. This process can be made by immobilization of them on a substrate surface or by using a stabilizing matrix. The distance of the particles in a matrix should be controlled [4].

Generally magnetic nanoparticles can be found in a 2D form like films, or 3D systems like compact materials. But compaction process may cause deterioration of the unique magnetic properties of the material. By using different type of matrices they can be stabilized. Usually non magnetic dielectric matrices are preferred like organic polymers. These matrices are used to make nanoparticles stable against the corrosion, oxidation and agglomeration so their single domain structure can be prevented. Coated or encapsulated nanoparticles can be used in many areas like xerography, magnetic ink, contrasting agents for magnetic resonance images, and ferrofluids [4].

Metallic nanoparticles find large application areas owing to their larger magnetization values than metal oxides. But their disadvantage is that their low stability against air, they are generally oxidized and this oxidation decreases their magnetizations. During the production method it is not possible to avoid the oxidation completely. Magnetization depends on the degree of oxidation on the metallic surfaces. So in order to get true information about magnetic characteristics, knowing the oxidation degree is important. Fe, Co, and Ni are the examples of the metallic magnetic nanoparticles. Fe-Co, Fe-Ni, Fe-Pt, Co-Pt alloys also show magnetic properties. In addition to these alloys, six of the nine rare earth elements (REE) from the periodic table exhibit ferromagnetic behavior. They are used in magnetic cooling systems [4].

In the magnetic nanomaterial area oxides like Fe oxides, Co oxides and Ni oxides are also find large applications. Especially iron oxides find large usage area like magnetic recording media, catalysts, pigments, gas sensors, optical devices, and

electromagnetic devices [4]. They have different structures and hydration states like 0, II and III and among them commonly observed states are II and III. There are are also another types of oxidation states [5]. Most abundant forms of iron oxides are hematite (α-Fe_2O_3), maghemite (γ-Fe_2O_3) and magnetite (Fe_3O_4). Maghemite and hematite have similar structures namely inverse spinel. 32 O^{2-} cubic close packed anions provide tetrahedral and octahedral coordination sites for the iron cations. Maghemite has only Fe^{3+} cations and they were found in both octahedral and tetrahedral coordinations. On the other hand in magnetite there are both Fe^{2+} and Fe^{3+} cations exist together. Fe^{3+} cations were placed both in octahedral and tetrahedral sites. Fe^{2+} cations occupy the tetrahedral sites. Due to this structural similarity betwen these oxides, X-ray diffraction method should not be used only to determine the phases. Other techniques should also be used as characterization tools for the determination of crystal structure [5].

0, II and III oxidation states of the iron metal and iron oxides have unpaired electrons in their d shells resulting in paramagnetic behaviour. But in maghemite and magnetite there is no complete cancellation, so there is non-zero magnetic moment [5].

Magnetic iron oxide nanoparticles have gained acceptance in several fields of application of nanomaterials, like in magnetic recording systems, magnetic refrigeration, magneto-optical solid devices, magnetic resonance imaging and in flow systems [6]. Especially maghemite (γ-Fe_2O_3) nanoparticles are used extensively in the field of biomagnetics for a broad range of applications, such as drug delivery [7,8,9], medical diagnosis [7], cell seperation [7,8] magnetic resonance imaging, sensing [7,10] as well as therapeutic applications [7] such as AC magnetic field-assisted cancer therapy, i.e. hyperthermia [7,8,11], magnetic refrigeration [9,10,12]. All these technological and medical applications require that the nanoparticles are superparamagnetic with sizes smaller than 20 nm with narrow size distribution to have uniform physical and chemical properties. It is reported that the critical size for maghemite nanoparticles is around 10 nm [9].

The aim of this study is to produce maghemite nanoparticles by using different production methods and to characterize them with appropriate techniques. Main focus area was synthesizing the maghemite which is not a stable phase at room temperature. According to the theoretical predictions in the literature [13], γ-Fe_2O_3 is only stable at a particle size on the order of 5 nm. As a result of increased particle size, maghemite's tendency of transforming into hematite phase increases. As reported before the main problem is to control the particle size of the produced nanoparticles.

In order to realize the aim of finding the most effective technique to produce this material, various methods were investigated and compared as a way of overcoming the difficulties of improving the quality of the produced material.

Main purpose of this study is producing maghemite by a typical method which will allow us to obtain maghemite phase in desired properties. To achieve this purpose Sol-Gel Processing and Microwave Synthesis methods were employed.

While searching for appropriate methods, suitable characterization techniques like XRD, TEM, BET, and VSM were performed to control the properties of the produced material whether it is suitable for certain applications.

This thesis is composed of six chapters. It gives a general information about nanoparticles and aim of the study in Chapter 1. Second chapter begins with again nanoparticles followed by iron oxides, their crystal structures and their applications. Given applications are especially for the maghemite phase. After that magnetic properties of iron oxide nanoparticles were explained in this chapter. In the last part of the chapter production methods for magnetic nanoparticles were given. In this part sol-gel process was explained in more detailed way since generally this method is preferred to produce maghemite nanoparticles in the literature. Third chapter includes the experimental procedure consisting both sol-gel method and microwave method. In sol-gel processing, two different routes used in the thesis were explained in detail. In the fourth chapter results from XRD (X-ray diffraction), SEM (scanning elecron microscopy), TEM (transmission electron microscopy), BET, and VSM

(vibrating sample magnetometry) were given and details of phenomena which may be responsible for the present experimental findings were presented. Chapter 6 gives the summary of the study. Finally in Chapter 5, conclusions and further suggestions were made.

CHAPTER 2

LITERATURE SURVEY

2.1 Nanoparticles

Materials that are composed of particles with dimensions less than 100 nm classifed as nanomaterials. When the size of the particles changes from micro to nano size regime many of the properties of the material change. These are physical, chemical, mechanical and magnetic properties of the materials.

Nanoparticles can be in the form of amorphous or crystalline state. In some studies it is proposed that nanoparticles should be considered as a sate of matter [14].

As the particle gets smaller, surface area to volume ratio increases since many of the atoms locate at the surface. As an example 20 nm iron particle has 10 % of its atoms at its surface, on the other hand 50 % of the atoms of 3 nm iron particle are located at the surface [5]. At this size surface reactivity of the material increases since many chemical reactions occur at the surface. High surface area is especially critical for performance of the fuel cell and battery technologies. The large surface area of the particles also inreases the interactions between the materials in nanocomposites, resulting in the high strength and high chemical resistance. Since dimensions of the nanoparticles are smaller than the wavelength of the light, these are useful for the packaging, cosmetic and coating applications [15].

Nanoparticles are also used in various different areas like catalysts, films for microelectronics, new magnetic materials, protective coatings on metals, plastics and glasses [16].

Many of the technological interests have been given to small atomic aggregations due to their unique properties between the isolated atoms and bulk solids [16].

Nanotechnology term is related with the sizes of the structural elements. Nanomaterials are generally classified according to their particles sizes. Figure 2.1 shows this classification. They can also be classified according to their geometrical form and dimensionality. They are cluster materials, fibrous materials, films and multilayer materials, and also polycrystalline materials [16].

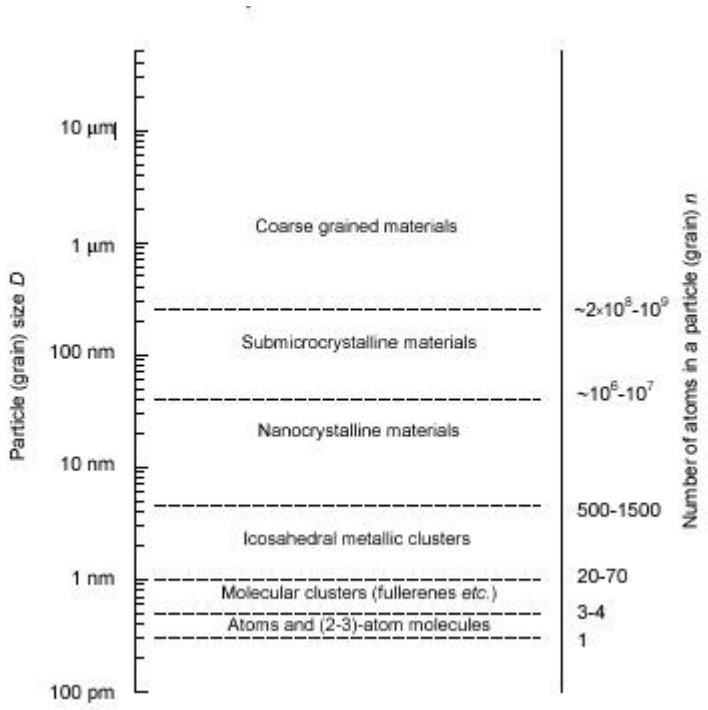

Figure 2.1 Classification of substances and materials on the basis of particle (grain) size D.

Nanoobject has the dimension between 1 and 100 nm and it has different properties than its bulk form. Physical properties, especially magnetic properties, are dependent upon the size of the nanoparticles. Thus many scientists are interested in the particles

that have sizes smaller than the magnetic domains in the corresponding bulk materials [4].

Nanotechnology is related with nanomaterials, their production methods and devices produced from those materials. Compact materials and nanodispersions are types of nanomaterials. Isotropic materials that contain nanometer sized structural elements, belong to first type nanomaterials. On the other hand nanodispersions contain homogeneous dipersion medium and isolated nanoinclusions dispersed in this medium. There are various distances in these dispersions from fraction of a nanometer to tens of nanometers. Other type contains nanopowders that their grains are separated by monoatomic layers of atoms, thus agglomeration can be prevented [4].

Nanoparticles can also be called as quasi-zero-dimensional (0D) nanoobjects and their dimensions are not more than 100 nm. Properties of nanoparticles are different from larger particles above 0.5 μm. Generally nanoparticles have spheroid shapes. If they have ordered arrangement of atoms they are called as nanocrystallites. Quantum dots are the nanoparticles that have discrete electronic energy levels and generally their compositions are similar with semiconductor materials [4].

Great importance are given to the nanoparticles since they are between bulk materials and molecules and atomic level structures. Nanoparticles that are smaller than 1 nm are called clusters in the literature. Nanoparticles have size distributions whereas molecular magnetic clusters consist of magnetic nanoparticles with similar sizes. Magnetic clusters magnetism is usually described by exchange-modified paramagnetism [4].

Magnetism of nanoparticles are different from classical magnetic materials because of their domain structure and their magnetism can beconsidered as nanomagnetism. Superparamagnetism, ultrahigh magnetic anisotropy and coercive force, and giant magnetic resistance terms are related with nanomagnetism. Magnetization and magnetic anisotropy of nanoparticles are greater than a bulk specimen, in addition

Curie or Neel temperatures between nanoparticles and the corresponding microscopic phases are also different. Chemical composition, the type and and the degree of defectiveness of the crystal lattice, the particle size and shape, the morphology, the interaction of the particle with the surrounding matrix and the neighboring particles are the important parameters that determine the properties of nanoparticles. However these properties are not easily controlled during the synthesis procedures [4].

2.2 Iron Oxides

There are 16 iron oxide types including oxides, hydroxides, or oxyhydroxides. But among these most important ones are hematite (α-Fe_2O_3), magnetite (Fe_3O_4) and maghemite (γ-Fe_2O_3) [17].

2.2.1 Hematite

Hematite (α-Fe_2O_3) is second most abundant mineral with the structure similar with corundum [17,18]. Among the iron oxides hematite is the most thermodynamically stable one and it is the oldest known iron oxide with a blood red colour (Figure 2.2).

Figure 2.2 Hematite ore [19].

Hematite has a hexagonal unit cell with six formula units per unit cells but it can also be classifed in the rhombohedral system. If it is in rhombohedral system, there are two formula units per cell. Its unit cell parameters are a = 0.5034 nm and c = 1.375 nm for hexagonal and a = 0.5427 nm and $\alpha = 55.3°$ for rhombohedral systems, respectively. Oxygen ions are stacked in the [001] direction. Fe^{III} ions occupied the two thirds of the sites, and there is a vacant site in the (001) plane. $Fe(O)_6$ octahedra is obtained by the arrangement of the cations. Three octahedra shares the edges and one face with each octahedron. Edges are shared with in the same plane, on the other hand one face is shared in the adjacent plane in the c axis. This face sharing distorts the ideal packing [17].

Hematite is an antiferromagnetic material. There is a small magnetic moment in the basal plane direction since moments of two sublattices don't cancel each other and spins are canted. Magnetic properties of hematite are effected from the preparation conditions of the sample.

At 263 K there is a phase transition in hematite, which is called as Morin transition. At this temperature antiferromagnetic phase turns to a weak ferromagnetic phase [20]. Magnetization of the two spin sublattices are reoriented from parallel to perpendicular to the [111] axis [21,22]. The spins of the hematite lie in the rhombohedral [111] direction at low temperatures, and at high temperatures they lie in the basal (111) plane in a canted position [20]. Crystallite size of the hematite influences the Morin transition temperature [23]. Both single and polycrystalline hematites show Morin transition. It decreases with decreasing particle size and if the size is smaller than 20 nm there is no such transition in the sample [24].

2.2.2 Magnetite

Magnetite (Fe_3O_4) is the most common iron oxide material with black colour (Figure 2.3) and it shows high magnetization [25]. It has the inverse spinel type structure [17]. There are 32 O^{2-} ions in the face centered cubic unit cell positions. The unit cell parameter is 0.839 nm.

Figure 2.3 Magnetite ore [19].

The structure of magnetite is quite different from the other iron oxides. There are both divalent (Fe^{II}) and trivalent (Fe^{III}) iron in its formula. Trivalent ions are in the tetrahedral and octahedral sites. Generally magnetite is nonstoichiometric, if divalent-trivalent ion ratio is 0.5 it is stoichiometric. Unit cell length differs from its original size **w**hen there are cation substitutions in the lattice [17].

Magnetite is a ferrimagnetic material and its Curie temperature is about 850 K. Below 850 K magnetic moments are antiparallel in the tedrahedral and octahedral sites giving to ferrimagnetic properties to the magnetite. At about 125 K there is a semiconductor-insulator phase transition(verwey transition) in the magnetite and its electrical conductivity decreases, also monoclinic symmetry is obtained [26]. At this temperature freezing of electron hopping occurs and resistivity, magnetization, magnetoresistive ratio and susceptibility values change sharply [27].

Magnetite behaves like a metal when the electrons orient in one direction, and it behaves like an insulator when they orient in the other direction. This is the half metallicity behavior of magnetite material and because of this property it is the most desired material for tunneling magnetoresistance devices [26]. Besides its half

metallic property, high polarity is another important nature of this material and thus it is important for ultahigh density magnetic storage media and magneto optical devices [28].

2.2.3 Maghemite

Maghemite (γ-Fe_2O_3) is another important iron oxide material with red brown colour (Figure 2.4). It has a spinel structure which is similar with magnetite. But in the maghemite all of the irons are in the trivalent state [17].

Figure 2.4 Maghemite ore [19].

Unit cell of maghemite is cubic and the unit cell length is 0.834 nm. There are 32 O^{2-} ions, 21 1/3 Fe^{III} ions and 2 1/3 vacancies in each unit cell. Vacancy ordering results in the superstructure form of synthetic maghemite and it is related with crystallite size [17].

Goethite, hematite and magnetite forms of iron oxides can transform to produce maghemite phase. The last part of the transformation is the oxidation of magnetite [17].

Maghemite is ferrimagnetic material at room temperature but when the size of the particles smaller than a certain limit ~10 nm it shows superparamagnetic property. Maghemite transforms into more stable hematite phase in the temperature range 370-600 °C. Its Curie temperature is between 547- 713 °C [17].

Magnetic properties of maghemite nanoparticles are affected by the surface-interface effects. When surface area of the particles decreases their saturation magnetization value also decreases [17]. Size, internal structure disorder, agglomeration and interparticle seperation influence the magnetic properties of maghemite [7].

Maghemite nanoparticles find large usage in biomedical applications like drug targeting, molecular biology, DNA purification, cell seperation, hyperthermia and magnetic resonance imaging [7]. These nanoparticles are used in industrial applications like magnetic recording, magnetic refrigeration, catalysis and many other applications. Earth and plenetary sciences are also interested in maghemite nanoparticles [7].

2.3 Applications of Iron Oxide Nanoparticles

Iron oxides are widely used compounds since they have excellent magnetic and catalytic properties. Due to their unique properties many different diciplines give great importance to these materials (Figure 2.5 and 2.6).

Magnetic nanoparticles with high saturation magnetization and high magnetic susceptibility values and sizes less than 200 nm are important for medical applications. These nanoparticles have been used in enzyme and protein immobilization, drug delivery, especially delivery of cancer drugs and as a contrast agent in magnetic resonance imaging (MRI) [29].

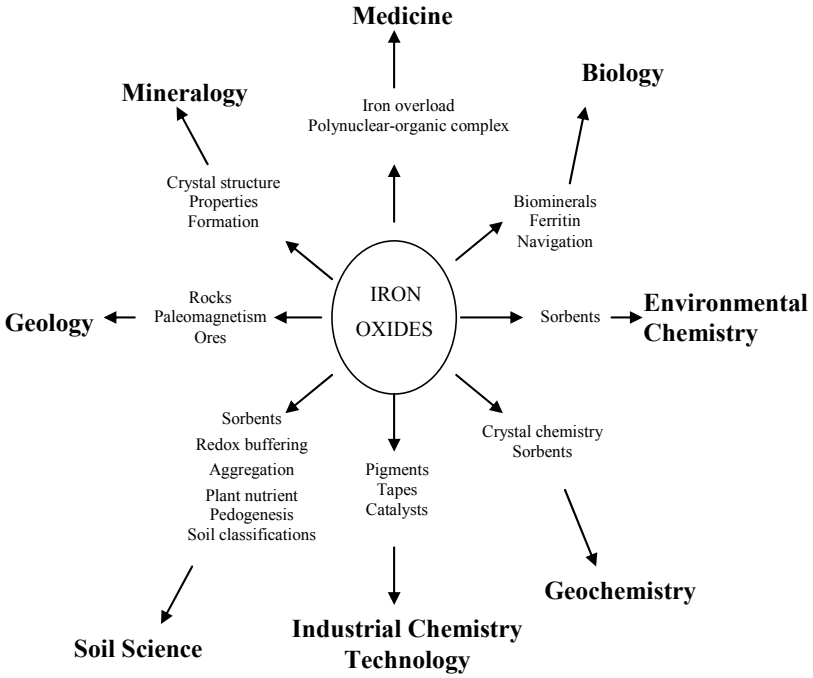

Figure 2.5 The multidisciplinary nature of iron oxide research [30].

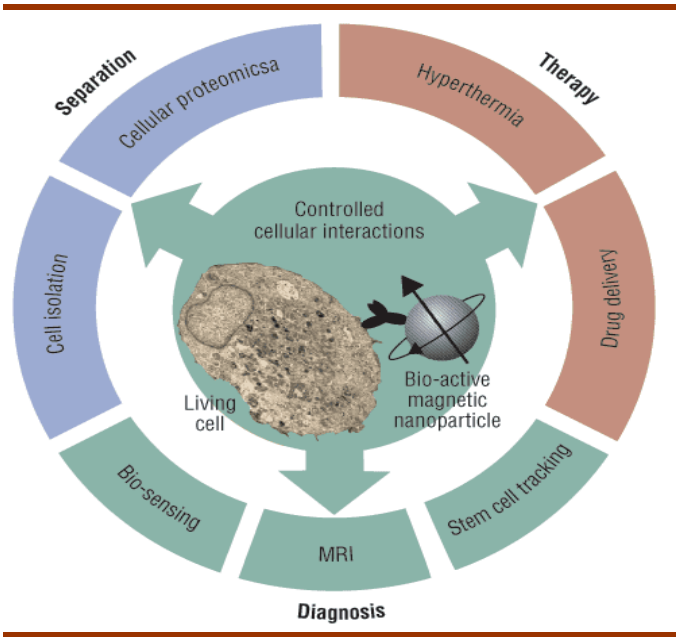

Figure 2.6 Biomedical applications of biologically activated magnetic nanoparticles [31].

All these applications require the narrow size distribution of nanoparticles and uniform chemical and physical properties [32]. The main reason of usage of iron oxide nanoparticles in these applications is their biocompatibility and nontoxicity [29].

Magnetic iron oxide nanoparticles have large surface areas due to small size and their surfaces are hydrophobic. Agglomeration occurs due to the hydrophobic interactions between particles. Agglomeration decreases the superparamagnetic properties of the nanoparticles and in order to use these nanoparticles in biomedical area, agglomeration should be prevented and surface modification should be done to increase their stability. Selection of coating materials like polymers or surfactants is important since they should have nontoxic, biodegradable and hydrophilic character. Some of the examples of polymers and surfactants that are used to modify the nanoparticles surface are polyethylene glycol (PEG), dexran, polyvinylpyrrolidone (PVP), polyvinyl alcohol (PVA), polypeptides, gelatin and chitosan**.** Also in some cases aluminum oxide and silica can be used as a stabilizer**.** Usually to prevent agglomeration stabilization occurs during the preparation of magnetic nanoparticles in chemical routes [29].

2.3.1 Magnetic Drug-Targeting and Gene Delivery

Targeted drug delivery is important especially for tumor diagnostics and therapeutics and it consist of basically two steps. One of them is delivery of drug to the desired organism and second one is the release of the drug in a controlled rate [33]. Drugs are targeted to specific sites with a magnetic field application by using magnetic drug delivery systems. With these systems prolonged release of the drug can be achieved [34].

Blood compartment exerts forces on the particles. Also magnet generates magnetic forces and by the competition between these forces drugs are localized in the targeted sites. Therapeutic systems are protected, transported and deposited to the desired

sites by using delivery systems. Targeted drug delivery systems have no side effects. In addition to cancer, magnetic carriers are also used in various diseases [34].
Drug carrier system should be small enough to allow the capillary distribution, should have biocompatible, non antigenic, non toxic and biodegradable properties. It has been reported that generally natural polysaccharides, liposomes and artificially synthesized polymers have been used as drug carriers since they have these requirements [33]. In a magnetically targeted drug delivery system, drug is binded to the magnetic nanoparticle, injected to the bloodstream and a magnetic field is applied to pull them out of suspension. But nanoparticles should have high stability and should have minimum aggregation. Because of this surface modification is necessary in the targeted drug delivery [33].

For drug delivery application nanoparticles should also allow a targetable delivery with being localized in a specific area. PEG is the most widely used coating material in the drug delivery application of nanoparticles**.** It has been shown that when nanoparticles are coated with PEG cellular response increased. For these applications size, charge and surface chemistry of the nanoparticles are important for blood circulation time in the body [32].

Magnetophoretic mobility (μ_m) is an important parameter in the drug delivery systems. It is the measure of the mobility of a magnetic carrier in a liquid medium under the influence of an applied magnetic field. Diameter of the carrier, effective susceptibility and the viscosity of the medium affects the magnetophoretic mobility. If the saturation magnetization of the magnetic carrier increases, the value of magnetophoretic mobility also increases [34].

2.3.2 Magnetic Resonance Imaging

Magnetic resonance imaging (MRI) is another important biomedical area in which nanoparticles are used in a broad manner. It is one of the most powerful techniques in biomedical research.

There are two relaxation times in this technique. First one is the longitudinal relaxation time (τ_1) and the second one is transverse relaxation time (τ_2) [35].

Nuclei of elements with a weak internal spin are aligned in the applied magnetic field direction. The nuclei are tilted away from its aligned direction when a force exerted perpendicular to the direction of the magnetic field. During this period nuclei absorbs energy. When the exerted force is removed, nuclei are aligned along its original direction with the field. Longitudinal relaxation time, τ_1 is the time that is required for the nuclei to return the field direction [34].

Different nuclei fall out of phase with each other due to being in an inhomogeneous magnetic field, and they emit the resonance signal and this signal interferes with each other. Thus there is a decay of received signal. Transverse relaxation time τ_2 is related with this process. Chemical compound, magnetic field strength and temperature affect τ_1 and τ_2 [34].

In most cases gadolinium or manganese based materials are used as contrast agents to increase the contrast between normal and diseased tissues. In recent years superparamagnetic iron oxide nanoparticles have been used instead of paramagnetic materials since they have high magnetic moments [36,37]. These high magnetic moment nanoparticles are desired since their enhancement in relaxation rates are better than conventional Gd based agents [29,38].

There are also two types of contrast agents; positive contrast agents enhance the signal and generally paramagnetic Gd based materials are used, on the other hand negative contrast agents reduce the signal and iron oxide nanoparticles are used in this case due to their higher magnetizations [35]. Superparamagnetic particles are desired in such applications since they don't retain any magnetization after removal of the magnetic field [29].

Mechanism of changing of relaxation times with magnetic particles are quite complex. When the magnetic field applied, particles show large magnetic moments. Their size and composition are important factors in the relaxation process [34].

2.3.3 Hyperthermia

Especially in the cancer therapy heating of organs and tissues is called hyperthermia. Heating occurs between 41-46 °C [34]. Usually tumor is heated more than healty tissues since blood flow is not normal in diseased tissues. Thus hyperthermia is the effective method in the cancer treatments [39].

In the classical hyperthermia there is reversible damage to cells and tissues, but radiation injury of tumor cells inreases. Modern clinical hyperthermia optimizes the thermal homogeneity at temperatures between 42-43 °C. It is reported that magnetic nanoparticles are used in magnetic hyperthermia about 50 years ago. Heating of oxide magnetic materials occurs in an external magnetic field due to the reorientation of the magnetization [34]. In the magnetic fluid hyperthermia method, ferromagnetic or superparamagnetic nanoparticles are injected into the tumor then irradiated with an ac magnetic field. Energy is transferred into heat with physical mechanisms. Magnetic properties of the particles and external field frequency affect the transformation efficiency [40].

2.4. Magnetic Properties of Iron Oxide Nanoparticles

Magnetic moments of the electrons determine the magnetic properties of the materials. Spin and orbital motions of the electrons effect the macroscopic magnetic properties in materials [41]. Spin moment is related with the spin of electron around its axis. Orbital motion is related with the electron spin which is originated along the orbit around the nucleus of the atom. Both of these two moments give the magnetic property to the material [42]. Figure 2.7.a and 2.7.b show these two moments.

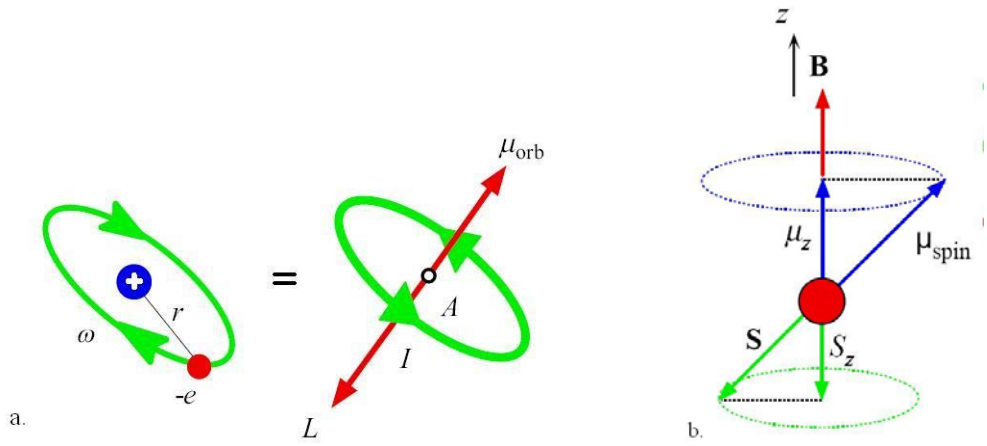

Figure 2.7 a. orbital magnetic moment, **b.** spin moment [43].

Diamagnetism, paramagnetism and ferromagnetism are the basic types of magnetism in the materials. Materials classification depends on the behavior of the material in the magnetic field [42]. Figure 2.8 shows a schematic representation of different types of arrangements of magnetic dipoles.

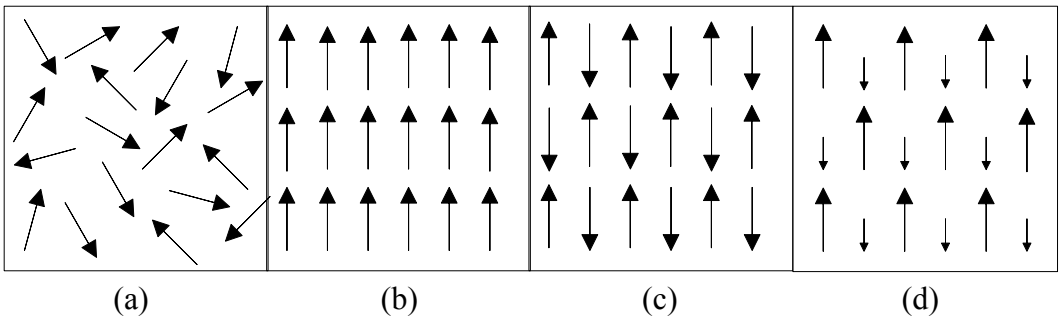

Figure 2.8 Different orientations of magnetic dipoles: (a) paramagnetic, (b) ferromagnetic, (c) antiferromagnetic, and (d) ferrimagnetic [43,44].

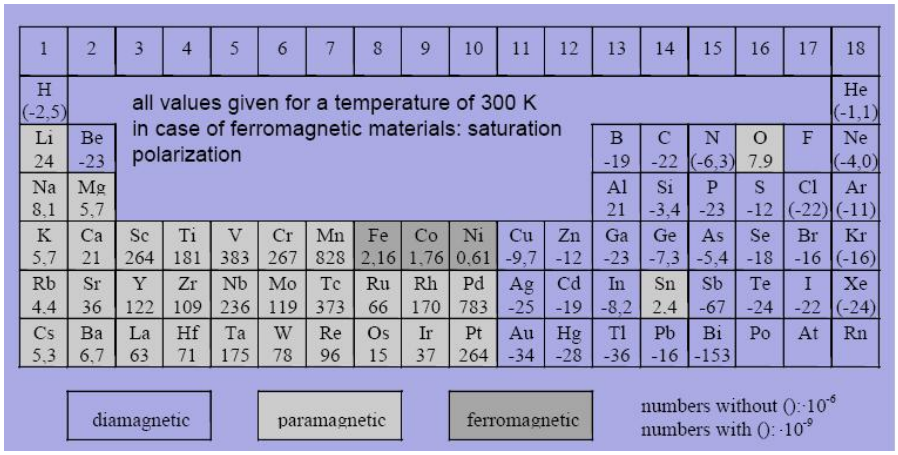

Figure 2.9 Periodic table that shows magnetic properties of the elements [45].

Figure 2.9 shows the elements with different magnetic properties. From the table it can be seen that most of the metals are paramagnetic and most nonmetals are diamagnetic. Iron, cobalt, nickel and below 16 °C gadolinium are ferromagnetic.

2.4.1 Diamagnetism

Diamagnetism is a basic property of all substances and involves a slight repulsion by a magnetic field [17]. Diamagnetic materials exhibit weak magnetism when they are placed in an external field (Figure 2.10). This weak form of magnetism is not permanent. Orbital motions of the electrons change in the magnetic field and this change causes the diamagnetism. This type of magnetism can be found in all materials when other magnetisms are not seen [46].

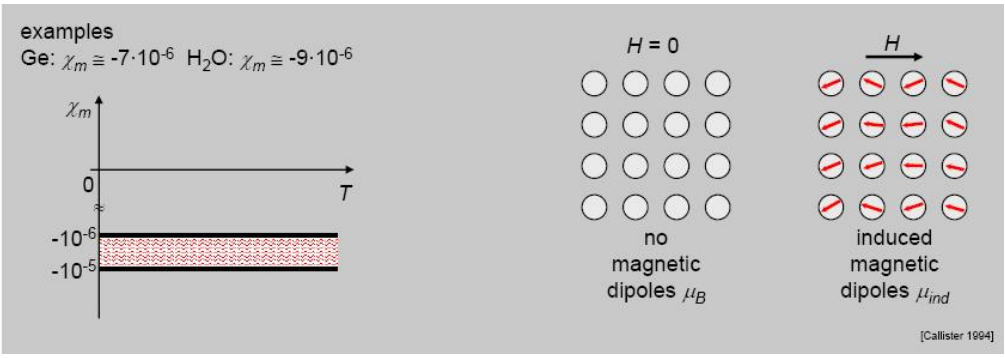

Figure 2.10 Magnetic polarization mechanisms in a diamagnetic material [46].

Diamagnetic materials have magnetic susceptibilites smaller than zero and their values are generally between 10^{-5} and 10^{-6} [30,45]. When a field is applied to this material it induces a magnetization to the material and it becomes a magnet. Its induced moment is opposite to the applied field and has a small value. If the material is not symmetric, field aligns it perpendicular to itself and minimizes the induced moment which is antiparallel to the field (Figure 2.11).

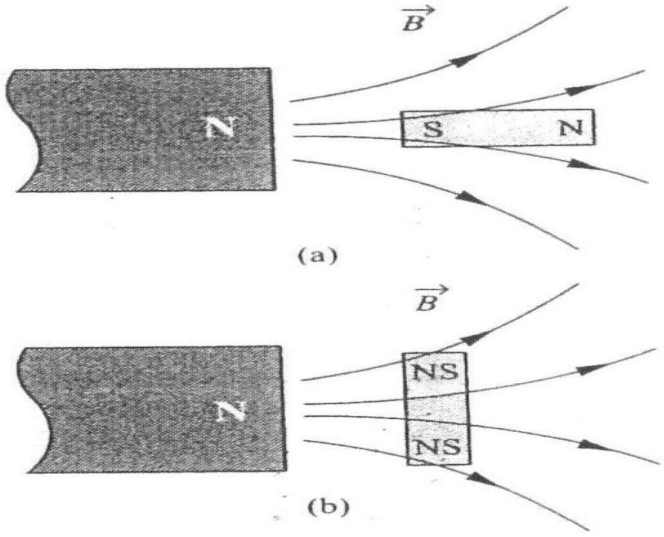

Figure 2.11 A magnetic field applied to an elongated material. (a) When $\chi>0$, the induced dipole is in the same direction as the applied field and the net force is attractive. (b) When $\chi<0$, (diamagnetic) the induced dipole is opposite to the field and to minimize this unfavorable antiparallel alignment the material rotates its axis perpendicular to the field. The net force is repulsive [45].

When an applied field acts upon on a conduction loop, there is a current inside the loop. This is the fundamental principle of electromagnetism which is called as Lenz's law. Induced current remains after the application of the field since the electron orbits are resistanceless from the atomic point of view. Conduction electrons of metals and superconductors also behave resistanceless and they exclude the applied field due to their diamagnetic behavior [45].

If the orbits of the electrons considered as current loops, diamagnetism of atoms, ions and molecules can be modeled. Current times the area of the loop gives the induced moment. Passage of the charge, and the frequency of the orbital motion affect the current. Due to this reason Langevin predicts the susceptibility like;

$$\chi = -\frac{NZe^2}{mc^2}\left\langle r^2 \right\rangle \qquad \text{Eq. 2.1}$$

In this equation N is the number of atoms per unit volume, m is the electron mass, c is the speed of the light, Z is the atomic number, e is the unit electric charge, and r is the radius of the orbital. According to this equation large atoms with high Z have high diamagnetic susceptibilities. Also in this equation there is no temperature effect [45].

2.4.2 Paramagnetism

When the magnetic moment of the atomic, ionic and molecular species are non zero, they exhibit paramagnetism. Their susceptibilities are greater than zero. In these materials there is also a diamagnetic behavior [45]. Paramagnetic materials have small susceptibilities larger than zero with the values between 10^{-3} and 10^{-5}. Due to this positive value, applied field is in the same direction with the induced moment. In figure 2.11 there is a permanent magnet which creates a field near the paramagnetic material. The field lines and induced dipoles are away from the north pole of the magnet. If the material is nonsymmetric its long axis is aligned parallel to the applied field [45].

Paramagnetic nonzero moments occur in most of the materials. Molecules that consist of odd number of electrons, transition metals that have partially filled d-shells and rare earth elements with partially filled f-shells can have spin moments [45].

Significant amount of polarization can be obtained with the small value of applied field. Thermal energy and magnetic moment alignment are the important parameters

for the paramagnetism and ferromagnetism. Langevin model of paramagnetism uses this competition which gives the importance of temperature for the magnetic properties of materials [45].

When the spin and orbital moments do not completely cancel each other, there is a dipole moment of atoms which is permanent in some solid materials. Atomic magnetic moments are randomly oriented when there is no magnetic field, so there is no net magnetization in the material [46]. Magnetic moments are partially aligned in the field direction when the field is applied. Figure 2.12 shows the polarization mechanism of paramagnetic substances.

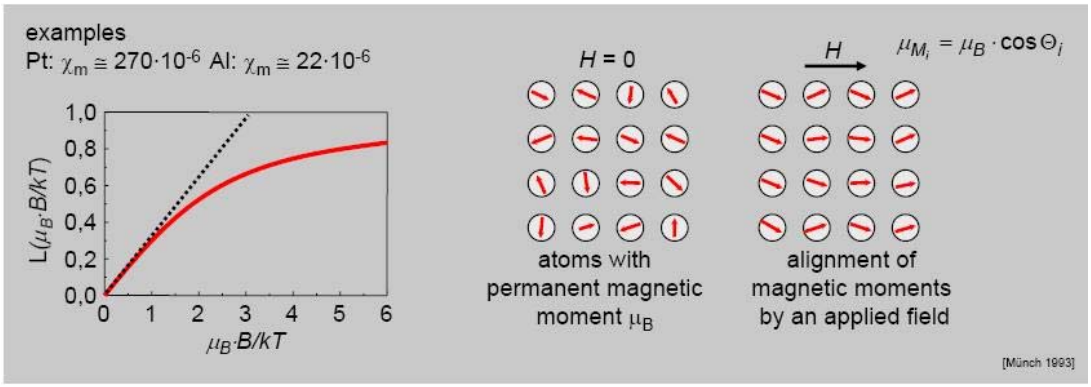

Figure 2.12 Magnetic polarization mechanisms in a paramagnetic material [46].

Due this orientation net positive magnetization occurs in the material with positive and small magnetic susceptibility, χ_M [30,42]. Moments are randomized by the temperature [12]. Cornell et al. described this behavior with Curie-Weiss law [30],

$$\chi_M = \frac{C_M}{T - T_C} \qquad \text{Eq. 2.2}$$

C_M is the Curie constant, T_C is the Curie temperature and T is the temperature. According to equation χ_M decreases with increasing temperature, since temperature increase changes the alignment of the magnetic moments due to thermal vibrations.

Iron oxides exhibit a transition behavior below a certain temperature. Curie temperature is the transition temperature of ferromagnetic and ferrimagnetic materials, on the other hand Nèel temperature is related with the antiferromagnetic materials.

Figure 2.13 shows the hysteresis behavior of diamagnetic and paramagnetic materials.

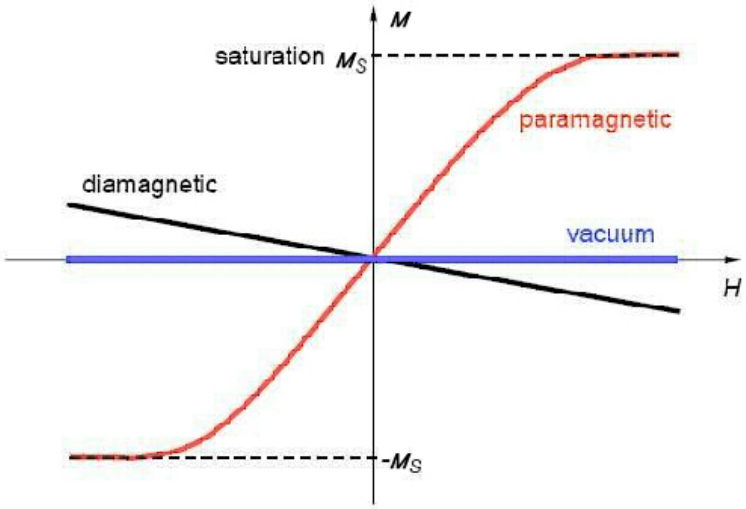

Figure 2.13 Hysteresis behavior of diamagnetic and paramagnetic materials [45].

2.4.3 Ferromagnetism

There are permanent magnetizations in some metallic materials even in the absence of magnetic field application. Both electron spin and orbital moments are responsible for this behavior [42]. This type of behavior is explained by ferromagnetism and generally transition metals iron (as BCC α ferrite), cobalt, nickel, and some of the rare earth metals such as gadolinium exhibit this magnetic bahavior [48]. Weiss theory describes the ferromagnetism in magnetic materials [45].

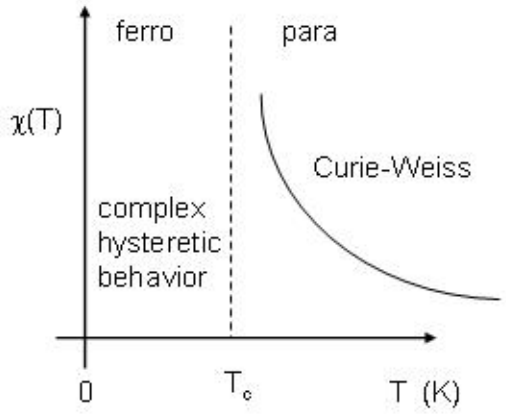

Figure 2.14 Curie-Weiss Law for ferromagnetism [45].

According to Figure 2.14, susceptibility increases with decreasing temperature. There is a critical temperature (T_C, Curie temparature), below which material is ferromagnetic, on the other hand above this temperature it behaves paramagnetically.

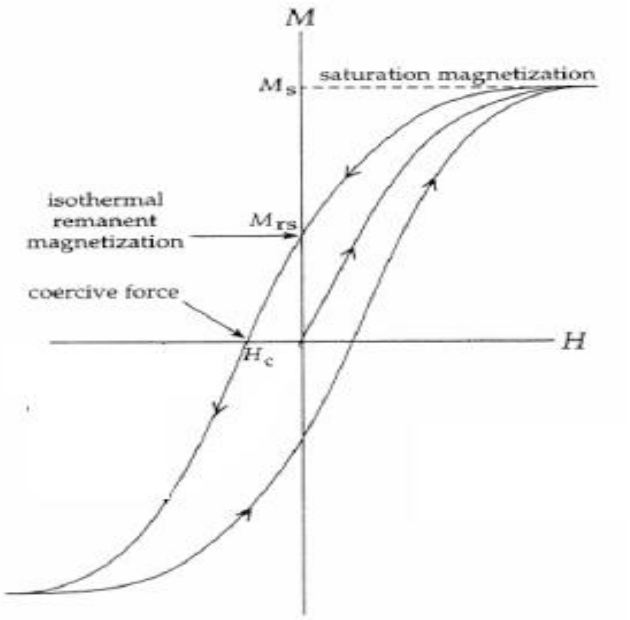

Figure 2.15 Hysteresis, remanence, and coercivity of ferromagnetic materials [43].

Figure 2.15 is the hysteresis curve of a ferromagnetic sample. According to this figure remanent magnetization is a measure of the remaining magnetization when field drops to zero. Coercive force is a measure of reverse field needed to drive the magnetization to zero after saturation.

Eq.2.2 diverges at T_C. In the case of zero applied field, there can be a net magnetization in the material. It can be said that there is a spontaneous magnetization. Weiss proposed that the atoms are interacting, to explain this result. It is alo proposed that the field is proportional to the materials magnetization.

2.4.4 Antiferromagnetism

When the spin moments of neighboring atoms or ions are aligned oppositely antiferromagnetism occurs. There is an antiparallel alignment in these materials [46]. Magnetic moments cancel each other and result in zero net magnetization [42].

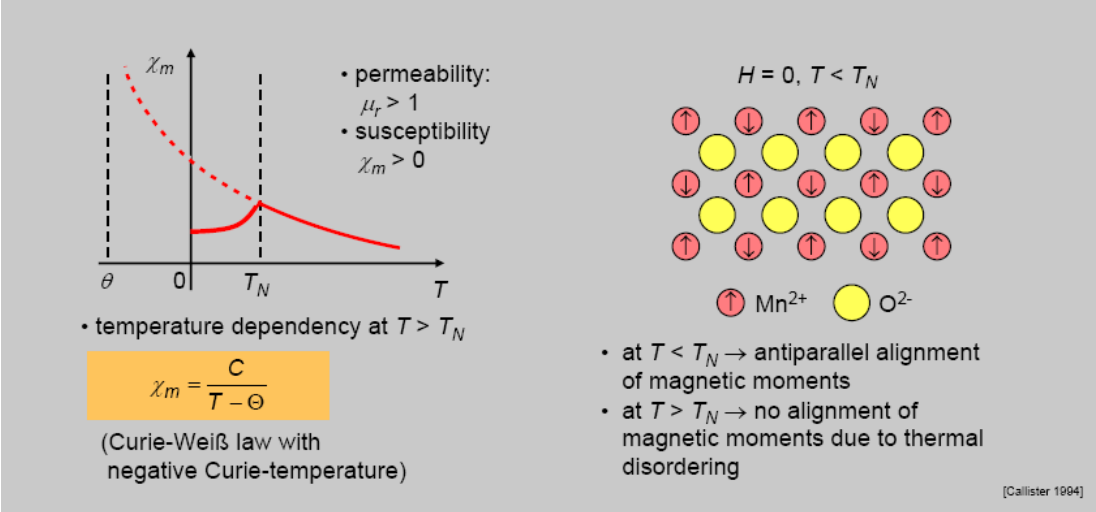

Figure 2.16 Magnetic polarization mechanisms in an antiferromagnetic material [46].

2.4.5 Ferrimagnetism

Ferrimagnetism is generally seen in ceramic materials and it is similar with ferromagnetism, only the source of the net moments are different [46]. Just like antiferromagnetic materials, ferrimagnetic materials have the same antiparallel alignment of magnetic moments. But the magnitude of the magnetic moments differs in opposite direction. Hence in the absence of a magnetic moment, there remains a net magnetic moment [41].

Figure 2.17 shows the alignment of dipoles and T_C temperatures of some ferrimagnetic materials.

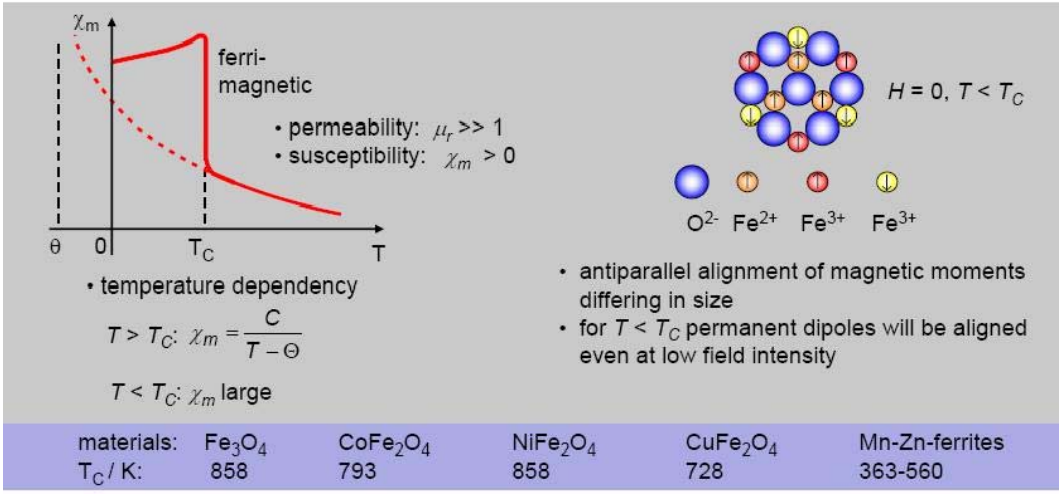

Figure 2.17 Magnetic polarization mechanisms in a ferrimagnetic material [46].

2.4.6 Superparamagnetism

Paramagnetic materials exhibit superparamagnetism at temperatures below the Curie or Nèel temperature. Superparamagnetic materials are composed of very small crystallites below 10 nm. Since the crystallite size is very small thermal energy overcomes the coupling forces and changes the magnetization direction. When there are fluctuations in the direction of the magnetization, average magnetic field drops to zero. This behavior is also observed in paramagnetic materials, but in the

superparamagnetic case whole crystallite aligns with the applied magnetic field due to the independent behavior of each individual atom [42].

Electron spins are aligned along the preferred crystallographic directions, thus magnetic anisotropy occurs and due to this effect superparamagnetism can be observed in the material. These preferred directions are along crystallographic axis or set of axes. Magnetization can change the direction if there is enough energy. Relaxation time τ is the required time for the spin reversal and it depends on the height of the energy barrier between the forward and reverse spin states and the temperature, according to

$$\tau \propto \exp\left(\frac{K_{eff}V}{kT}\right) \qquad \text{Eq. 2.3}$$

The height of the energy barrier between the forward and reverse states is the product of the particle volume, V, and the anisotropy constant K_{eff} (which is, to some extent, a function of particle size). If the thermal energy of the particles is higher than the activation energy barrier between the spin states, rapid fluctuations occur and superparamagnetic relaxation is observed.

Iron oxides that have the size smaller than 10 nm show superparamagnetism at the room temperature since superparamagnetism depends on the size and the anisotropy constant. If the temperature decreases and relaxation time increases superparamagnetic relaxation can be prevented. Blocking temperature T_B is the temperature that particles are ordered below it and it is given in the following formula:

$$T_B = \frac{K_{eff}V}{25k} \qquad \text{Eq. 2.4}$$

In Figure 2.18 different magnetism types are shown. M_S is the saturation magnetization and at the saturation point all of the spins are aligned with the applied

field. H_C is the coercive field, M_R is the remanent magnetization. Superparamagnetic and paramagnetic materials have no hysteresis loops on their M-H curves.

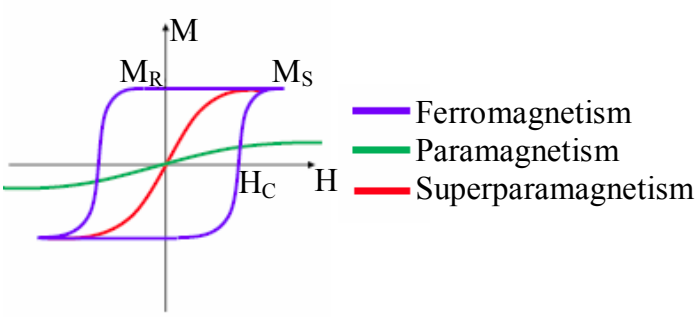

Figure 2.18 Magnetization (M) vs. applied field (H) for ferromagnetic, paramagnetic and superparamagnetic materials [44].

2.5 Preparation Methods of Iron Oxide Nanoparticles

Production methods of magnetic nanoparticles should give particles with uniform size and shape. Uniform particles can be produced by using precipitation from a homogeneous solution and by controlling the particle growth in a process. In such processes precursor in aerosol or vapour is decomposed to produce particles. Gold colloids, sulfur sols, metal oxides and hydrous oxides can be prapared by these preparation methods [47].

To produce magnetic nanoparticles and composites with magnetic nanoparticles, there are various techniques based on solutions, aerosol/vapour phases or organic and inorganic matrices [47].

2.5.1 Magnetic nanoparticles

2.5.1.1 Precipitation from solution

In these methods magnetic nanoparticles are produced in a controlled size and shape that is suitable for biomedical applications. Usually homogeneous precipitation is

preferred that includes separation of the nucleation and the nuclei growth steps. Figure 2.19 shows the mechanism of formation of uniform particles [47].

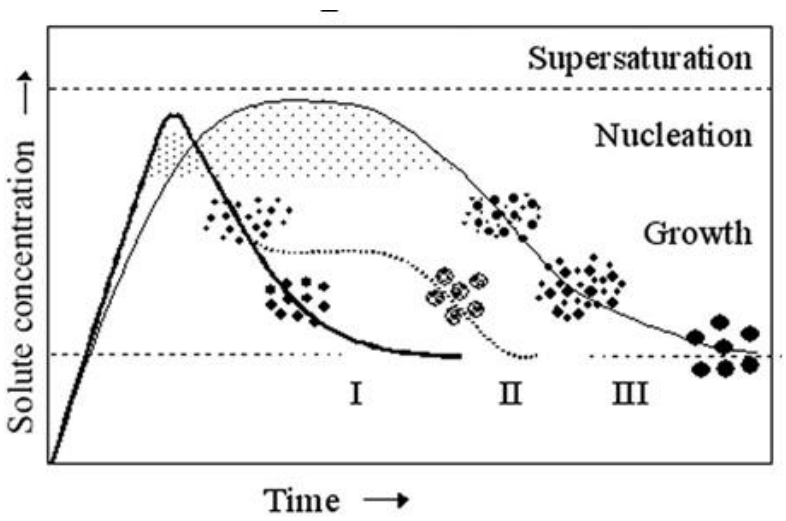

Figure 2.19 Mechanism of formation of uniform particles in solution: curve I: single nucleation and uniform growth by diffusion; curve II: nucleation, growth and aggregation of smaller subunits; curve III: multiple nucleation events and Ostwald ripening growth [47].

When the concentration of constituent species reaches a critical supersaturation, nucleation occurs in the form of homogeneous precipitation. After the nucleation, nuclei grow uniformly by diffusion of solutes from the solution to their surface until the final size is obtained. If there is no nucleation during the growth process monodisperse particles can be obtained according to the classical model proposed by LaMer and Dinegar. Uniform particles can also be obtained after multiple nucleation steps by Ostwald ripening process [47].

Coprecipitation, microemulsions, polyol process and decompositon of organic precursors are the examples of solution methods that are used for the production of iron based nanoparticles [48].

2.5.1.2 Coprecipitation

There are two methods in this technique to produce spherical magnetic nanoparticles. Ferrous hydroxide suspensions and oxidizing agents are used in the first one. In the literature spherical magnetite nanoparticles with a size range of 30-100 nm is obtained. In the other method mixtures of ferric and ferrous hydroxides are used. Controlling the pH and ionic strength of the medium yields the control on the mean particle sizes. Also chemical composition is affected by these parameters. Smallest particles can be obtained by using polyvinylalcohol (PVA) with iron salts. Some modifications by using dextran can be applied to this technique for the production of nanoparticles for in vivo biomedical applications and this is the most common technique to produce magnetic nanoparticles used as NMR contrast agents [47].

2.5.1.3 Microemulsions

In the water-in-oil (W/O) microemulsions, microdroplets of the aqueous phase are trapped in the surfactant. Surfactant molecules are dispersed in an oil phase. Particle nucleation, growth and agglomeration are limited by the small sized microcavities. Small sized magnetic nanoparticles in the range of 4-12 nm are prepared by Pileni and co-workers by using microemulsions [49].

The W/O microemulsions are transparent, isotropic and thermodynamically stable and these are used to produce nanoparticles for both in vivo and in vitro applications since the preparation method is simple [47].

2.5.1.4 Polyols

Especially polyol technique is used for producing the nanoparticles for magnetic resonance imaging. In this technique dissolved metallic salts are reduced and metals are directly precipitated from a polyol solution. In the literature firstly noble metals like Ru, Pd, Pt and Au and other metals like Co, Ni and Cu were prepared by this method. Then Fe based materials are produced by using polyol technique [50,51].

In this process liquid polyol is used as a solvent, reducing agent and sometimes as a complexing agent. Polyol slightly or highly dissolve the metal precursor. For less reducable metals solution is stirred and heated to a boiling point of the polyol. Kinetics of the precipitation should be controlled to produce particles with well defined size and shape. Also by separating the nucleation and growth processes, uniformly shaped particles can be obtained [47].

2.5.1.5 High Temperature Decompositon of Organic Precursors

Magnetic iron oxide nanoparticles with narrow size distribution and good crystallinity can be obtained by the decomposition of iron precursors with the organic surfactants. Magnetic nanoparticles with these properties are potential materials especially for magnetic resonance imaging, magnetic cell separation or magnetorelaxometry applications [47].

Nanocrystals of maghemite obtained by injecting the $FeCup_3$ (Cup: N-nitrosophenylhydroxylamine) solutions into long chain amines at 250-300 °C in the study of Alivisatos and co-workers [52]. The size of these maghemite nanoparticles range between 4-10 nm and they are highly crystalline and dispersible in organic solvents. Hyeon and co-workers used $Fe(CO)_5$ with surfactants and mild oxidants to produce 13 nm sized maghemite nanoparticles [53]. In another work of Sun and Zeng magnetite nanoparticles are produced by using iron(III) acetlyacetonate, phenyl ether, alcohol, oleic acid and oleylamine by a high temperature reaction [54].

2.5.1.6 Sonochemical Assisted Synthesis

Maghemite and magnetite nanoparticles can also be prepared by sonochemical assisted synthesis. Acoustic cavitation generates a localized hot spot in the sonochemistry. Acoustic cavitation means that the formation, growth and collapse of bubbles occur in an irradiated liquid. The temperature of the localized hot spot is 5000 K and its lifetime is in the nanosecond level [47].

Maghemite nanoparticles can also be prepared by electrochemical methods in organic medium. Size distribution is dependent upon the current density [47].

2.5.1.7 Spray and Laser Pyrolysis

Spray and laser pyrolysis methods are considered as promising tecniques for the production of magnetic nanoparticles for in vivo and in vitro applications. Final state of the particles are different in these two techniques. There is an agglomeration of ultra fine particles in the spray pyrolysis. Laser pyrolysis results in less agglomeration due to the shorter reaction time than spray pyrolysis method [47].

In spray pyrolysis solution is sprayed into a series of reactors to obtain solid phase. In these reactors aerosol droplets evaporate and in the droplet solute condensation occurs. At high temperature particles are precipitated after drying and thermolysis steps [47].

Dense particles are obtained from microporous solids after sintering. Produced particles have predictable shape and size of them are predicted from the original droplets. This technique has many advantages over the precipitation from homogeneous solution since it is simple, rapid and continuous. Phosphorescent nanoparticles can also be prepared by this technique [47].

Generally Fe^{3+} salts and organic compounds are used to produce maghemite nanoparticles by this method. Fe^{3+} reduced to mixture of Fe^{2+} and Fe^{3+} with the magnetite formation, then magnetite is oxidized and maghemite particles are obtained. If there is no reducing agent used in the process, the final phase is hematite [47].

Maghemite nanoparticles are also produced between the sizes of 5-60 nm by using alcoholic solutions. The type of iron salts affects the morphologies of the particles obtained. 6 nm sized maghemite nanoparticles are obtained by using Fe(III) nitrate,

on the other hand the size of the nanoparticles increases up to 60 nm by using Fe(III) chloride solution. In addition to these materials acetylacetonate solutions and Fe(II) ammonium citrate can be used to produce maghemite nanoparticles with different sizes [55].

Mixture of gases are heated with a carbon dioxide laser in the laser pyrolysis technique. A critical concentration of nuclei is reached in the reaction zone above a certain laser power and pressure. Then, in the presence of an inert gas particles are transferred to a filter. Small sized nanoparticles with narrow size distribution can be obtained by using laser pyrolysis technique. One of the most important advantages of this technique is extremely low amount of agglomeration of particles [47].

CO_2 laser pyrolysis method can be used to prepare well crystalline maghemite nanoparticles with narrow size distribution [56]. If $Fe(CO)_5$ is used as precursor, ethylene is also used as an absorbent to carry the carbonyl vapour to the reaction zone since this precursor does not absorb the radiation at the 10.6±0.05 μm laser wavelength [47].

2.5.2 Magnetic Composites

Generally superparamagnetic nanocrystals are dispersed in diamagnetic matrixes for in vitro biomedical applications. By using these matrixes functional and biocompatible nanocomposites can be obtained [47]. Uniform and smooth coatings can be prepared via deposition methods by controlling the precursor properties, temperature and pH. Layer by layer self assembly method is an important method to produce superparamagnetic composites. This method can be used for ultrathin films, nanocomposites core-shell materials and hollow capsules [57]. Polyelectrolytes, nanoparticles and proteins are used to coat the colloidal particles by using this method. Dense and hollow spherical superparamagnetic iron oxide nanoparticles are prepared in the Caruso and co workers study [58].

2.5.2.1 Encapsulation of Magnetic Nanoparticles in Polymeric Matrices

Oxidation of particles, toxicity and susceptibility to leaching are prevented by coating the nanoparticles with an organic polymer. This coating also increases the compatibility, chemical stability and dispersibility. Mechanical energy is needed in this method to obtain dispersibility in the production of nanocomposites. Magnetic nanoparticles are dispersed in the aqueous albumin, chitosan or PVA polymers [47].

Superparamagnetic latex is produced by emulsion polymerization. 5 nm sized superparamagnetic iron oxide is produced by using double hydrophilic diblock copolymer. This material controls the nucleation and growth steps and also it provides steric stabilization [47].

2.5.2.2 Encapsulation of Magnetic Nanoparticles in Inorganic Matrices

Usage of inorganic matrices in the production of superparamagnetic nanocrystals is very effective and simple method. The most preferred matrix is silica [47].

Iron ammonium citrate and tetraethoxysilane are used to coat silica on the hollow spherical particles of maghemite via aerosol pyrolysis. In the first stage precipitation occurs by the evaporation of the methanol solvent. Precipitation of the iron salt solid shell is due to the low solubility of the iron ammonium citrate. In the second stage shrinkage of the iron salt solid shell occurs and lastly silica coated hollow spheres are produced by the decomposition of the precursors. Dense maghemite particles are obtained when the salt concentration increases. W/O microemulsion method can also be used for the productionof silica coated iron oxide nanoparticles [47].

2.5.3 Sol- Gel Process

Sol-gel technology has started about 30 years ago with oxide materials. After that time it has been used for non-oxide materials like nitrides, carbides, fluorides and

sulfides, etc. Recently sol-gel processing of organic and inorganic materials are gaining importance for encapsulation of enzymes, antibodies and bacteria in the biotechnology area [59].

Sol-gel term was firstly used for solution processes that formed by initial colloid followed by a gel. Then the term was started to be used for solution processes including hydrolysis and formation of a gel without any colloid formation. Colloidal sol-gel process can be described as following [60];

Precursor material ⟹ Dispersible Oxide ⟹ Sol ⟺ Gel ⟹ Oxide

In the sol-gel technology, first researches were based on dense and bulk materials and many of the researchers have given an importance to how to densify porous gels into glasses and ceramics. Nowadays great attention is being given to the sol-gel processing of mesoporous and macroporous materials with good chemical and photonic properties and controlled pore sizes. Various products can be processed with different shapes in the sol gel area. Powders, fibers, thin films and coatings are the products that can be produced by sol-gel processing. However in the sol-gel film depositon there are still some technical problems and they should be solved to produce these materials practically in the industrial applications. The process parameters should be improved for the coating of plastic materials and self standing thick films which use different deposition techniques like ultrasonic pulverization of aerosols and electrophoretic deposition. Beside the conventional sol- gel methods there are also non hydrolytic sol-gel methods and they have been used to produce unique materials [59].

Metal alkoxides, metal salt solutions and metal complex solutions are dissolved and they are called “solution” precursors in the sol-gel process. Among these generally metal alkoxides are used [61]. Inorganic salts or alkoxides are used as starting materials and hydrous metal oxides or hydroxides are formed by their chemical processing [60]. Most of these materials react with water via hydrolsis and condensation reactions to give amorphous oxides or oxy-hydroxide gels [61].

After gelation of colloidal dispersions by dehydration or pH control, material is calcined to produce stable oxides like SiO_2, Al_2O_3, ZrO_2, TiO_2, etc. Forms of the particles produced vary between polymer chains and highly cross-linked species when there is a change in the conditions under which the precursor material is processed [60].

Sol-gel process has many advantages in the production of ceramics and glasses. It is a low temperature synthesis method and simple equipments are needed. At low temperatures it is difficult to obtain organic molecule doped inorganic materials, therefore sol-gel process is a better choice to produce these materials. In these processes dopants are added to the initial solution, then gelation and drying steps are applied, respectively. Usually methanol, ethanol or water are used to dissolve the dopant materials [59].

Various shapes with large areas can be coated in an inexpensive way by using deposition methods in sol-gel processing. Various shaped products like monoliths, powders, spheres, fibres and thin coatings can be produced by sol-gel process by controlling the viscosity of the sols. Final shape of the product obtained after dehydration, gelation or freezing and after these steps calcining, firing, drying or ultraviolet curing is applied. Besides the advantages, this method has some disadvantages like high cost of alkoxides, high shrinkage amounts during production and sometimes porosity resulting from residual carbon [60].

Sometimes the control of the hydrolysis of the alkoxides in the multi component ceramic production can be difficult. Instead of using metal alkoxides, in most cases it is reported that usage of metal salts is better since their handle is easier than metal alkoxides and they can easily be converted to oxides. Chlorides, acetates, nitrates and sulfides that have high solubility in water and organic solvents can be used as metal salts in the sol-gel process. But among these materials solubility of acetates are lower than that of other materials [59].

In sol-gel processing, purity and homogeneous mixing of precursors, and availability of obtaining different shapes like fibers, thin films, optical elements etc. and low energy consumption due to low temperature processing are the advantages [59].

As reported above, various methods can be used to prepare iron oxide nanoparticles. Among these methods, most widely used technique is the sol-gel process. Different production methods are reported that used in the literature for the production of iron oxide nanoparticles are given in Table 2.1. As seen in the table most researchers preferred the sol-gel method to produce these nanoparticles.

Table 2.1 Production methods of iron oxide nanoparticles.

Production Method	Experimental (Precursors)	Obtained Phase	Magnetic properties	Particle size	Reference
Chemical co-precipitation technique of ferric and ferrous ions in alkali solutions through the pipette drop and piezoelectric nozzle method	$FeCl_2.4H_2O$ and $FeCl_3.6H_2O$, HCl, distilled water	γ- Fe_2O_3	Typical superparamagnetic behavior with T_B of 75 and 120 K for piezoelectric and pipette methods, respectively.	Pipette drop method;5-8 nm Piezoelectric nozzle method;3-5 nm	[62]
Vaporization-Condensation process	α- Fe_2O_3 powders	γ- Fe_2O_3	Strong decrease of the saturation magnetization in the sample (D~15 nm) when compared with that of the bulk material. In sample (D~45 nm) the reduction of the saturation magnetization amounts only around 20 %. Mean T_B ~ 38±15 K	D~15 nm	[63]
Mechanical processing (in particular high energy ball milling)	Metallic iron powder	γ- Fe_2O_3 and Fe_3O_4 (after 12 h), pure γ- Fe_2O_3 (after 48 h), pure γ- Fe_2O_3 (after 72 h)	Transition between a ferromagnetic and paramagnetic behavior is observed around 760 K.	After 12 h; 10-100 nm After 48 h; 15 nm	[64]

Table 2.1 (Continued) Production methods of iron oxide nanoparticles.

Production Method	Experimental (Precursors)	Obtained Phase	Magnetic properties	Particle size	Reference
Sol - gel and mechanical crystallization at room temperature (mechanical activation was conducted in a high energy mill at 900 rpm for 10, 20, 30, 40 h)	TEOS, $Fe(NO_3)_3.9H_2O$ Ethanol	After 10 h; Fe_3O_4 After 30 h; γ-Fe_2O_3 After 40 h; α-Fe_2O_3	For 10 h; saturation magnetization value ~ 3.89 emu/g, for 30 h; ~8.45 emu/g γ- Fe_2O_3 in silica matrix; 62.6 emu/g (theoretical value of bulk γ- Fe_2O_3; 76 emu/g) for 40 h; ~6.22 emu/g (because of γ-α transformation)	Fe_3O_4: 3-4 nm γ- Fe_2O_3: 11 nm γ- Fe_2O_3: 16 nm (after 40 h)	[65]
Novel non-hydrolytic synthetic method	$Fe(CO)_5$, octyleter, oleic acid, ethanol	γ- Fe_2O_3	T_B ~ 25K (4 nm) T_B ~ 185 K (13 nm) T_B ~ 290 K (16 nm)	4-16 nm	[66]
Dispersing in aqueous medium	$FeCl_2.6H_2O$, $FeCl_3.3H_2O$, PVA, water	γ- Fe_2O_3	The saturated magnetization and coercive force show low magnetic values owing to the presence of a nonmagnetic layer	22 nm (without PVA) 10-15 nm (with PVA)	[67]

Table 2.1 (Continued) Production methods of iron oxide nanoparticles.

Production Method	Experimental (Precursors)	Obtained Phase	Magnetic properties	Particle size	Reference
Microwave processing of $Fe(NO_3)_3.nH_2O$ followed by low temperature annealing	High purity $Fe(NO_3)_3.nH_2O$	γ- Fe_2O_3 low-temp. annealing following microwave processing leads to γ- Fe_2O_3 and α- Fe_2O_3	-	5-6 nm	[68]
Microwave-hydrothermal synthesis	$FeSO_4.7H_2O$, $FeCl_3.6H_2O$, NaOH	γ- Fe_2O_3	Superparamagnetic with T_B: 200 K	10 nm	[69]
Microwave assisted synthesis	$FeCl_3$, PEG, $N_2H_4.H_2O$	α- Fe_2O_3, Fe_3O_4	Small hysteresis loop with $M_s(\alpha$- $Fe_2O_3)$:~10 emu/g $M_s(Fe_3O_4)$: ~60 emu/g	4-6 nm (after MW heating ellipsoidal nanocrystals with 50 nm width, 120 nm length)	[70]
Microwave synthesis	$FeCl_3.6H_2O$, $FeSO_4.7H_2O$, ammonia,ethyl alcohol, methyl alcohol, acetone, urea	Fe_3O_4	Superparamagnetic nanoparticle M_s: 70.48 emu/g magnetic fluid M_s: 6.56 emu/g	8-9 nm	[71]
Microwave irradiation	$FeCl_3.6H_2O$, urea	Amorphous Fe_2O_3	Superparamagnetic at room temperature M_S: ~1 emu/g	3-5 nm	[72]

Table 2.1 (Continued) Production methods of iron oxide nanoparticles.

Production Method	Experimental (Precursors)	Obtained Phase	Magnetic properties	Particle size	Reference
Forced precipitation in an organic solvent	Fe(III)chloride 2-propanol	Precipitation in water; γ+α Precipitation from iron nitrate in water; α 2-propanol; γ+α	-	~ 5 nm After 300 °C surface area: γ- Fe_2O_3; 70-120 m^2/g	[73]
Homogeneous precipitation	$FeCl_3.6H_2O$, urea, PEG, sodium dodecyl benzene sulphonate or triethylamine	350 ^0C; α- Fe_2O_3+ γ- Fe_2O_3 650 ^0C; α- Fe_2O_3	-	γ- Fe_2O_3 ; 30 nm diameter, 100-120 nm length, Surface area; 50 m^2/g	[74]
Homogeneous precipitation	Iron(III) sulphate, urea	α- Fe_2O_3	-	40-45 nm (surface area: 148.5 m^2/g)	[75]
Precipitation or co-precipitation	$FeCl_2$, $Fe(NO_3)_3$, $NaNO_3$, NaOH	Fe_3O_4 γ- Fe_2O_3 doesn't form directly in solution by precipitation of ferric ions, but a small proportion of Fe^{+2} induces the crystallization of all the iron to spinel.	γ- Fe_2O_3; positive charge density ~ 0.3 C/m^2 ionic strength $10^{-2}/5.$ 10^{-2} mol/l	1.6-12.5 nm	[76]

Table 2.1 (Continued) Production methods of iron oxide nanoparticles.

Production Method	Experimental (Precursors)	Obtained Phase	Magnetic properties	Particle size	Reference
Colloidal suspensions of the magnetite can be directly oxidized by aeration to γ- Fe_2O_3	$FeCl_2$, $FeCl_3$	Fe_3O_4 γ- Fe_2O_3	-	Fe_3O_4: 8.5±1.3 nm Needle like γ- Fe_2O_3: 20-50 nm in length, 4-6 nm width	[77]
Reverse micelle technique	-	γ- Fe_2O_3	Superparamagnetic blocking temperature; T_B: ~147 K (9 nm) T_B: ~166 K (10 nm) T_B: ~303 K (11 nm)	9 nm (200 °C) 10 nm (250°C) 11 nm (300 °C)	[78]
Sol - gel (Colloidal, inorganic polymeric, complexing sol gel)	$Fe(NO_3)_3.9H_2O$ glycol Y_2O_3	γ- Fe_2O_3 (300 ^{0}C) α- Fe_2O_3 (450 ^{0}C)	-	γ- Fe_2O_3: 10 nm α- Fe_2O_3: 32.6 nm	[79]
Hydrolysis, oxidation and subsequent dehydration of tetrapyridino-ferrous chloride	Tetrapyridino-ferrous chloride	γ- Fe_2O_3 (needle like) XRD; no trace of α- Fe_2O_3	-	5 nm	[80]
Mild oxidation of $Fe(CO)_5$	$Fe(CO)_5$, Oleic acid(surfactant), oxidant	γ- Fe_2O_3	-	~7 nm	[81]

Table 2.1 (Continued) Production methods of iron oxide nanoparticles.

Production Method	Experimental (Precursors)	Obtained Phase	Magnetic properties	Particle size	Reference
Sol - gel	TEOS, $Fe(NO_3)_3.9H_2O$	γ- Fe_2O_3	T_B ~ 54 K (S/V=0.037) T_B ~ 88 K (S/V=0.100) T_B ~ 236 K (S/V=0.300)	6±2 nm (S/V=0.037) 4.5±1.5 nm (S/V=0.100) 2.5 ± 1 nm (S/V=0.300)	[82]
Sol - gel	$FeCl_3.6H_2O$, propylene oxide (PO), TMO, TMOS, TEOS	Fe-Si mixed oxide	-	5-20 nm	[83]
Sol - gel	TEOS, $Fe(NO_3)_3.9H_2O$ Ethanol-ethylene glycol	γ- Fe_2O_3	Superparamagnetic behavior, high values of coercive field	3-6 nm	[12]
Sol - gel	TEOS, $Fe(NO_3)_3.9H_2O$ Ethanol	Above 900 °C; α-Fe_2O_3 appears	Superparamagnetism μ_{eff}: 2.8 (700 °C treated sample) μ_{eff}: 14 (900 °C treated sample)	3-4 nm	[84]
Sol - gel	TEOS, $Fe(NO_3)_3.9H_2O$ Ethanol	Above 900 °C; α-Fe_2O_3 appears At higher temperetures α-SiO_2 At 1100 °C; ε-Fe_2O_3	-	6-25 nm	[85]

Table 2.1 (Continued) Production methods of iron oxide nanoparticles

Production Method	Experimental (Precursors)	Obtained Phase	Magnetic properties	Particle size	Reference
Sol - gel	$FeCl_3.6H_2O$, alcohol, TEOS, dI water, HNO_3	γ- Fe_2O_3	Change from paramagnetic to ferromagnetic resonance observed	5-12 nm	[86]
Sol - gel	$Fe(NO_3)_3.9H_2O$ Ethylene glycol	γ- Fe_2O_3 at 300 °C in O_2 atm; α- Fe_2O_3 at 800 °C in N_2 atm; mixture of magnetite, wustite, metallic iron	-	18 nm	[87]
Sol - gel	TEOS, $Fe(NO_3)_3.9H_2O$ Ethanol	γ- Fe_2O_3	M_s: 0.39-8.04 emu/g	-	[6]
Sol – gel	Ferric chloride, hexahydrate, ferric nitrate nonahydrate, ethanol, TEOS	γ- Fe_2O_3	Superparamagnetic behavior Saturation magnetization at 77 K compared to RT was 67.7% and 42.7% higher	9.42-10.17 nm	[88]

CHAPTER 3

EXPERIMENTAL PROCEDURE

In this thesis preparation of maghemite nanoparticles were carried out by mainly two processing methods. One of them is sol-gel processing, the other is microwave processing. Maghemite nanoparticles are generally prepared by sol-gel method in the literature. Throughout the thesis two different route of sol-gel processing were reported. In the first route TEOS was used as the precursor material, in the second route ethylene glycol and diethylene glycol were used. S/V ratio, iron salt type and heat treatment temperature are important parameters in TEOS route of sol-gel processing. Another part of the study is related with the microwave processing. In this method different microwave powers and durations were employed in order to see their effect on the produced samples.

3.1 Preparation of Maghemite Nanoparticles by Sol-Gel Method

The stabilization of nanometric γ-Fe_2O_3 is usually achieved by dispersing maghemite in a polymeric, glassy or ceramic matrix. Matrix support, which in principle, modifies the properties of nanomaterials, thus opening new possibilities to the control of their performance [89]. The use of an inorganic matrix as a host for nanocrystalline particles can provide an effective way for tailoring a uniform particle size and controlling the homogeneous dispersion of ultrafine metal oxide clusters [84]. The sol-gel derived oxide matrices act as excellent support for the dispersion of metal or metal oxide magnetic particles. Recently, γ-Fe_2O_3 nanoparticles are accommodated in an inert, inorganic, transparent and temperature resistant sol-gel matrix. In this case the process is frequently based on the hydrolysis of the

precursors, such as tetraethoxysilane (TEOS) and subsequent condensation of hydrolysed TEOS in a medium containing a hydroalcoholic solution of the metal salt [90].

In this study, the preparation of γ-Fe_2O_3 nanoparticles through two different sol-gel methods were reported. In the first sol-gel method, iron nitrate ($Fe(NO_3)_3.9H_2O$) and TEOS were used, in the second method, different from conventional sol-gel method, ethylene glycol and diethylene glycol were used as the starting materials.

3.1.1 TEOS Route

For this sol-gel method a series of iron oxide/silica nanocomposites with 0.25 Fe/Si molar ratio were prepared by adding 5 ml of tetraethylorthosilicate (TEOS) to an initial solution which was obtained by dissolving 0.0055 moles of iron nitrate ($Fe(NO_3)_3.9H_2O$) into 15 ml and 22.5 ml of ethanol. The sample contained 25 wt % $Fe_2O_3/(Fe_2O_3+SiO_2)$. The hydrolysis reaction was promoted only by the hydration water of the salt. After stirring for 1 hour, clear sols having approximately a pH value of 1 were obtained. The sols were poured into glass vessels. The surface/volume (S/V) ratio which is calculated by dividing the evaporation surface (the section of the vessel) by the volume of the sol was taken between 0.03 and 0.05. The vessels were closed using a seal with a small punched hole and the sols were allowed to gel in an oven at 50 °C for 15 days. Further, they were kept at 150 °C for 24 h for the elimination of residual water. Finally, the samples were treated at a higher temperature, with steps of 50 °C from 150 °C up to 500 °C, kept for 30 min at each temperature and up to 900 °C with steps of 100 °C, kept for one hour at each temperature. Some of the samples were only heated to 400 °C for 4 h in air to observe the effect of heat treatment temperature on the phases produced in the Fe_2O_3-SiO_2 nanocomposite.

Another series of iron oxide/silica nanocomposites with 0.25 Fe/Si molar ratio were prepared by adding 5 ml of tetraethylorthosilicate (TEOS) to an initial solution which was obtained by dissolving iron chloride ($FeCl_3.6H_2O$) into 15 ml and 20 ml of ethanol to investigate the effect of metal salt on the phases produced in the Fe_2O_3-

SiO_2 nanocomposite. The different experimental conditions of the gelation process for each sample are summarized in Table 3.1.

Table 3.1 Experimental conditions employed for each prepared sample for the TEOS route of sol-gel process.

Precursors	S/V ratio (mm^{-1})	Gelation temperature and time	Thermal treatment
TEOS Ethanol $Fe(NO_3)_3.9H_2O$	0.03 0.04 0.05	50 °C 15 days	400 °C 4 h
TEOS Ethanol $Fe(NO_3)_3.9H_2O$	0.03 0.04 0.05	50 °C 15 days	900 °C 1 h (Stepwise)
TEOS Ethanol $FeCl_3.6H_2O$	0.04	50 °C 15 days	400 °C 4 h

3.1.2 Ethylene Glycol - Diethylene Glycol Route

In this study, iron nitrate ($Fe(NO_3)_3.9H_2O$) and ethylene glycol were used as starting materials. 7 g of $Fe(NO_3)_3.9H_2O$ was dissolved in 27.5 g of ethylene glycol and afterwards heated at 60 °C or 80 °C for 2 h in N_2 gas flow or air under continuous stirring. The gel thus obtained was transferred to a Petri dish and dried in air at 110 °C for 24 h. Samples are heat treated at 300 °C for 2 h in air atmosphere. Also instead of ethylene glycol, some samples were prepared by using diethylene glycol. In order to see the temperature effect, samples were heated at different temperatures between 300 and 750 °C for 2 h in air atmosphere. The different experimental conditions for this ethylene glycol-diethylene glycol route are summarized in Table 3.2.

Table 3.2 Experimental conditions employed for each prepared sample for the ethylene glycol - diethylene glycol route of sol-gel process.

Sample name	**Precursors**	**Stirring temperature, time and atmosphere**	**Heat treatment temperature(°C) and time**
OAE1	Ethylene glycol, Iron nitrate ($Fe(NO_3)_3.9\ H_2O$)	60 °C 2 h, air	300, 2h
OAE2		60 °C 2 h, N_2	
OAE3		80 °C 2 h, N_2	
OAE32H			
OAD300	Diethylene glycol, Iron nitrate ($Fe(NO_3)_3.9\ H_2O$)	80 °C 2 h, N_2	300, 2h
OAD350			350, 2h
OAD400			400, 2h
OAD450			450, 2h
OAD500			500, 2h
OAD700			700, 2h
OAD750			750, 2h

Heat treatment is a critical step for obtaining the desired phase of iron oxide. In this part samples were heat treated in an air atmosphere in the furnace but the critical point is the heat treatment period in the furnace. For example OA3 and OAE32H samples were similar samples, their precursors and stirring conditions were the same, the only difference appears at the heat treatment step. OA3 sample was heat treated in the furnace at 300 °C for 2 h and left in the furnace until the furnace temperature decreases to room temperature. On the other hand similarly prepared OAE32H sample was heat treated in the furnace and after 2h it was removed from the furnace followed by cooling to room temperature. Intensity of the maghemite peaks are

higher for the quickly removed sample than the other one in their respective XRD spectras.

3.2 Microwave Synthesis of Maghemite Nanoparticles

Iron oxide nanoparticles can also be prepared by microwave method [91]. Microwave frequency radiation may be used as an efficient and environmental-friendly alternative to traditional energy sources for solid state synthesis. Microwaves are electromagnetic waves which are characterized by wavelengths in the centimeter range, generated by electronic devices whose power outputs range from microwatts to megawatts. The microwaves can be applied to materials in the form of either continuous or pulsed waves. In the continuous mode of operation, energy is supplied at a constant power level, whereas in the pulsed mode, the microwave energy is turned on and off in a manner at predetermined periods to give a desired average power level [92]. It has long been known that molecules undergo excitation with electromagnetic radiation. The water molecule is the target for domestic microwave ovens; like any other molecule with a dipole, it absorbs microwave radiation. Microwave radiation is converted into heat with high efficiency, so that "superheating" becomes possible at ambient pressure. Microwaves offer several potential advantages over other heating methods:

- Fast heating rates, particularly above the glass transition temperature.
- Minimal thermal lag effects, since the energy is directed at the material and not transmitted through vessels.
- Good thermal control through the use of pulsing techniques.
- Minimized thermal gradients, resulting in more homogeneous cure, smaller thermal stresses, trapped volatiles, and material degradation.
- Floor space for equipment can be less than conventional thermal equipment [92].

In the microwave procedure high purity iron nitrate ($Fe(NO_3)_3.9\ H_2O$) was used as the starting material. Samples were placed in three different crucibles, each was 10 g, and hold in a microwave oven (850 W) for 5, 10, and 15 min. After microwave

processing, samples were annealed in the furnace at 230 °C for 24, 48, and 72 h. In this way 12 samples were prepared. Table 3.3 shows the preparation conditions of these samples.

Table 3.3 The preparation conditions of microwave processed samples at 850 W.

	Microwave durations		
	5 min	**10 min**	**15 min**
As microwave processed	A1	B1	C1
24 h (230 °C)	A2	B2	C2
48 h (230 °C)	A3	B3	C3
72 h (230 °C)	A4	B4	C4

Different samples were also microwave processed at varying powers (630-900 W) for different durations in order to observe the effect of microwave power and duration. The preparation conditions of these samples were presented in Table 3.4.

Table 3.4 The preparation conditions of microwave processed samples at different microwave powers between 630-900 W.

Sample name	**Microwave power(W)**	**Microwave Duration (min)**
Y9005	900	5
Y90010		10
Y90015		15
Y8103	810	3
Y8105		5
Y81010		10
Y81015		15
Y7203	720	3
Y7205		5
Y72010		10
Y72015		15
Y6305	630	5
Y63010		10
Y63015		15

3.3 Preparation of Maghemite Nanoparticles by Modified Microwave System

In the last part of this study the domestic microwave oven was modified and different samples were prepared using this new system. The conventional microwave ovens close itself in a short time because the electronics and magnetron of the microwave system are affected by microwaves reflected from the walls which heat those parts (electronics and magnetron). That is, the air flow supplied by the conventional fan is not enough to cool the necessary parts of the system. Therefore experiments requiring longer time periods can't be performed in such conventional systems.

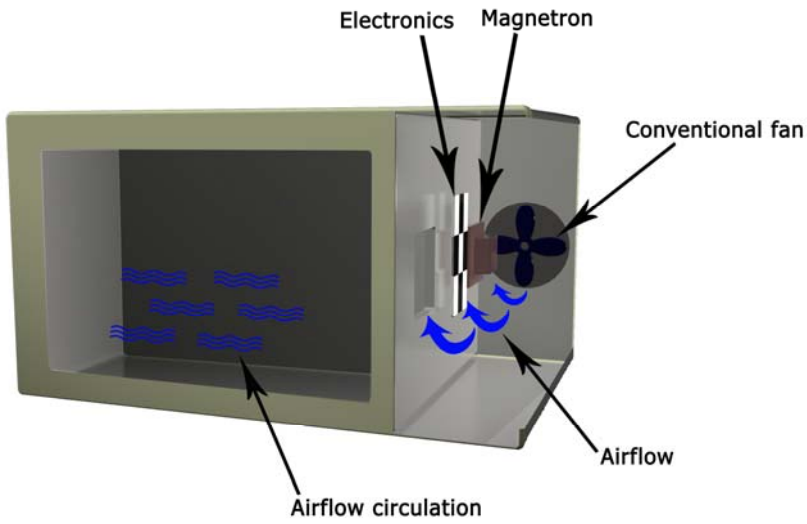

Figure 3.1.a Conventional microwave system.

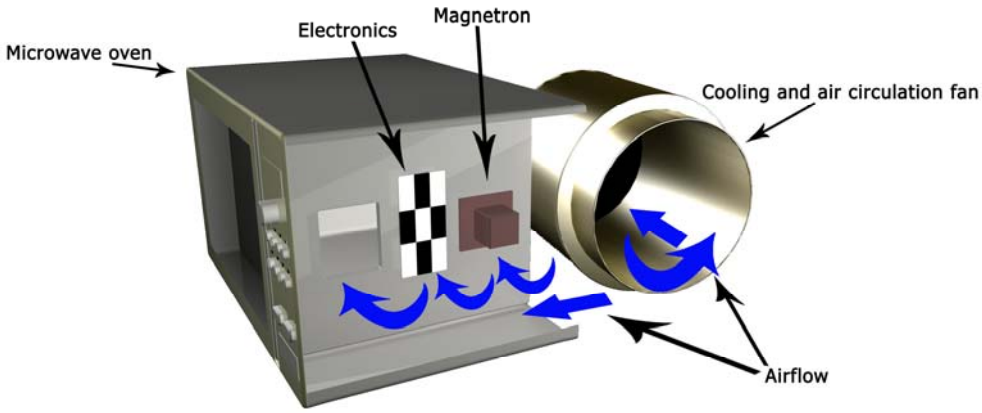

Figure 3.1.b Modified microwave system.

The modified fan system provides the air flow such that the electronics and magnetron can be kept cool during the experiments. Air flow circulation is created inside the oven by flowing air passing through the electronics and magnetron in the cavity of the microwave oven. Table 3.4 shows the preparation conditions of the modified microwave samples.

3.4 Characterization of the Nanoparticles

3.4.1 Structural and Morphological Analysis

3.4.1.1 XRD and SEM Analysis

For the structural analysis of the nanoparticles X-ray diffraction (XRD) analyses were performed using Rigaku D/MAX 2200/PC Diffractometer with monochromatic Cu-K_α radiation (λ = 1.54056 Å) between 2θ values of 10°-90°. The crystal structure of the samples was determined by using Hanawalt's method. Average particle sizes were estimated by using Scherrer's Formula, $t = \frac{0.94 \times \lambda}{B \times \cos\theta}$, which is a technique based on measuring the full width of x-ray diffraction peaks at the half maximum height of the peak. In the formula, t is the average particle size, λ is the wavelength of radiation of the x-ray beam used, B is the width of the peak at the half of the maximum intensity (in

radians) and θ is the half of the diffraction angle 2θ [93]. For maghemite particle size determination, the most intense diffraction peak, (311) was used.

Table 3.5 Preparation conditions of the modified microwave samples.

Sample name	Microwave conditions	Heat treatment in the furnace	Crystallite size (nm)	Phases
OB2	900 W, 20 min	200 °C, 24h	23.8	γ, α
OB3	900 W, 20 min	200 °C, 3h	7.8	γ, α
OB4	900 W, 30 min	No heat treatment	6.8	γ, α
OB6	900 W, 30 min	300 °C, 2h	24.4	γ, α
OB8	900 W, 5 min	400 °C, 2,5h	29.8	γ, α
OB9	900 W, 5 min	350 °C, 2h	19.8	γ, α
OB10	900 W, 40 min	No heat treatment	9.1	γ, α
OB11	810 W, 5 min	No heat treatment	7.9	γ, α
OB12	810 W, 5 min	300 °C, 2h	23.1	γ, α
OB13	900 W, 40 min	300 °C, 2h	12.2	γ, α

Actually, B is the full width of the peak at the half of the maximum intensity (FWHM) after correcting for peak broadening which is caused by the diffractometer. Peak broadening caused by the diffractometer was calculated by the estimation of FWHM value of almost perfect crystalline structure. For this measurement, a crystalline iron sample was used and the calculations showed that the broadening due to the machine is almost negligible. Therefore, in the particle size calculations by Scherrer method, FWHM was considered to be coming from the observed (311) maghemite peaks in XRD spectra.

For the morphological analysis of sol-gel synthesized samples by TEOS route, JEOL JSM-6400 Scanning Electron Microscope (SEM) equipped with an Energy Dispersive

Spectrometer (EDS analyser) was used. The difference in the surface morphology between iron salts, iron nitrate and iron chloride, were reported using these SEM images.

3.4.1.2 TEM Analysis

TEM (Transmission Electron Microscopy) can be used for many different purposes in nanoparticle characterization. It can be used generally for structural characterization and chemical characterization, also the particle size distributions can be studied using TEM. However, one of the disadvantages of TEM instrument is the limited depth of resolution [2]. Another problem about TEM characterization is the difficulty of sample preparation. But sample preparation of maghemite nanoparticles was not as difficult as the sample preparation of other TEM samples.

TEM micrographs and electron diffraction results were obtained by using JEOL JEM 3010 300 kV microscope at Kırıkkale University, JEOL 2100 HRTEM Transmission Electron Microscopy at TUBITAK Marmara Research Center (MAM), and JEOL JEM-2100F Field Emission Transmission Electron Microscopes at Anadolu University and Middle East Technical University-Central Laboratory.

The samples used for TEM observations were prepared by dispersing small amount of the iron oxide nanoparticles in acetone ultrasonically, placing a small droplet of the suspension onto carbon coated copper grids. This method of preparation leads, to some extent, to a separation of the particles according to their size. The type of grids used in this study was holey and lacey type carbon coated copper grids.

3.4.2 BET Surface Area Analysis

Single point and multi point BET surface area analyses were conducted through Quantachrome Corporation, Autosorb-1-C/MS system available at the Central Laboratory of Middle East Technical University. Samples were heated at 200 °C for 2 h during these measurements under N_2 atmosphere.

Gas adsorption is a successful method for particle surface area analysis. It allows us to determine the specific surface area, porosity and pore size distribution. In the adsorption process a vapour is in contact with the solid phase, some part of it is taken up and some part remains on the solid surface. In physical adsorption, there is Van der Waals attraction between the adsorbate and the solid surface, also there is low heat of adsorption. Physical adsorption can involve multiple layers of adsorbate, thus pore size measurement is possible. It is also a reversible process [94].

Usually nitrogen is used as the adsorbate material. Ar, CO_2, CO, O_2 and C_4H_{10} are the other examples of adsorbate materials that used in these analyses. Surface area is the external surface area of a solid object including surface attributable to the pores [94].

BET theory is a rule for the physical adsorption of gas molecules on a solid surface and serves as the basis for an important analysis technique for the measurement of the specific surface area of a material. In 1938, Stephen Brunauer, Paul Hugh Emmett, and Edward Teller published an article about the BET theory in a journal for the first time; "BET" consists of the first initials of their family names [94].

The concept of the theory is an extension of the Langmuir theory, which is a theory for monolayer molecular adsorption, to multilayer adsorption with the following hypotheses: (a) gas molecules physically adsorb on a solid in layers infinitely; (b) there is no interaction between each adsorption layer; and (c) the Langmuir theory can be applied to each layer. The resulting BET equation is expressed by Eq. 3.1:

$$\frac{1}{v((P_0/P)-1} = \frac{1}{v_m C} + \frac{C-1}{v_m C}\left(\frac{P}{P_0}\right) \qquad \text{Eq. 3.1}$$

P and P_0 are the equilibrium and the saturation pressure of adsorbates at the temperature of adsorption, v is the adsorbed gas quantity (for example, in volume

units), and v_m is the monolayer adsorbed gas quantity. c is the BET constant, which is expressed by Eq.3.2:

$$c = \exp\left(\frac{E_1 - E_L}{RT}\right) \qquad \text{Eq. 3.2}$$

E_1 is the heat of adsorption for the first layer, and E_L is that for the second and higher layers and is equal to the heat of liquefaction [94].

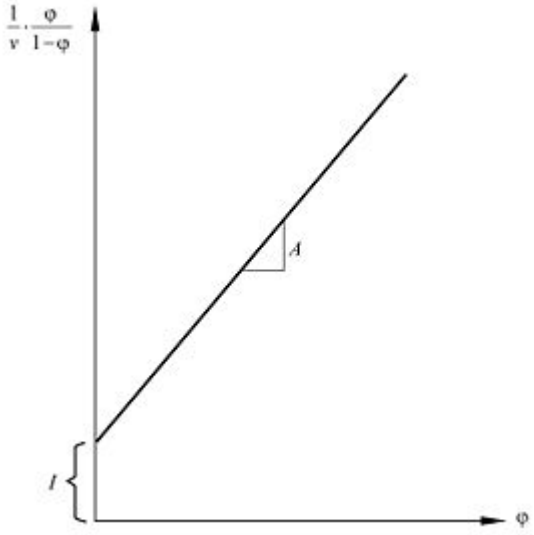

Figure 3.2 BET plot [94].

Equation (1) is an adsorption isotherm and can be plotted as a straight line with $1 / v[(P_0 / P) - 1]$ on the y-axis and $\varphi = P / P_0$ on the x-axis according to experimental results. This plot is called a BET plot. The linear relationship of this equation is maintained only in the range of $0.05 < P / P_0 < 0.35$. The value of the slope A and the y-intercept I of the line are used to calculate the monolayer adsorbed gas quantity v_m and the BET constant c. The following equations (Eq. 3.3 and 3.4) can be used:

$$v_m = \frac{1}{A + I} \qquad \text{Eq. 3.3}$$

$$c = 1 + \frac{A}{I} \qquad \text{Eq. 3.4}$$

The BET method is widely used in surface science for the calculation of surface areas of solids by physical adsorption of gas molecules. A total surface area S_{total} and a specific surface area S are evaluated by the following equations (Eq. 3.5 and 3.6):

$$S_{BET,total} = \frac{(v_m Ns)}{V} \qquad \text{Eq. 3.5}$$

$$S_{BET} = \frac{S_{total}}{a} \qquad \text{Eq. 3.6}$$

N: Avogadro's number

S: adsorption cross section

V: molar volume of adsorbent gas

a: molar mass of adsorbed species

In the BET method there are both single point and multipoint methods. In single point BET specific surface area is determined by using a single on the isotherm. In the multipoint method minimum three points are taken [94].

High surface area values are indicative of samples that contain nanometer sized particles.

3.4.3 Magnetic Characterization

To determine the magnetic properties of the materials generally vibrating sample magnetometer (VSM) is used. Many types of magnetometers have been developed and are now commercially available. They have been extensively reviewed by Foner and can be broadly classified into two categories: (i) Those employing direct techniques, such as measurement of the force experienced by the specimen in a non-

uniform field (Guoy, Faraday, Kahn balances); (ii) Those based on indirect techniques such as measurement of magnetic induction due to relative motion between the sample and the detection coils system (vibrating sample, vibrating coil, SQUIDs) or use of galvanomagnetic effects such as the Hall effect [95,96].

The vibrating sample magnetometer (VSM) developed originally by Foner, has however, been the most successful for low temperature and high magnetic field studies of correlated electron systems due to its simplicity, ruggedness, ease of measurement and reasonably high sensitivity. Also different types of samples can be characterized by this magnetometer [96].

Magnetic properties of powders, thin films and bulk specimens can be measured by this system. Vibrating sample magnetometer can operate at different temperatures in the range of 2 and 1050 K and it uses DC magnetic field [97].

The VSM is based upon Faraday's law according to which an *e.m.f.* is induced in a conductor by a time-varying magnetic flux. In VSM, a sample magnetized by a homogenous magnetic field is vibrated sinusoidally at a small fixed amplitude with respect to stationary pick-up coils [97].

Magnetic measurements at different temperatures from 123 K to 293 K were performed by using ADE Magnetics Model EV9 VSM. Zero-field cooled (ZFC) susceptibilities were measured by cooling samples in zero magnetic field and then by increasing the temperature in an applied field of 100 Oe, while field-cooled (FC) curves were recorded by cooling the samples in an applied field of 100 Oe.

Magnetic measurements of the samples that were produced by microwave synthesis were done by using Lake Shore Model 7407 Vibrating Sample Magnetometer. Hysteresis M–H curves were recorded at different temperatures and to applied fields of 21 kOe (2.1 T). The results were presented in terms of mass magnetization in cgs-units, i.e., emu/g.

CHAPTER 4

RESULTS AND DISCUSSION

Aim of this study was to prepare maghemite (γ-Fe_2O_3) nanoparticles by using different production methods. Among the iron oxide phases maghemite is the least stable one, it tends to transform into hematite (α-Fe_2O_3) at elevated temperatures.

Different production methods are reported that used in the literature for the production of maghemite nanoparticles, but among these sol-gel and microwave methods were used in this study. Maghemite nanoparticles are important for many different areas, especially these nanoparticles are widely used in biomedical applications. Most of the applications require that nanoparticles are superparamagnetic with small particle size and narrow size distribution.

During the study, the process temperature and time were the main experimental parameters. Since maghemite phase is not stable at higher temperatures, experiments were carried out at lower temperatures to obtain the desired phase. In the conventional sol-gel route, the effect of the iron salt used for the production of these nanoparticles were investigated.

In the microwave procedure, microwave power is the important parameter to obtain the desired phase. Generally hematite phase appears together with the maghemite phase at high microwave powers and extended durations. Since it is considered that the microwave power is not homogeneous in the oven, microwave system was modified and some experiments were carried out with the modified microwave system.

The nanoparticles were characterized by X-Ray Diffraction (XRD), scanning electron microscopy (SEM), transmission electron microscopy (TEM), surface area analysis (BET), and vibrating sample magnetometry (VSM).

4.1 TEOS Route of Sol-Gel Processing

4.1.1 Structural Characterization (XRD)

X-ray diffraction patterns for the nanocomposites obtained by heating the initial gels from nitrate salts at 400 °C and 900 °C are shown in Figures 4.1 and 4.2. Together with the broad peaks corresponding to amorphous SiO_2 (2θ = 23-27°), the peaks of the diffractograms obtained by heat treating the gels at 400 °C can be identified mainly as γ-Fe_2O_3 (maghemite) crystalline phase. The broad peaks are characteristic of small particles with a mean crystallite size, estimated from the (311) reflection, of 12 to 15 nm. There are some small peaks corresponding to α-Fe_2O_3 (hematite) on the same XRD spectra. However, the diffractograms obtained by heat treating the gels at 900 °C can be identified as consisting of α-Fe_2O_3 (hematite) antiferromagnetic crystalline phase and iron silicate (fayalite) peaks. The mean crystallite size calculated is about 23 nm. The broadening of the peaks near the base line suggests that a significant fraction of the samples consists of smaller particles. In the case of samples obtained from nitrate salts, temperatures higher than 400 °C give rise to the transformation of maghemite into hematite and fayalite due to a reaction with the matrix.

X-ray diffraction patterns for the nanocomposites obtained when $FeCl_3.6H_2O$ is used as a precursor, the iron oxide obtained is α-Fe_2O_3 (hematite). These differences in the resulting iron oxide phases could originate partially during the hydrolysis of the iron salts inside the silica pores. It is well-known that the composition and structure of iron (III) (hydrous) oxide formed in water depend on the preparation conditions such as Fe^{+3} concentration, the nature of the anion present and pH [98]. Hydrolysis of the iron salt proceeds by the formation of monomers and dimers of iron (III) ions, followed by the condensation of polymeric species. The polymers formed in the case

of nitrates are presumed not to include the nitrate ion in the polymer chain, whereas the polymers formed in the chloride solution contain some chloride ions in place of the hydroxyl ions [99]. The next step in the precipitation process is the formation of oxybridges. In the presence of chloride ions, β-FeOOH is produced initially which later converts to α-Fe_2O_3 by heating [100]. From nitrate solutions, γ-FeOOH can be precipitated which directly transforms by heating to γ-Fe_2O_3 [101]. Therefore, γ-Fe_2O_3 nanocomposites should be preferentially formed through the reduction-oxidation of initially precipitated iron oxide-hydroxide polymeric material. However, it is clear that the nature of our nanocomposites formed in an organic medium (ethanol) depends on the type of the salt precursor [98]. Therefore, only nitrate salts were used as the starting material in this study. X-ray diffraction patterns given in Figures 4.1 and 4.2 were obtained for different S/V ratios ranging between 0.03 to 0.05 prepared from nitrate salts. Apart from the typical broad halo due to amorphous silica always present, for the samples gelated with lower S/V ratio, the X-ray patterns show well defined peaks. As the S/V ratio increases, it can be observed that peaks progressively broaden and the peak intensities start to decrease (Figure 4.1). From these results it can be concluded that the evaporation process during gelation plays an important role in the crystallization of the γ-Fe_2O_3 particles. The higher evaporation rate seems to be decisive for obtaining samples with smaller particle sizes (15 nm when S/V ratio is 0.03 compared to 12 nm when S/V ratio is 0.05). By changing the S/V ratio it is possible to control the gelation process, in such a way that higher S/V ratio leads to smaller pore size of the matrix. The matrix structure is an important factor affecting the particle size of the nanocomposites [102].

A schematic diagram of the proposed mechanism for the formation of γ-Fe_2O_3 (maghemite) nanoparticles in the silica matrix is presented in Figure 4.3. TEOS is hydrolyzed by the hydration water of the iron salt and condenses at temperatures lower than 80 °C, giving rise to the initial gel. The pore of the gel constitutes the

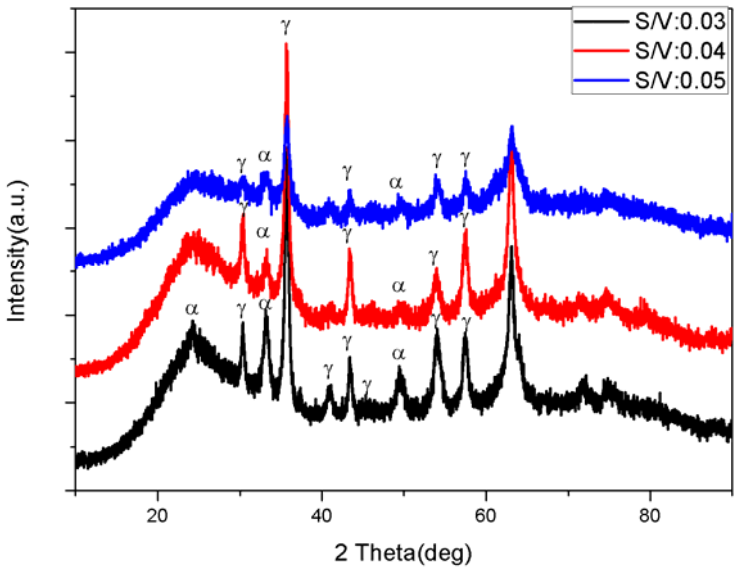

Figure 4.1 X-ray diffraction patterns of iron oxide nanocomposites heated at 400 °C with different S/V ratios and prepared from nitrate salts.

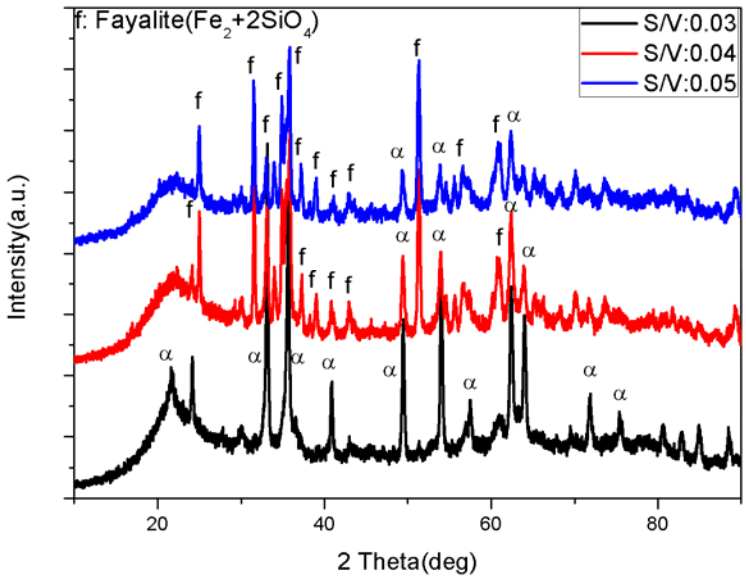

Figure 4.2 X-ray diffraction patterns of iron oxide nanocomposites heated at 900 °C with different S/V ratios and prepared from nitrate salts.

ideal environment for the nucleation of some iron oxide-hydroxide polymers which show magnetic behavior. Later heat treatment up to 400 °C promotes the formation and growth of γ-Fe_2O_3 nanoparticles on the preformed nuclei. The size of the final particle depends on the preparation conditions such as the concentration of the iron salt, the treatment temperature and the S/V ratio.

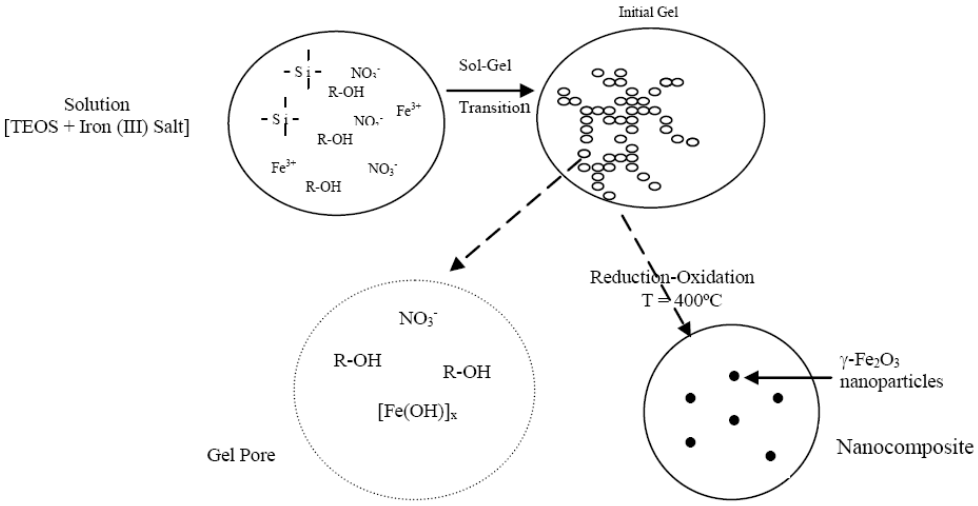

Figure 4.3 Schematic diagram of the mechanism of formation of γ-Fe_2O_3 nanoparticles in the silica matrix.

4.1.2 Magnetic Characterization (VSM)

The hysteresis loops of the samples heat treated at different temperatures for different S/V ratios are shown in Figures 4.4 to 4.6. The saturation magnetization values at 10 K increase up to a maximum of 6 emu/g obtained for the sample heat treated at 400 °C for S/V ratio equal to 0.03 (Figure 4.1). Larger S/V ratios such as 0.04 lead to an increase in the apparent saturation magnetization of the composite (heat treated at same temperature) to the value of 12 emu/g. The saturation magnetization values are, in all cases, far from the reported value for bulk γ-Fe_2O_3 (74 emu/g), but these values are in fairly good agreement with the values measured in γ-Fe_2O_3 particles of similar size [63,103,104]. Surface and finite size effects have been reported as being responsible for the decrease in the magnetic properties of

nanoparticles [103]. Also, the nanocomposites heat treated at 400 ^{0}C contain small amount of antiferromagnetic α-Fe_2O_3 (hematite) as indicated in the XRD spectra given in Figure 4.1. The samples were not composed of entirely γ-Fe_2O_3 (maghemite) crystalline phase.

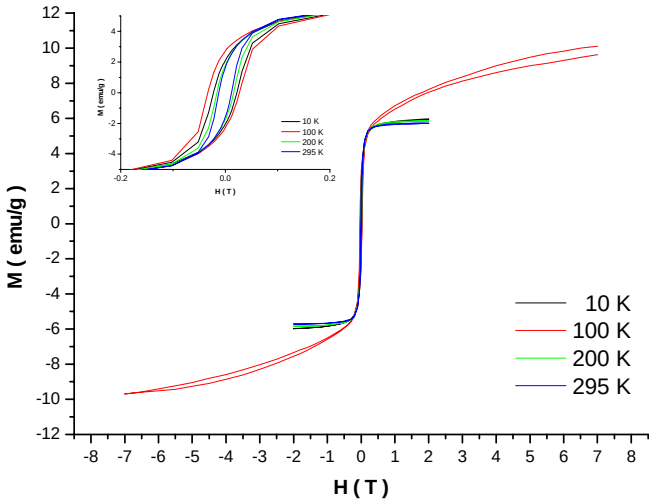

Figure 4.4 Hysteresis loops (M-H curves) of nanocomposites heat treated at 400 °C for the S/V ratio of 0.03. The curves were recorded at the temperatures between 10 and 295 K.

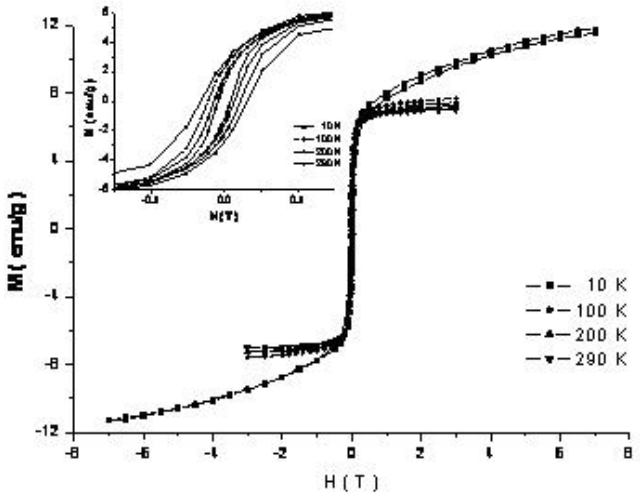

Figure 4.5 Hysteresis loops (M-H curves) of nanocomposites heat treated at 400 °C for the S/V ratio of 0.04. The curves were recorded at the temperatures between 10 and 290 K.

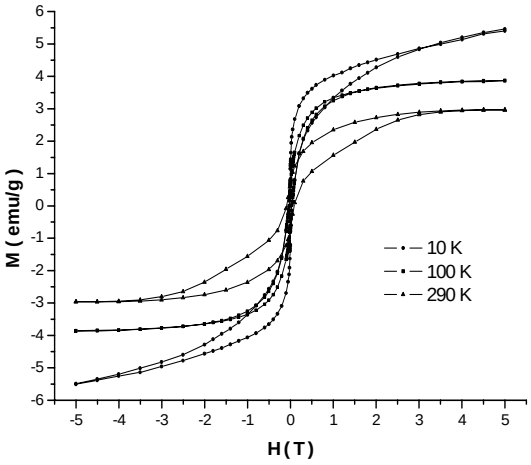

Figure 4.6 Hysteresis loops (M-H curves) of nanocomposites heat treated at 900 °C for the S/V ratio of 0.03. The curves were recorded at the temperatures between 10 and 290 K.

As shown in the Figure 4.6, nanocomposites prepared from nitrate salts at a temperature of 900 °C show a decrease in the saturation magnetization value to 4 emu/g where S/V ratio is 0.03. The same value is recorded to be 11 emu/g for the same sample prepared at 400 °C. This decrease is mainly due to the presence of the nonmagnetic iron oxide phases of hematite and fayalite appeared at 900 °C as can be seen from XRD spectra of Figure 4.2.

4.1.3 Morphological Characterization (SEM)

Figure 4.7 and 4.8 are the SEM images of sol-gel samples which were produced from nitrate salts and chloride salts, respectively. From these figures it can be concluded that nitrate sample has smoother surface than chloride sample. This different behavior is a result of using different starting gels for the production of nanocomposites. The gel obtained from iron nitrate salt shows a compact appearance as a result of its higher degree of network connectivity (polymeric gel) whereas the one from the iron chloride appears more loose and highly hygroscopic (colloidal gel). In addition, there is small superparamagnetic nuclei formation during the hydrolysis and condensation of the gel through the use of iron nitrate salt. Maghemite

nanoparticle formation takes place through a reduction-oxidation reaction which occurs during the burning of the organic species trapped inside the gel pore [90].

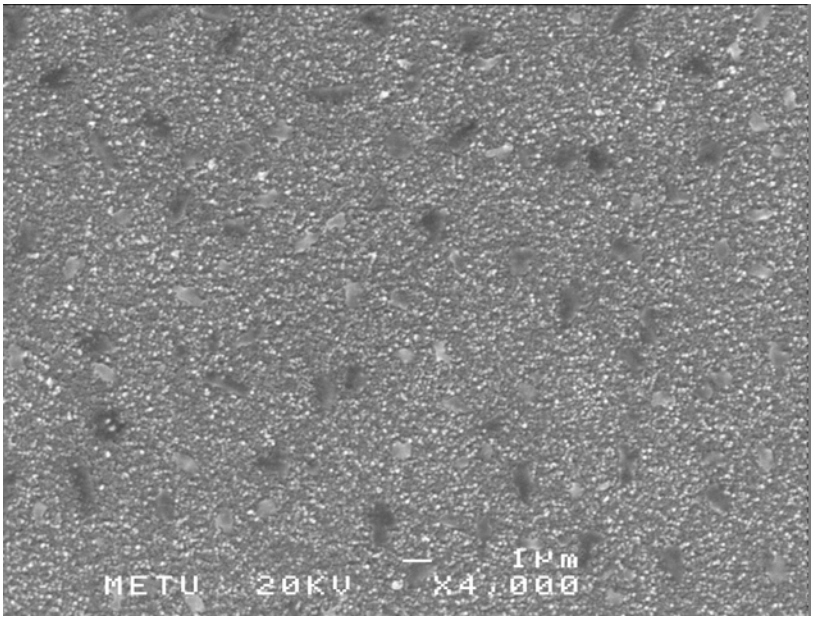

Figure 4.7 SEM image of S/V = 0.04 sample heat treated at 400 °C and prepared from nitrate salts.

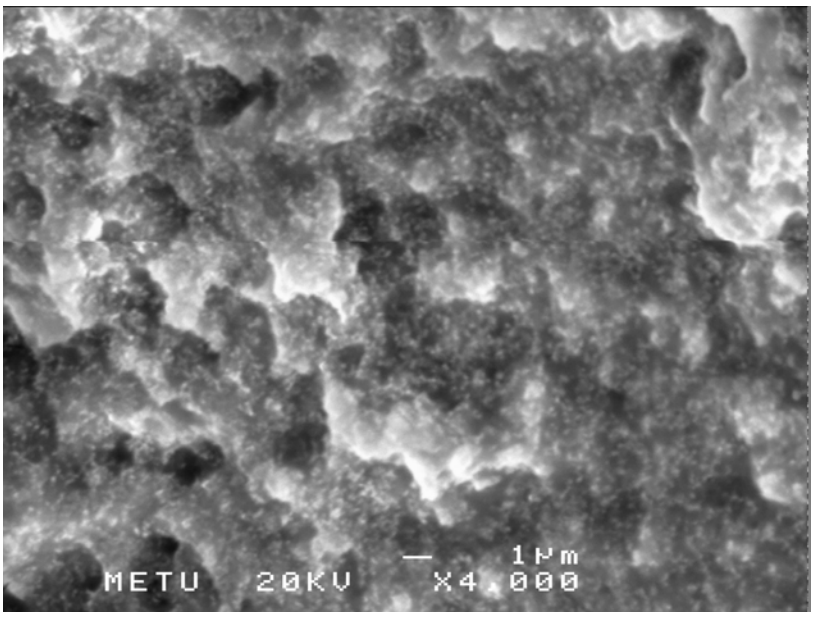

Figure 4.8 SEM image of S/V = 0.04 sample heat treated at 400 °C and prepared from chloride salts.

Table 4.1 summarizes the results of the samples which were prepared by TEOS route of sol-gel processing.

Table 4.1 Results of the samples which were prepared by TEOS route of sol-gel processing.

Sample	Conditions	Crystallite size (nm) (Scherrer Method)	Phases	VSM Saturation magnetization
3A S/V:0.03	400 °C, Nitrate	15.0	α, γ	6 emu/g (10 K) 11 emu/g (100 K)
4A S/V:0.04		12.7	α, γ	12 emu/g (10 K)
5A S/V:0.05		12.0	α, γ	-
3 S/V:0.03	900 °C, Nitrate	23.3	α, Fayalite	4 emu/g (100 K)
4 S/V:0.04		23.4	α, Fayalite	-
5 S/V:0.05		23.4	α, Fayalite	-

4.2. Ethylene Glycol - Diethylene Glycol Route of Sol-Gel Processing

4.2.1 Structural Characterization (XRD)

Figures 4.9 and 4.10 are the XRD patterns of samples which were produced by ethylene glycol - diethylene glycol route of sol-gel method at different temperatures. From the XRD studies it can be concluded that some of the samples have higher amount of maghemite phase on their diffraction patterns, while the others have

higher amount of hematite phase. By using Scherrer equation, approximate particle sizes were calculated for these samples and they are between 4 and 48 nm. Firstly ethylene glycol ($C_2H_6O_2$) was used as the precursor to obtain maghemite nanoparticles. Ethylene glycol based sol-gel synthesis is different from conventional sol-gel synthesis. The formation of sol in ethylene glycol system do not rely on hydrolysis and condensation reactions, but on the formation of chain or network large molecules from complexation of ethylene glycol [105]. Then following experiments were conducted with diethylene glycol ($C_4H_{10}O_3$) precursor. It is considered that diethylene glycol could give smaller particle size of maghemite nanoparticles due to being larger molecule. Table 4.2 shows the calculated particle sizes of the samples. As seen in the Table 4.2, OAE32H sample and OAD300 sample were heat treated at the same temperature and the size of the diethylene glycol sample (OAE32H) is smaller than that of the diethylene glycol sample (OAD300).

Table 4.2 Approximate crystallite sizes for the samples which were produced by ethylene glycol - diethylene glycol route of sol-gel method.
(E: Ethylene glycol, D: Diethylene glycol)

Sample name	**Heat treatment temperature (°C)**	**Phases**	**Particle size (nm) (Scherrer Method)**
OAE1	300	α, γ	16.0
OAE2	300	α, γ	7.8
OAE3	300	α, γ	8.4
OAE32H	300	α, γ	8.4
OAD300	300	α, γ	4.0
OAD350	350	α, γ	8.0
OAD400	400	α, γ	12.1
OAD450	450	α, γ	24.2
OAD500	500	α	24.2
OAD700	700	α	48.5
OAD750	750	α	34.6

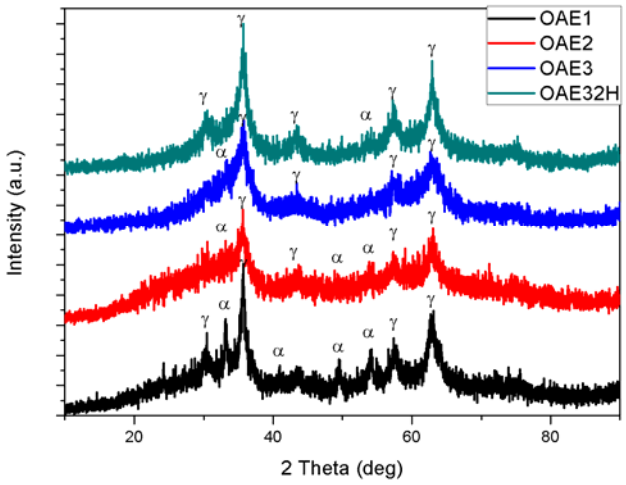

Figure 4.9 XRD patterns of samples which were produced by ethylene glycol route of sol gel method and heat treated at 300 °C.

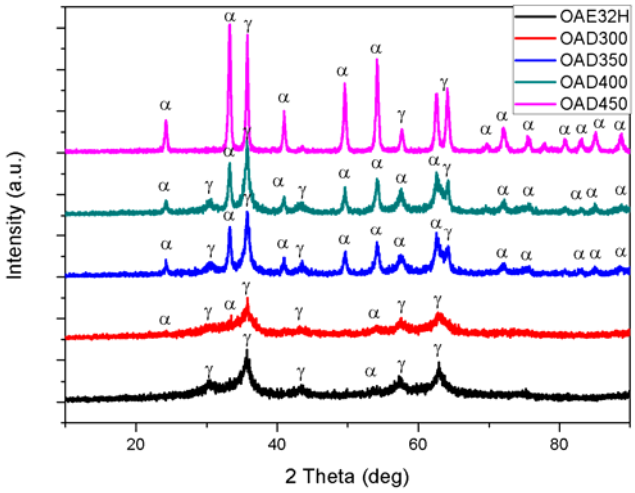

Figure 4.10 XRD patterns of samples which were produced by ethylene glycol - diethylene glycol route of sol gel method and heat treated at different temperatures between 300 and 450 °C.

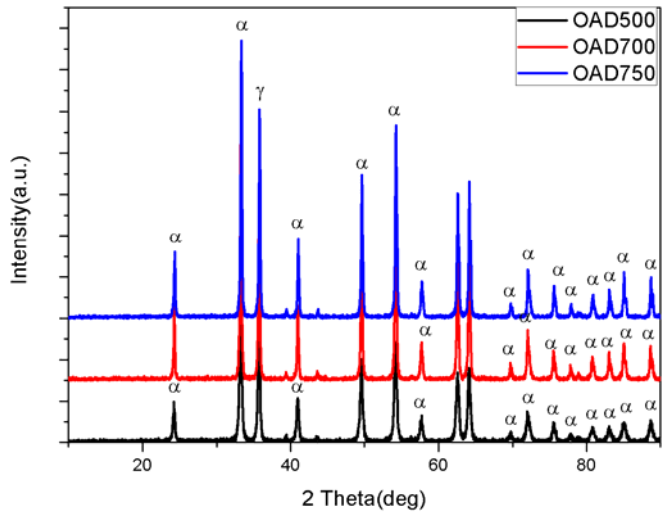

Figure 4.11 XRD patterns of samples which were produced by diethylene glycol route of sol gel method and heat treated at different temperatures between 500 and 750 °C.

Figure 4.9 shows the XRD patterns of samples that were heat treated at 300 °C by using ethylene glycol as the precursor. The differences in the preparation conditions of these samples were given in detail in Table 3.2 in Chapter 3. Among these samples OAE32H sample has more maghemite phase with a higher intensity than the other samples, so further studies are based on this sample.

XRD patterns which belong to Figure 4.10 show that all samples contain both maghemite and hematite phases. But OAE32H and OAD300 samples that were heat treated at 300 °C contain more maghemite phase than the other samples. As the heat treatment temperature increases, the intensity of hematite peaks also inreases. Also approximate particle sizes, obtained from the Scherrer equation, increase when the samples heated at higher temperatures. Same condition also holds for Figure 4.11, as the temperature increases from 500 to 750 °C, calculated particle sizes of the samples increase.

Since XRD patterns of these samples contain both maghemite and hematite phases, a quantitative analysis was made to obtain the amounts of different phases in the samples.

Quantitative analysis by diffraction is based on the fact that the intensity of the diffraction pattern of a particular phase in a mixture of phases depends on the concentration of that phase in the mixture. The relation between intensity and concentration is not generally linear, since the diffracted intensity depends markedly on the absorption coefficient of the mixture and this itself varies with the concentrations as given in Equation 4.1 [106] :

$$\frac{I_\alpha}{I_\gamma} = \frac{w_\alpha(\mu_\alpha / \rho_\alpha)}{w_\alpha(\mu_\alpha / \rho_\alpha - \mu_\gamma / \rho_\gamma) + \mu_\gamma / \rho_\gamma} \qquad \text{Eq. 4.1}$$

This equation permits quantitative analysis of a two phase mixture, provided that the mass absorption coefficients of each phase are known. When the mass absorption coefficients of the two phases are equal, Eq. 4.1 becomes simply

$$\frac{I_\alpha}{I_{\alpha p}} = w_\alpha \qquad \text{Eq. 4.2}$$

where I is the intensity of the γ and α phases, μ is the mass absorption coefficient, ρ is the density and finally w is the weight percentages of the phases. The subscript p denotes diffraction from the pure phases.

The mass absorption coefficients of γ- and α- Fe_2O_3 phases are the same, thus the ratio of relative intensities allows directly a quantification. However, the most intense peak of maghemite (311) [JSPDS No: 39-1346] is unfortunately overlapped by the (110) hematite [JSPDS No: 33-0664] peak. In order to avoid overlapping problems, hematite (104) peak (relative intensity: 100) and maghemite (220) peak (relative intensity: 35) were used for the quantitative measurements [107].

In this study these calculations were made according to Equation 4.2 and results are presented in Table 4.3.

Table 4.3 Weight percentages of the samples produced by ethylene glycol - diethylene glycol route of sol-gel method. (E: Ethylene glycol, D: Diethylene glycol)

Sample name	Maghemite (wt%)	Hematite (wt%)
OAE32H	80.0	20.0
OAD300	77.5	22.5
OAD350	30.0	70.0
OAD400	28.7	71.3

4.2.2 Morphological Characterization (TEM)

The shape of the magnetization curves for powder samples are strongly dependent on the sample particle size distribution. Finding the correct distribution is therefore necessary to help the interpretation of the magnetic behavior of these nanoparticles. TEM study was conducted to observe this distribution for some of the ethylene glycol - diethylene glycol route of sol-gel samples in this study. Figures 4.12-4.22 are the TEM images and their size distributions of these samples that were produced by ethylene glycol- diethylene glycol route. Approximate particle sizes were calculated from TEM images of these samples and these results are given in Table 4.4. As shown in the table, particle size measurement results of the two methods, XRD and TEM, are almost consistent with each other. In the case of nanoparticles, the average particle size measured by XRD is smaller than those measured by TEM. A number of well defined atomic planes are necessary for coherent diffraction in XRD. However, the atoms at the nanoparticle surfaces are not regularly arranged and they do not diffract coherently. Therefore, the measured particle size is smaller than the real size when measuring nanoparticles with XRD.

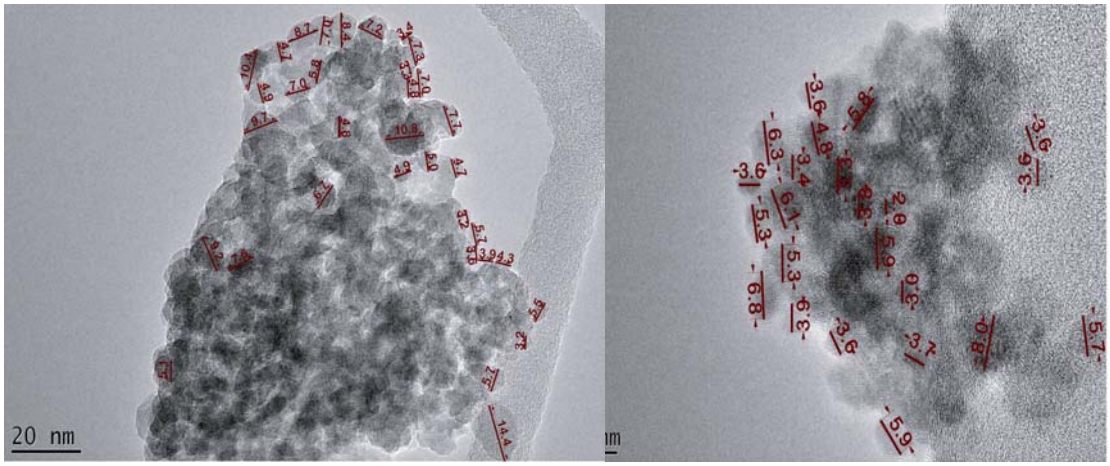

Figure 4.12 TEM micrographs of the sample which was produced by sol-gel method (diethylene glycol) and heat treated at 300 °C. The numbers on the TEM images indicate the particle sizes measured using these images.

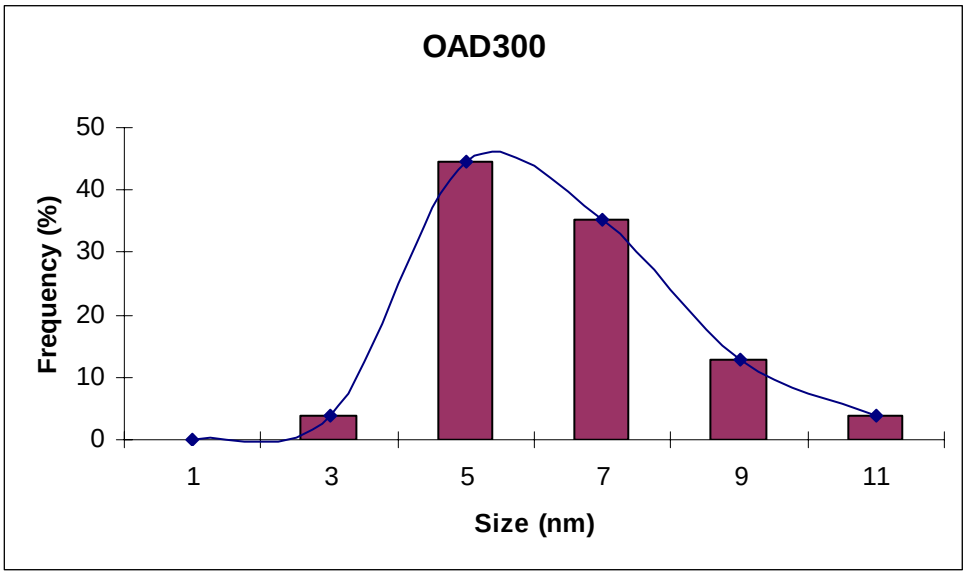

Figure 4.13 Particle size distribution of the sample of Figure 4.12 which was produced by sol-gel method (diethylene glycol) and heat treated at 300 °C.

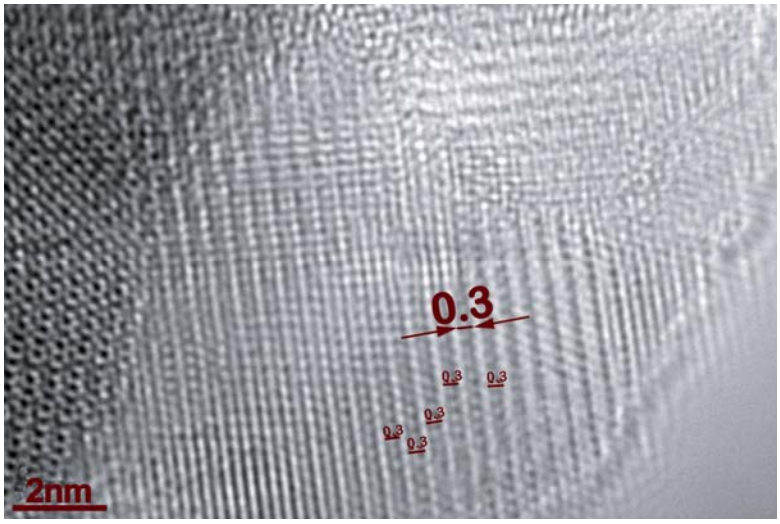

Figure 4.14 HRTEM micrograph of the sample which was produced by sol-gel method (diethylene glycol) and heat treated at 300 °C.

From the HRTEM image of the sample produced by diethylene glycol and heat treated at 300 °C, it can be concluded that the sample has high crystallinity (Figure 4.14). Interplanar spacing (d) value of this sample was also measured as 3.0 nm from the image and it was seen that this result is similar with the d value of the (220) plane as shown in the Table 4.5.

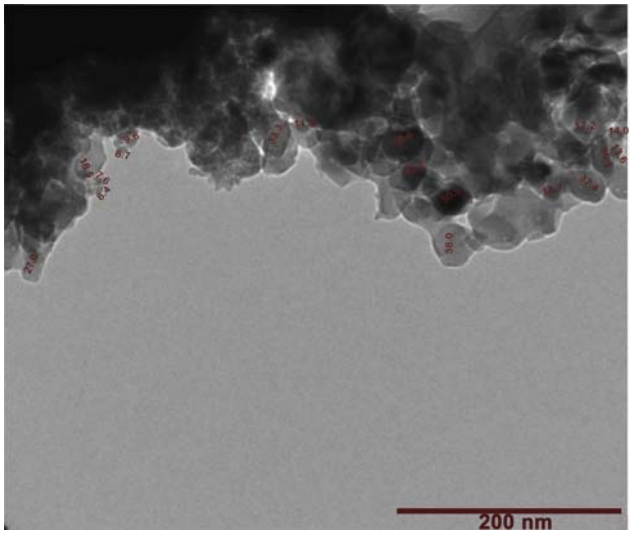

Figure 4.15 TEM micrograph of the sample which was produced by sol-gel method (diethylene glycol) and heat treated at 350 °C.

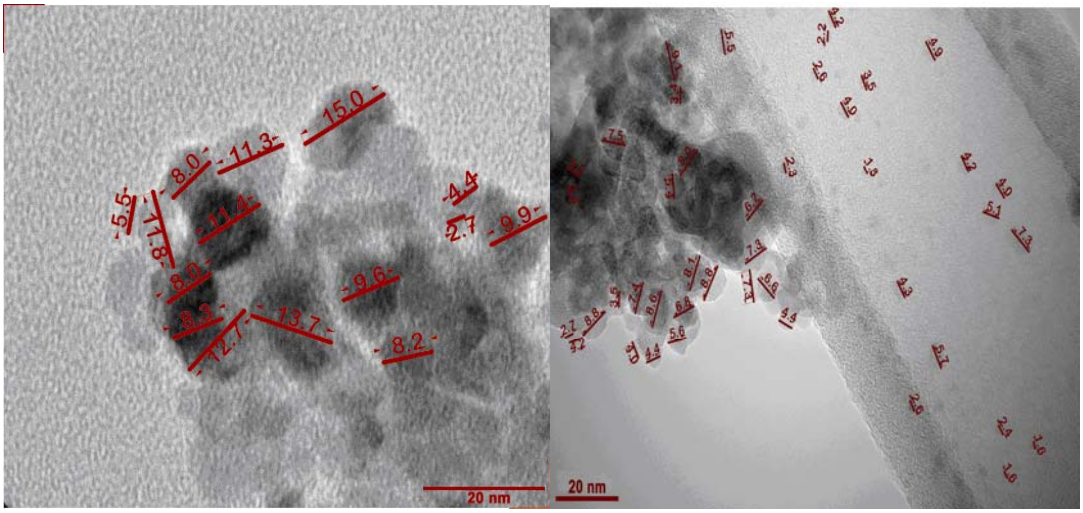

Figure 4.16 TEM micrographs of the sample which was produced by sol-gel method (diethylene glycol) and heat treated at 350 °C. The numbers on the TEM images indicate the particle sizes measured using these images.

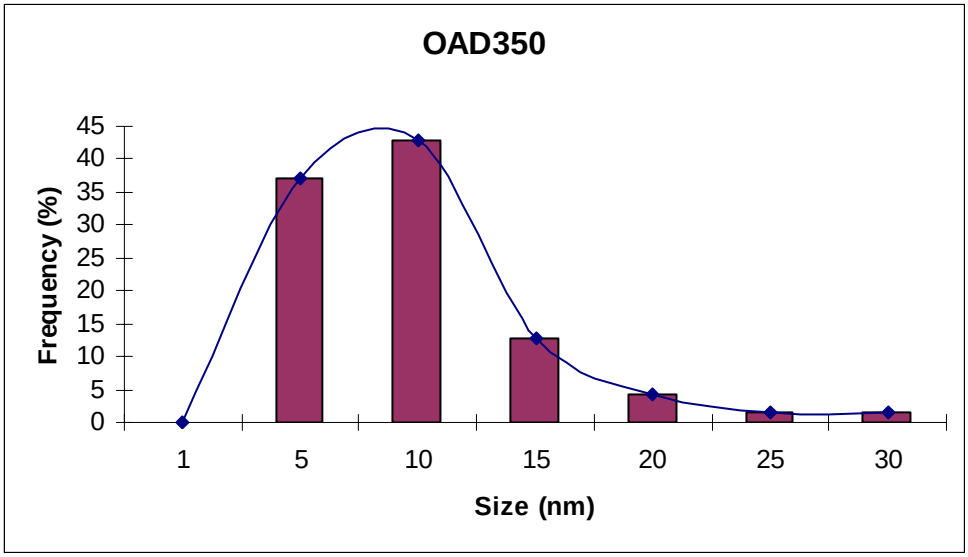

Figure 4.17 Particle size distribution of the sample of Figure 4.16 which was produced by sol-gel method (diethylene glycol) and heat treated at 350 °C.

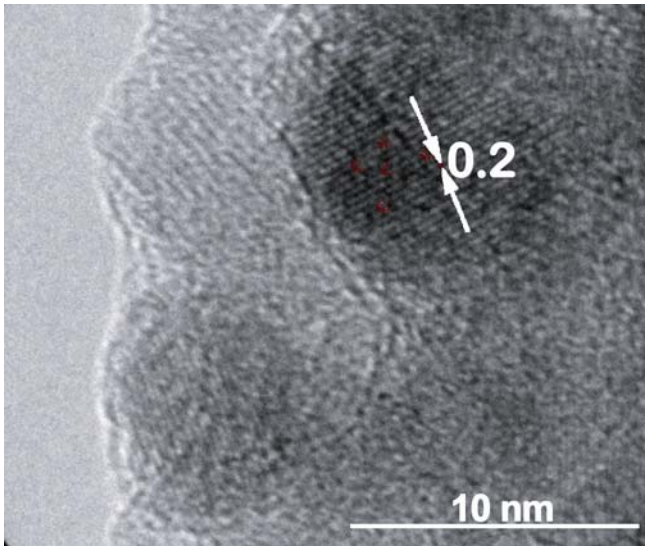

Figure 4.18 HRTEM micrograph of the sample which was produced by sol-gel method (diethylene glycol) and heat treated at 350 °C.

Interplanar spacing (d) value of the sample produced by using diethylene glycol and heat treated at 350 °C was also measured (Figure 4.18) and the result is consistent with the d value of the (321) plane of the maghemite phase (Table 4.5).

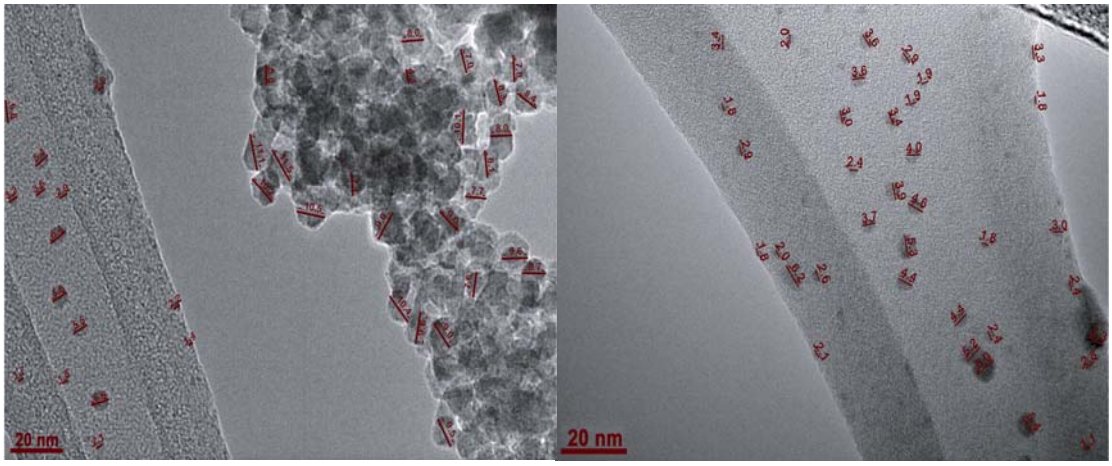

Figure 4.19 TEM micrographs of the sample which was produced by sol-gel method (diethylene glycol) and heat treated at 400 °C. The numbers on the TEM images indicate the particle sizes measured using these images.

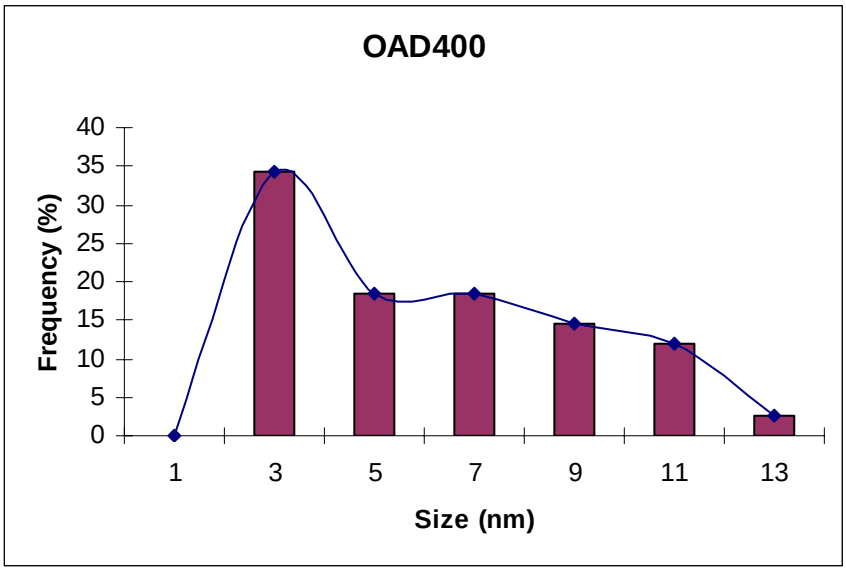

Figure 4.20 Particle size distribution of the sample of Figure 4.19 which was produced by sol-gel method (diethylene glycol) and heat treated at 400 °C.

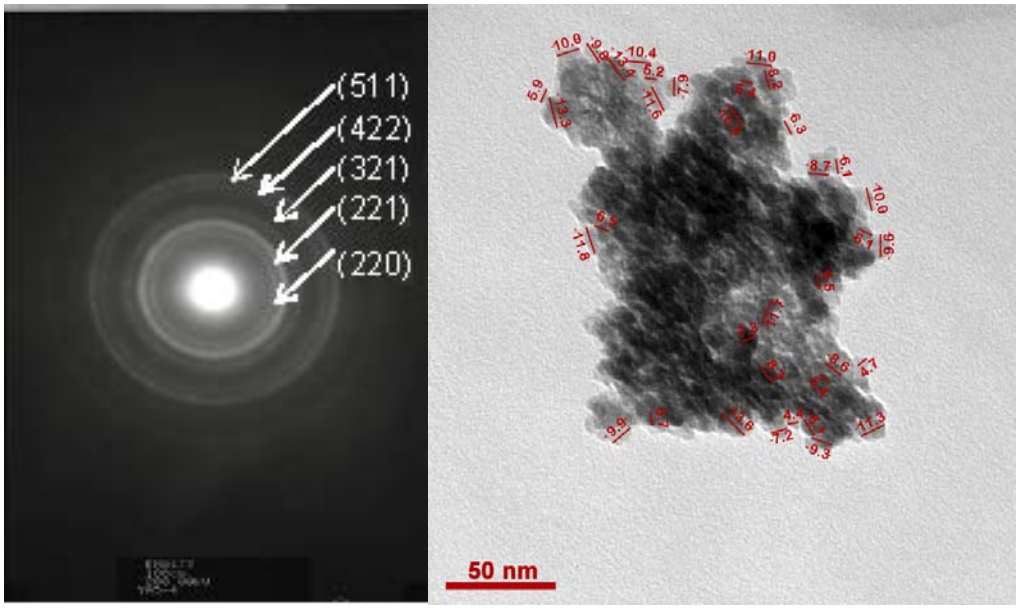

Figure 4.21 TEM micrograph and diffraction pattern of the sample which was produced by sol-gel method (ethylene glycol) and heat treated at 300 °C. The numbers on the TEM images indicate the particle sizes measured using these images.

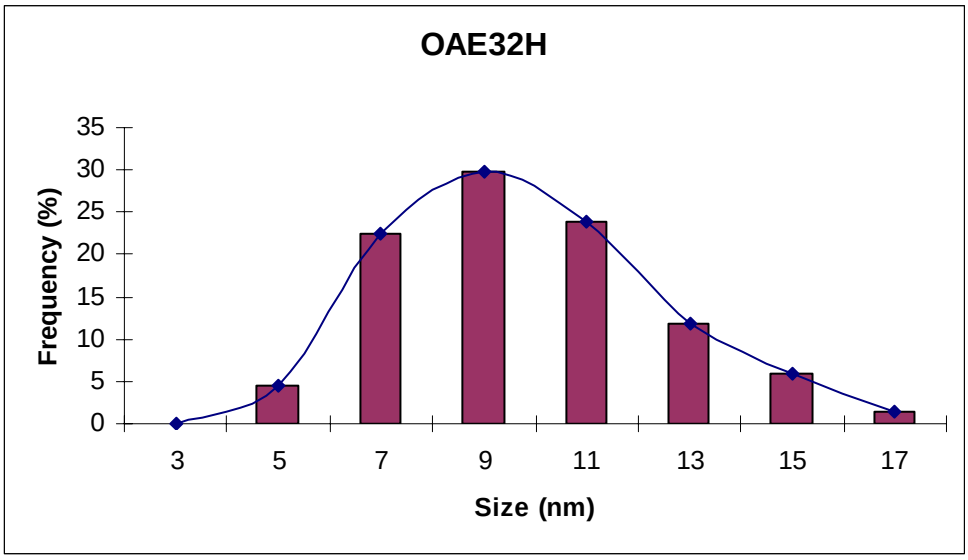

Figure 4.22 Particle size distribution of the sample of Figure 4.21 which was produced by sol-gel method (ethylene glycol) and heat treated at 300 °C.

As given in the table 4.4 and shown in the figures 4.12-4.22, the particle sizes are generally below 10 nm, although there are some particles greater than 10 nm and having larger particle sizes. However, all TEM images indicate that these particles are spherical and these particles show 3-dimensional assemblies demonstrating the uniformity of the nanoparticles. Electron diffraction, X-ray diffraction, and high resolution transmission electron microscope (HRTEM) images of the nanoparticles showed the highly crystalline nature of the γ-Fe_2O_3 structures.

By using the radii in the diffraction pattern of Figure 4.21, the interplanar spacings of the samples were calculated from equation 4.3 [11] where L is the camera length, R is the measured radius from the diffraction pattern, λ is the wavelength and d is the interplanar spacing. λ is 0.019 Å for the 300 kV microscope.

$$\frac{R}{L} = \frac{\lambda}{d} \qquad \text{Eq. 4.3}$$

From the electron diffraction study, it is observed that interplanar spacing (d) values of the ethylene glycol sample matched with the maghemite phase.

Table 4.4 Approximate crystallite sizes for the samples by XRD and TEM method, which were produced by ethylene glycol - diethylene glycol route of sol-gel method. (E: Ethylene glycol, D: Diethylene glycol)

Sample name and heat treatment temperature (°C)	**Particle size (nm) (Scherrer Method)**	**Particle size (nm) (TEM Method)**
OAE32H, 300	8.4	8.75 ± 0.35 7-9 nm ~ 29.85 % 9-13 nm ~ 35.82 % (Figure 4.19)
OAD300, 300	4.0	5.35 ± 0.27 1-5 nm ~ 48.14 % 5-7 nm ~ 35.18 % 7-11 nm ~ 16.66 % (Figure 4.12)
OAD350, 350	8.0	7.64 ± 1.46 1-5 nm ~ 37.14 % 5-10 nm ~ 42.85 % 10-15 nm ~ 12.85 % (Figure 4.15)
OAD400, 400	12.1	5.15 ± 0.76 1-3 nm ~ 34.21 % 3-7 nm ~ 36.84 % 7-13 nm ~ 28.94 % (Figure 4.17)

Table 4.5 Electron diffraction (ED) results for the maghemite nanoparticles obtained for the sample which was produced by sol-gel method (ethylene glycol) and heat treated at 300 °C.

	1	**2**	**3**	**4**	**5**
ED results-d(Å)	2.99	2.75	2.21	1.69	1.57
Theoretical values-d(Å)	2.95	2.78	2.23	1.70	1.60
Crystalline plane (hkl)	(220)	(221)	(321)	(422)	(511)

4.2.3 Magnetic Characterization (VSM)

Magnetic measurements at different temperatures from 123 K to 293 K were performed by using ADE Magnetics Model EV9 Vibrating Sample Magnetometer (VSM). Figures 4.23-4.26 are FC-ZFC curves of these samples. Zero-field cooled (ZFC) susceptibilities were measured by cooling the samples in zero magnetic field and then by increasing the temperature in an applied field of 100 Oe, while field-cooled (FC) curves were recorded by cooling the samples in an applied field of 100 Oe.

The temperature dependence of magnetization of nanoparticles exhibits a cusp that corresponds to the blocking temperature, T_B [108]. The difference in T_B is attributed to the size difference and the existence of a broadened distribution of energy barriers. Furthermore, Kim et al. studied the effect of surface coating on the blocking temperature. Without coating, due to the increase in the surface area to volume ratio, the attractive force between nanoparticles will increase, and agglomeration of the nanoparticles will take place. These agglomerated nanoparticles act as a cluster, resulting in an increase of the blocking temperature [108]. The significance of this temperature is that the whole sample becomes superparamagnetic above this temperature, the particles are free to align with the field during the measurement

period. At room temperature and the temperatures above the T_B, the particles have sufficient thermal energy to overcome the energy barrier and magnetic spins are free to fluctuate between orientations. This process is called superparamagnetic relaxation. Below the T_B, the spins are frozen, or blocked, resulting in a disordered state common to superparamagnetic materials. The zero field curve (ZFC) exhibits maximum and this maximum point shifts to a lower temperatures for smaller particle sized samples, which defines a typical blocking process of an assembly of superparamagnetic particles [109].

In this study blocking temperatures were found as approximately 220 K, 300 K and 300 K for the samples heat treated at 300, 350 and 400 °C, respectively using M-T curves (M: Magnetization, T: Temperature). T_B was found approximately as 265 K for the ethylene glycol sample of sol-gel processing. These results show that these samples behave superparamagnetically at the room temperature. Since the aim of the study is to produce maghemite nanoparticles that can be used in biomedical applications at room temperature, the results obtained seem to be quite satisfactory.

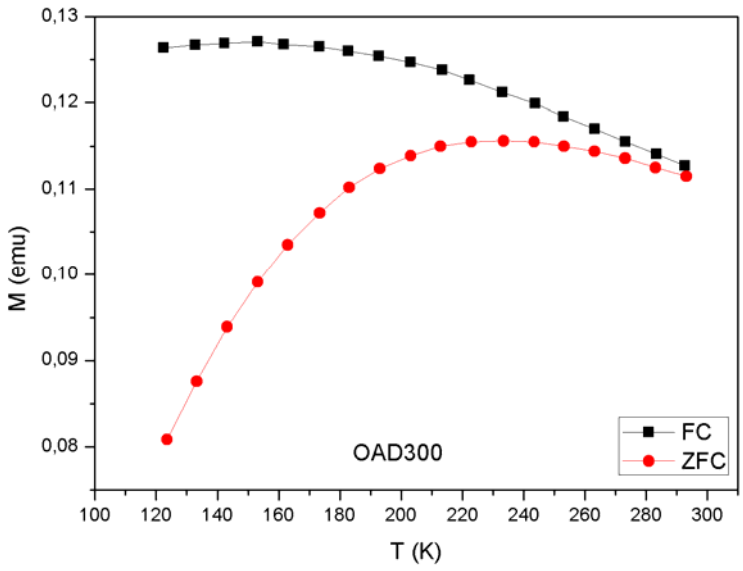

Figure 4.23 M-T curves for the sample produced by sol-gel method (diethylene glycol) and heat treated at 300 °C using zero field cooling and field cooling procedures at the applied field of 100 Oe.

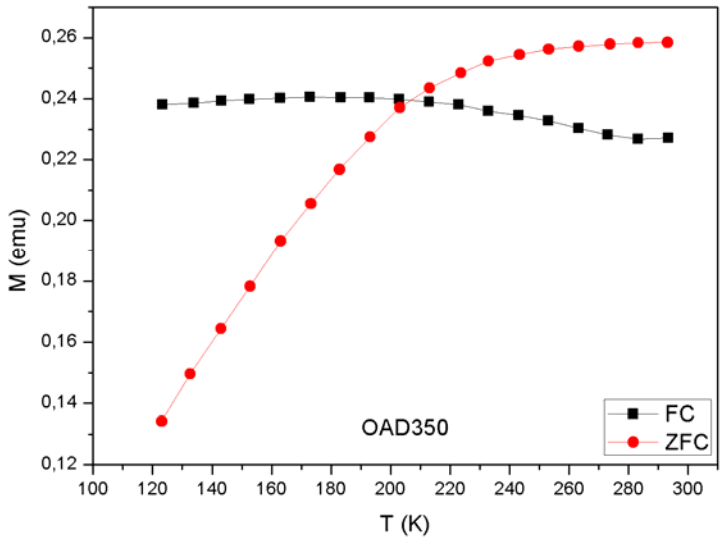

Figure 4.24 M-T curves for the sample produced by sol-gel method (diethylene glycol) and heat treated at 350 °C using zero field cooling and field cooling procedures at the applied field of 100 Oe.

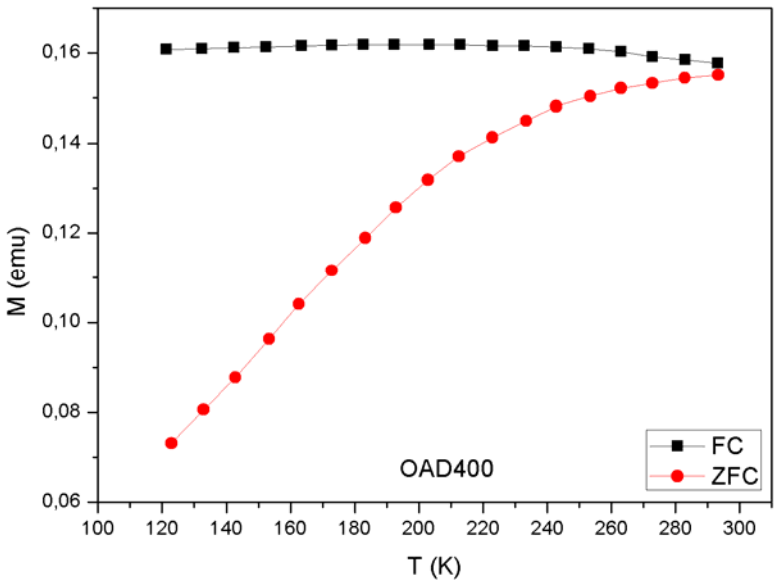

Figure 4.25 M-T curves for the sample produced by sol-gel method (diethylene glycol) and heat treated at 400 °C using zero field cooling and field cooling procedures at the applied field of 100 Oe.

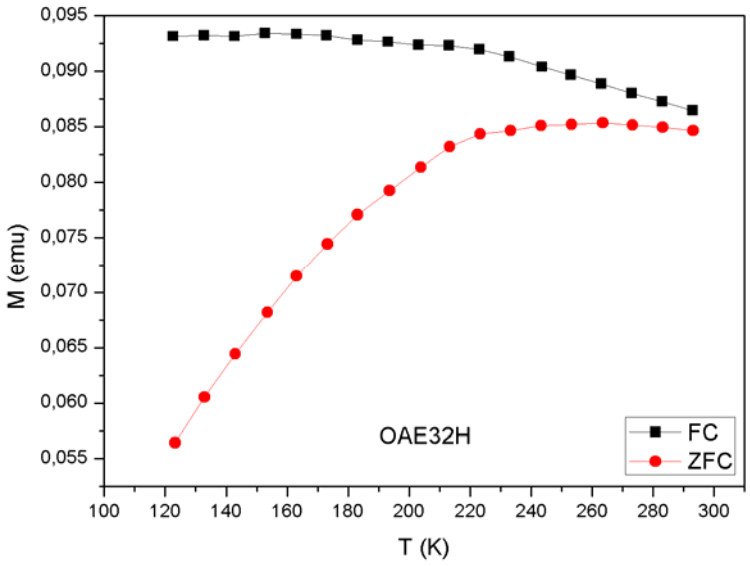

Figure 4.26 M-T curves for the sample produced by sol-gel method (ethylene glycol) and heat treated at 300 °C using zero field cooling and field cooling procedures at the applied field of 100 Oe.

Magnetic nanoparticles behave very differently from bulk or thin film systems. Saturation magnetization value of bulk maghemite is reported in the literature as 74 (emu/g). However γ-Fe_2O_3 maghemite nanoparticles have lower value of saturation magnetization when compared to bulk form. It could be attributed to nanoscale dimension and the surface effects [63,104].

When the size of the particles reduced below the single domain limit (~15 to 20 nm for iron oxide), they exhibit superparamagnetism at room temperature [63,110], followed by a spin-glass like transition at low temperature. Superparamagnetism is essentially a result of non-interacting, thermally fluctuating nanoparticle moments where the particle volume dependent effective anisotropy energy (KV) of each particle is easily overcome by the thermal energy (k_BT). The effect of this is that the nanoparticles have a large moment with high saturation magnetization but a non-hysteretic M-H curve with zero remanence and coercivity [110].

Figures 4.27-4.31 are the M-H (M: Magnetization, H: Applied Magnetic Field) curves of the samples. These samples show no hysteresis at all the temperature ranges. M_s (saturation magnetization) values were found as approximately 27, 22 and 16 emu/g for the diethylene glycol samples heat treated at 300, 350 and 400 °C, respectively. M_s value was found as 28 emu/g for the ethylene glycol sample.

In this study saturation magnetization (M_s) values of the sol-gel processed samples are quite high when compared with the results in the literature (Table 2.1) Also obtained blocking temperatures (T_B) of the sol-gel samples are comparable with the similar sized nanoparticles given in the literature. As the size decreases T_B shifts to lower temperatures [78]. T_B values obtained from this study are indicative of the room temperature usage of these nanoparticles in the desired applications.

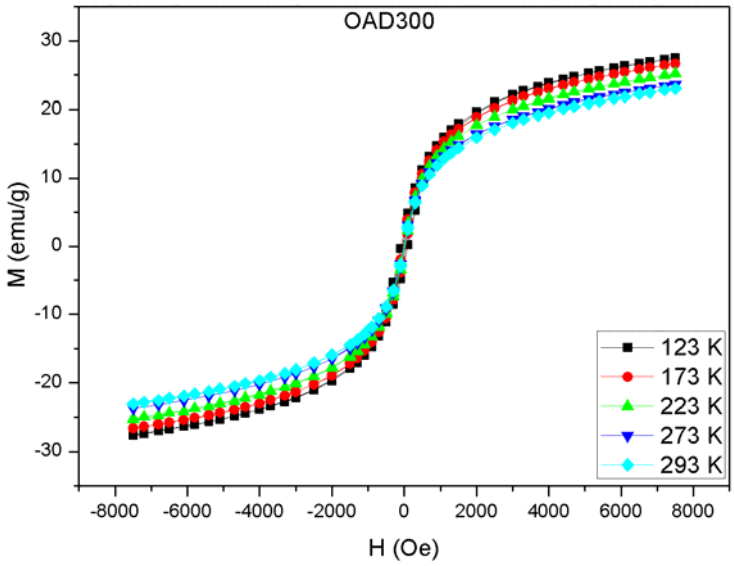

Figure 4.27 M–H curves obtained at different temperatures for the sample produced by sol-gel method (diethylene glycol) and heat treated at 300 °C.

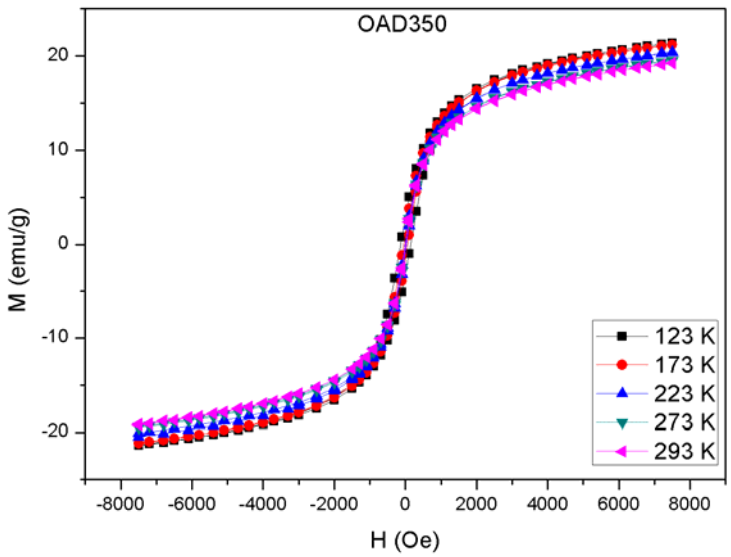

Figure 4.28 M–H curves obtained at different temperatures for the sample produced by sol-gel method (diethylene glycol) and heat treated at 350 °C.

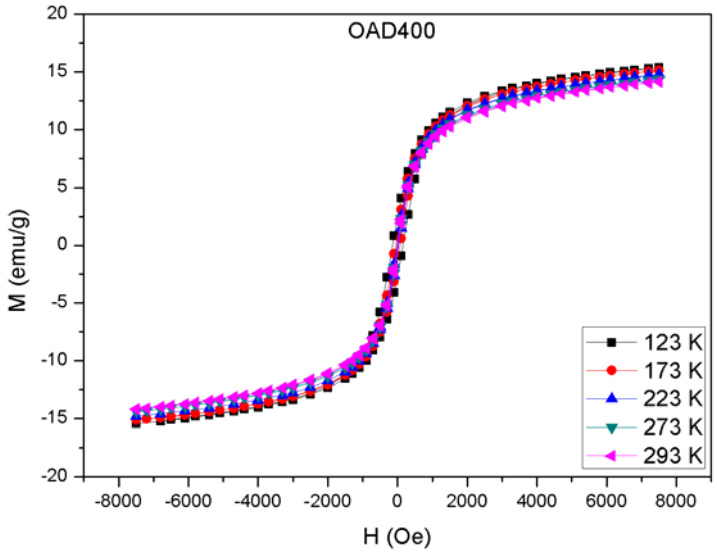

Figure 4.29 M–H curves obtained at different temperatures for the sample produced by sol-gel method (diethylene glycol) and heat treated at 400 °C.

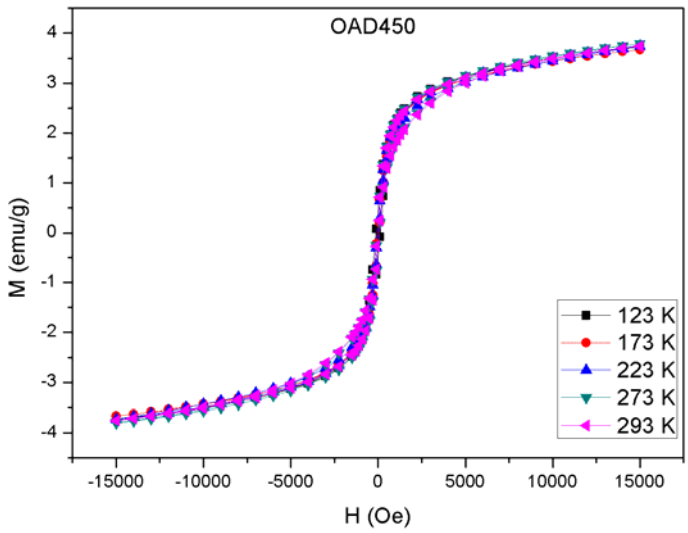

Figure 4.30 M–H curves obtained at different temperatures for the sample produced by sol-gel method (diethylene glycol) and heat treated at 450 °C.

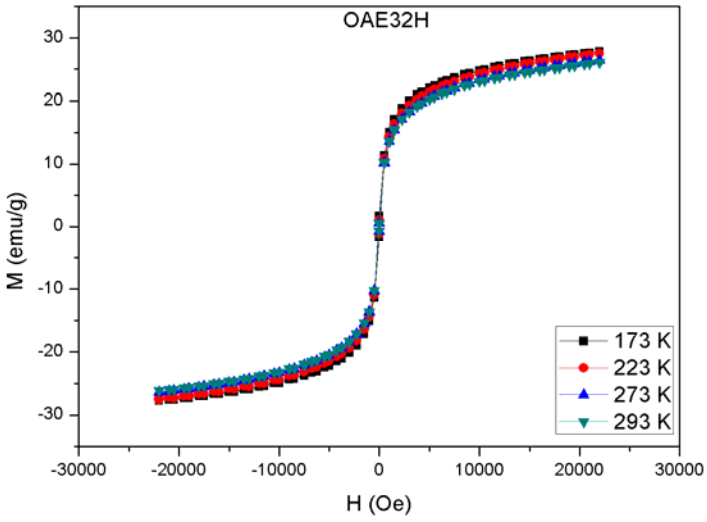

Figure 4.31 M–H curves obtained at different temperatures for the sample produced by sol-gel method (ethylene glycol) and heat treated at 300 °C.

In this study M-H curves are used to determine the magnetization behavior of the samples. If the figures do not show any hysteresis behavior and have sigmoid shape, it can be concluded that the sample behaves superparamagnetically. Another important method for the determination of superparamagnetic behavior is the FC-

ZFC characteristic where these curves are used to determine the blocking temperature (T_B) of the samples. Finally M - H/T curves are used to determine the superparamagnetic behavior, when they coincide with each other it can be said that the sample behaves superparamagnetically. Since M - H curves are lacking a precise description of M versus H due to random orientation of the particles, M - H/T curves become a universal method for the determination of superparamagnetic behavior. Figures 4.32-4.36 are the M - H/T curves of these samples produced by ethylene glycol-diethylene glycol route of sol-gel processing.

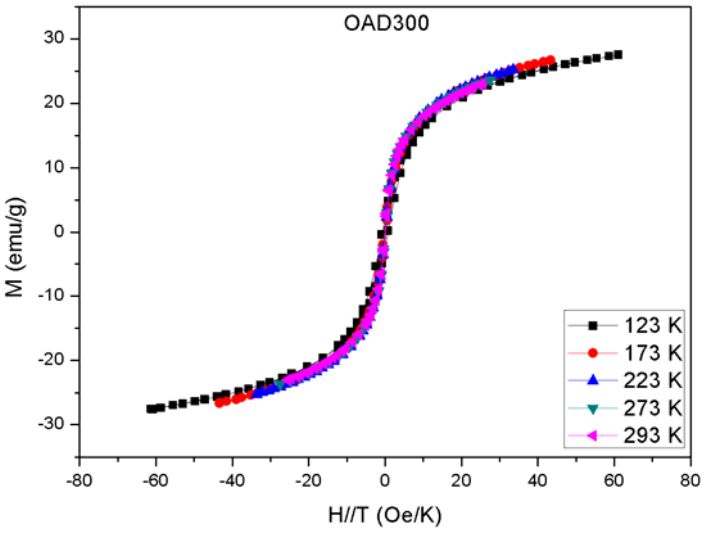

Figure 4.32 M - H/T curves obtained at different temperatures for the sample produced by sol-gel method (diethylene glycol) and heat treated at 300 °C.

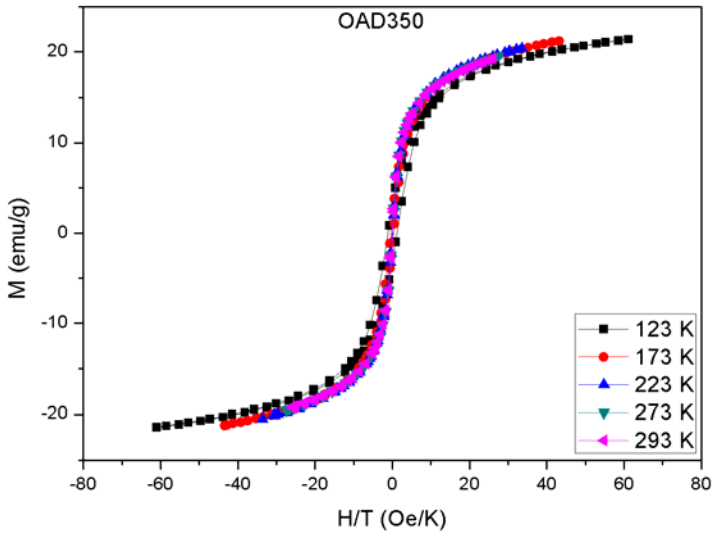

Figure 4.33 M - H/T curves obtained at different temperatures for the sample produced by sol-gel method (diethylene glycol) and heat treated at 350 °C.

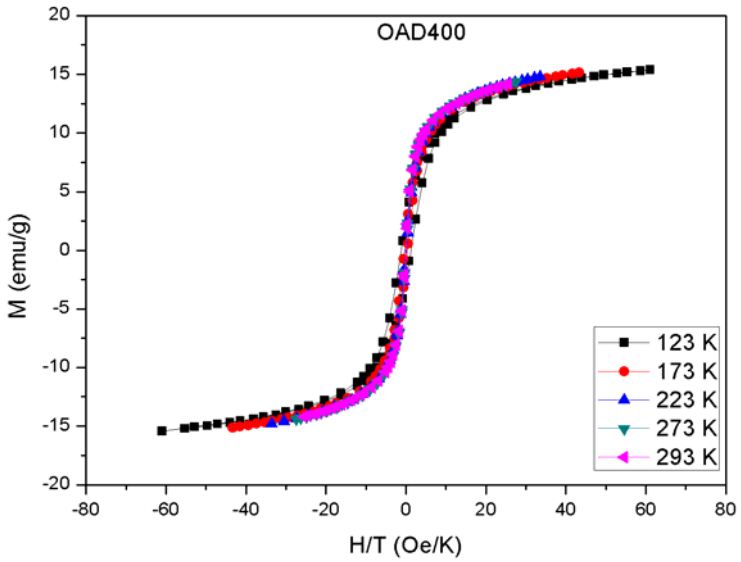

Figure 4.34 M - H/T curves obtained at different temperatures for the sample produced by sol-gel method (diethylene glycol) and heat treated at 400 °C.

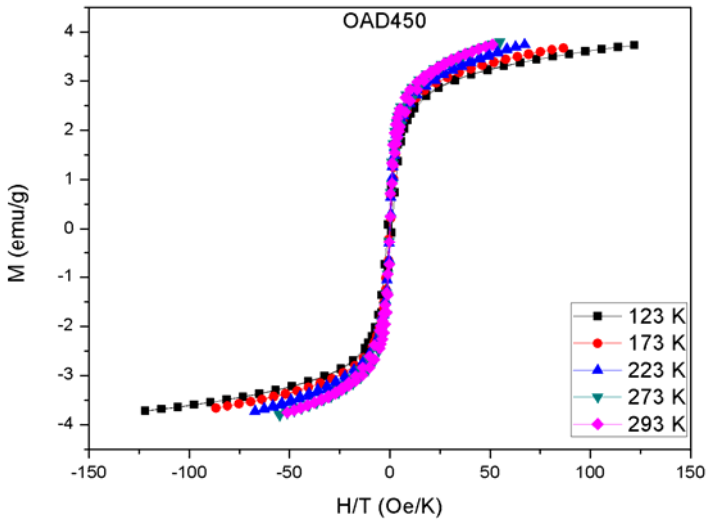

Figure 4.35 M - H/T curves obtained at different temperatures for the sample produced by sol-gel method (diethylene glycol) and heat treated at 450 °C.

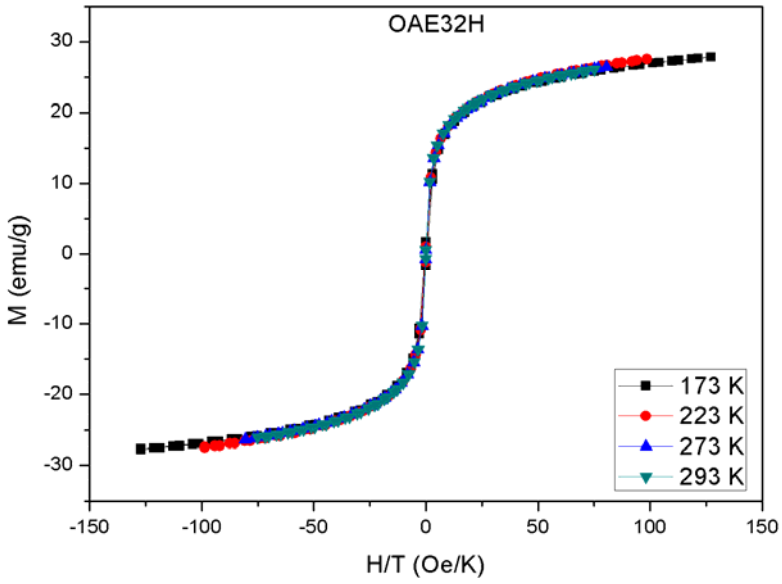

Figure 4.36 M - H/T curves obtained at different temperatures for the sample produced by sol-gel method (ethylene glycol) and heat treated at 300 °C.

Two key qualities remain for a superparamagnetic system: 1) lack of hysteresis and 2) data of different temperatures superimpose onto a universal curve of M versus H/T. From the results, it can be concluded that the samples that were heat treated at 300, 350 and 400 °C, show superparamagnetic behaviour [45,111,112].

VSM results of the samples heat treated at 500, 700 and 750 °C showed different magnetic properties than the other samples due to containing mainly hematite phase (Figure 4.11). M-T curves of these samples indicated a transition temperature called as Morin temperature in the literature (Figures 4.37-4.39). Hematite (α-Fe_2O_3) has a rhombohedral structure and a magnetic phase transition occurs at ~ 263 K, known as the Morin temperature, characterized by a reorientation of the magnetization of the two spin sublattices from parallel to perpendicular to the [111] axis in the antiferromagnetic phase. Also, due to the anisotropic superexchange interaction, spins are slightly canted out of the basal plan, giving rise to a weak ferromagnetic state. In particular, it is known that the spin reorientations in hematite are determined to a large extent by the presence of impurities or substitutions and by the particle size and morphology [24,113,114]. The diethylene glycol samples heat treated at 500, 700 and 750 °C exhibited Morin temperatures in the range 260-273 K and this variation is attributed to the variation in the particle sizes (Table 4.6).

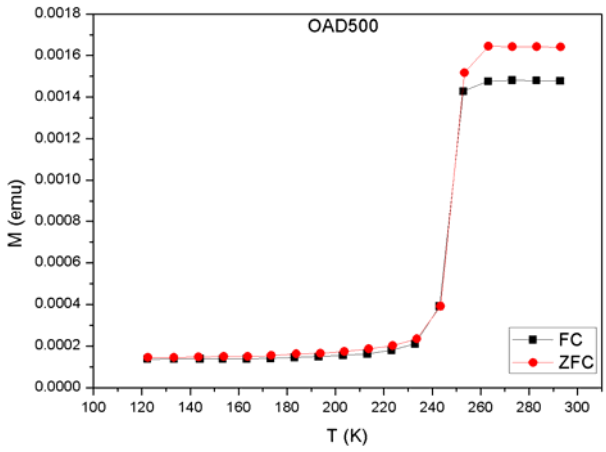

Figure 4.37 M-T curves for the sample produced by sol-gel method (diethylene glycol) and heat treated at 500 °C using zero field cooling and field cooling procedures at the applied field of 100 Oe.

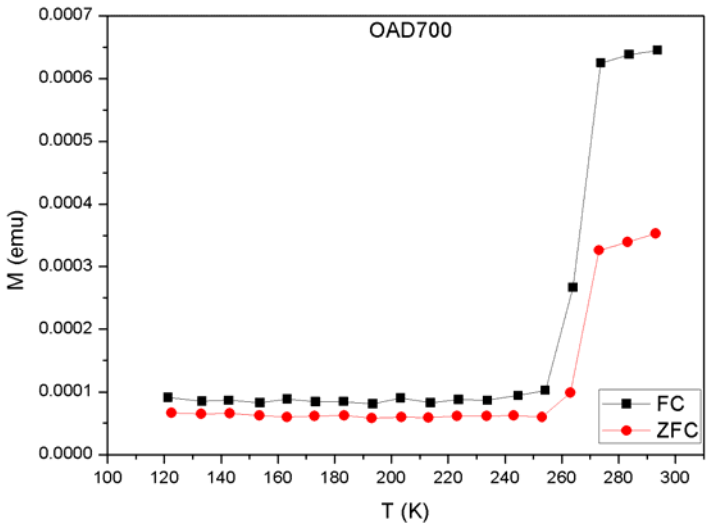

Figure 4.38 M-T curves for the sample produced by sol-gel method (diethylene glycol) and heat treated at 700 °C using zero field cooling and field cooling procedures at the applied field of 100 Oe.

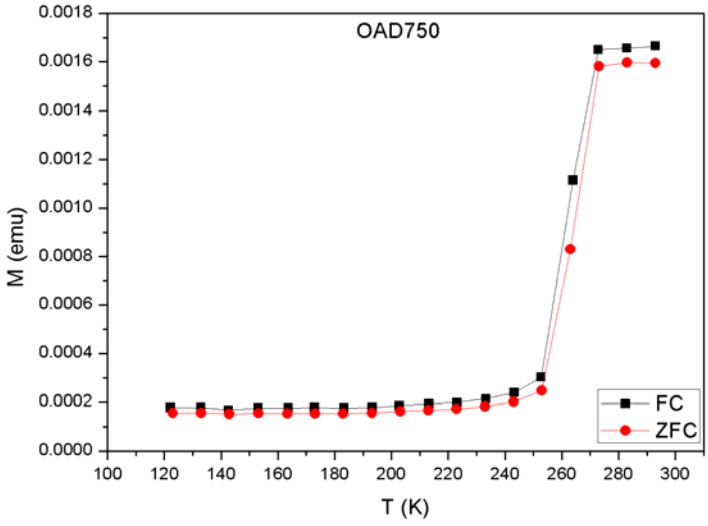

Figure 4.39 M-T curves for the sample produced by sol-gel method (diethylene glycol) and heat treated at 750 °C using zero field cooling and field cooling procedures at the applied field of 100 Oe.

The diethylene glycol samples heat treated at 500, 700 and 750 °C which exhibited Morin temperatures in the range 260-273 K yield M-H curves with a paramagnetic slope at lower temperatures (123, 173 and 223 K), on the other hand at 273 and 293 K the same samples showed a hysteretic behaviour according to magnetic measurements. This transition in magnetic behavior is attributed to Morin transition in the hematite phase (Figure 4.37-4.39).

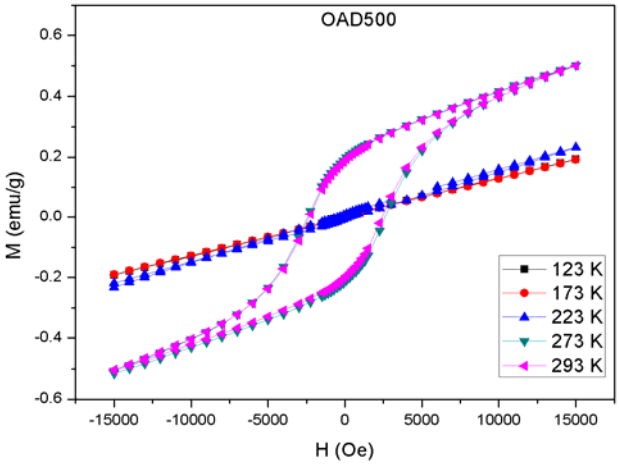

Figure 4.40 M–H curves obtained at different temperatures for the sample produced by sol-gel method (diethylene glycol) and heat treated at 500 °C.

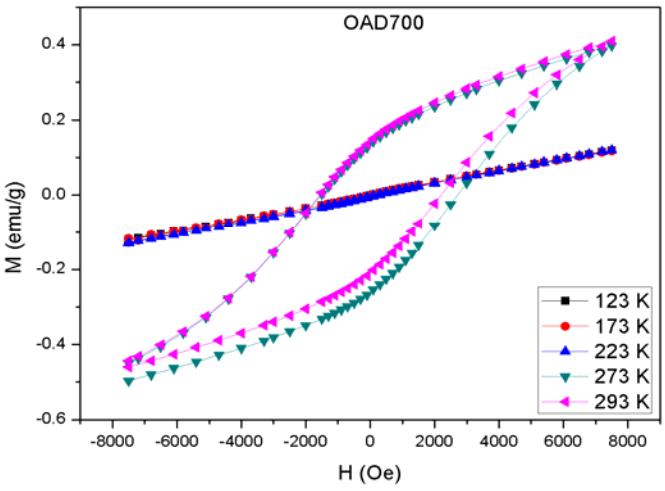

Figure 4.41 M–H curves obtained at different temperatures for the sample produced by sol-gel method (diethylene glycol) and heat treated at 700 °C.

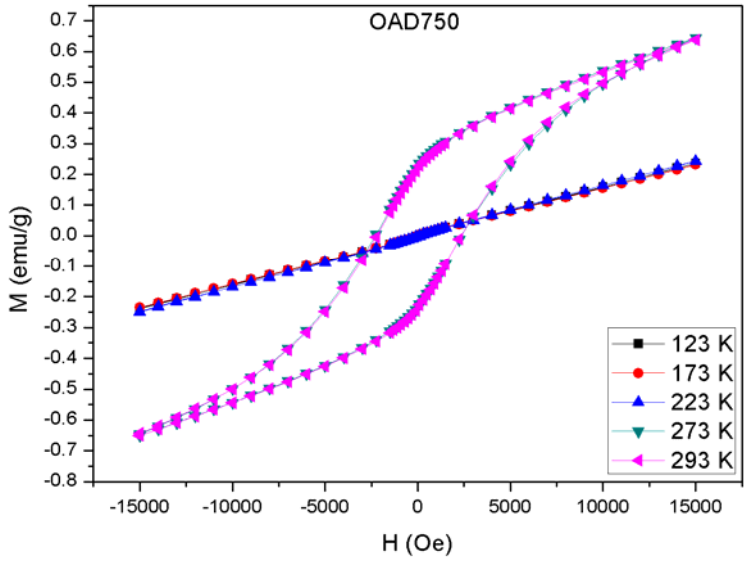

Figure 4.42 M–H curves obtained at different temperatures for the sample produced by sol-gel method (diethylene glycol) and heat treated at 750 °C.

Table 4.6 summarizes the magnetic properties of sol gel processed samples of ethylene glycol-diethylene glycol route which were heat treated between 300 and 750 °C. As it can be seen from the Table 4.6, the highest magnetization value (28 emu/g) belongs to ethylene glycol sample (OAE32H) which was heat trated at 300 °C. Since the amount of maghemite phase is higher in this sample than the other samples with the value of 80 % (Table 4.3). The saturation magnetization values of the other samples (OAD300, OAD350, OAD400) are also quite high when compared with the results of the sol-gel processed samples from the literature given in Table 2.1 such as 8 emu/g as the maximum value [6].

Table 4.6 Magnetic properties of the samples which were produced by ethylene glycol - diethylene glycol route of sol-gel method.

Sample	Phases	M_s (emu/g), T_B (K), T_{Morin} (K)
OAE32H	α, γ	28, T_B : 265
OAD300	α, γ	27, T_B : 220
OAD350	α, γ	22, T_B : 300
OAD400	α, γ	16, T_B : 300
OAD450	α, γ	-
OAD500	α, γ	T_{Morin}: 240-260
OAD700	α	T_{Morin}: 260-273
OAD750	α	T_{Morin}: 260-273

4.2.4 Analysis of Magnetization Curves

If a magnetic field H is applied to a randomly oriented assembly of magnetic dipoles which are assumed to have no mutual interactions and do not interact with any other system, there is no change in the mean orientation along the applied field, i.e. there is no induced magnetization in the system. This is only true for non-quantum-mechanical or classical moments which might be termed as classical or Langevin paramagnetism. It applies to assemblies of particles with permanent freely rotating moments which are too large for quantum treatments to be significant (superparamagnetism) [115]. In this case the total moment of the macroscopic body will be proportional to μ, the number of atoms per unit volume N, and the degree of alignment. The alignment is measured by cos θ, and since there are many moments, the average alignment can be obtained from the probability of having a given cos θ. In a system in thermal equilibrium at temperature T, this probability is given by the Boltzmann distribution and the integration yields the Langevin function

$$L(x) = \coth(x) - \frac{1}{x} \qquad \text{Eq. 4.4}$$

In Equation 4.4, the parameter x = μ H / k T is the ratio of magnetic alignment energy to thermal randomizing energy, and hence gives emphasis to the competition between these two terms where k is the Boltzmann constant [45].

Observed experimental results show that the magnetizations of nanoparticles produced in this study originate from two contributions;

- one due to the superparamagnetic particles and
- the other due to the blocked particles.

Superparamagnetic part can be described by Langevin function $L(x) = \coth(x) - \frac{1}{x}$ from a minimum particle size up to a critical size, and the blocked part can be described by hyperbolic tangent function (tanh(x)) from the critical size up to a maximum particle size [116].

Using this assumption magnetization curves can be described by

$$M(H) = C1.L(x) + C2.\tanh(x) \qquad \text{Eq. 4.5}$$

Mathcad programme was used to obtain best fit of Eq. 4.5 to the magnetization data using least-squares procedure.

Langevin model was used in the Mathcad programme as the only function by considering that the samples consist of small sized particles with narrow size distribution, however the results were not satisfactory (Figure 4.43). Best fit was obtained when it is assumed that there is a size distribution of particles. According to this assumption smaller particles behave as superparamagnetic and described by Langevin function, on the other hand larger blocked particles described by tangent hyperbolic function. Correlation coefficients of both models are in the range between 0.98-0.99. The results are given in the Table A.1 in the appendix.

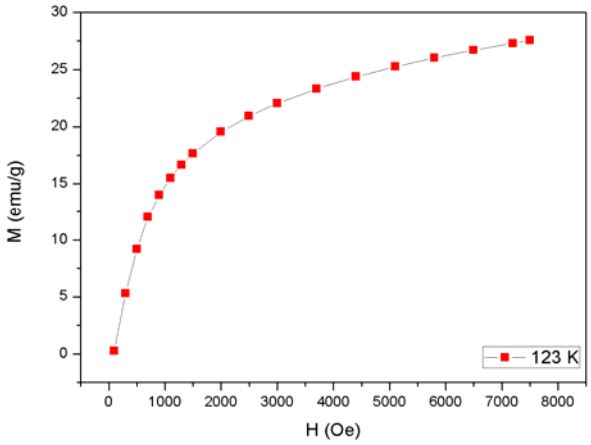

a.

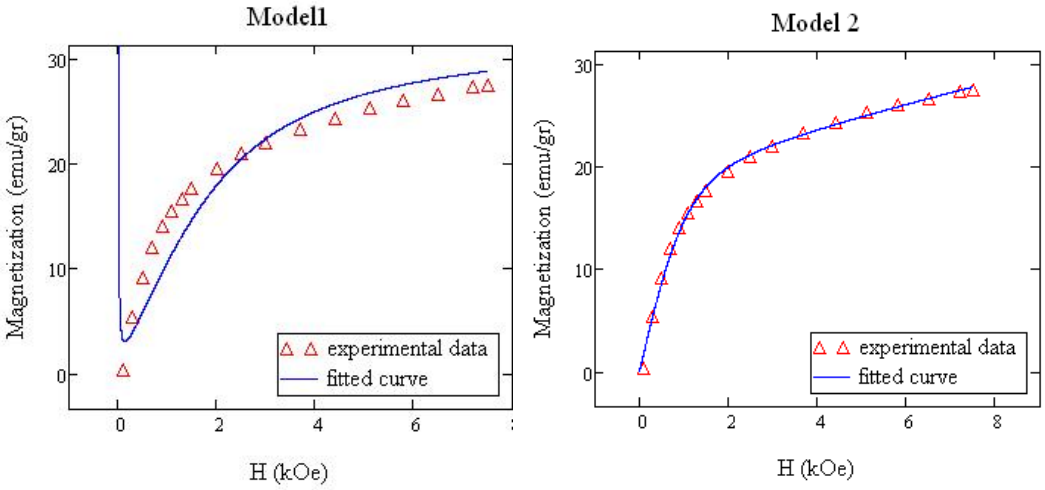

b. **c.**

Figure 4.43 a. M-H curve (123 K) of sol-gel sample produced by using diethylene glycol and heat treated at 300 °C, **b.** It's fitted curve by using only Langevin function, **c.** It's fitted curve by using Langevin and tangent hyperbolic functions.

Figures 4.44-4.46 show the fitted curves of the samples at different temperatures and Table 4.7 gives the values of the parameters C1 and C2 obtained from the fitting.

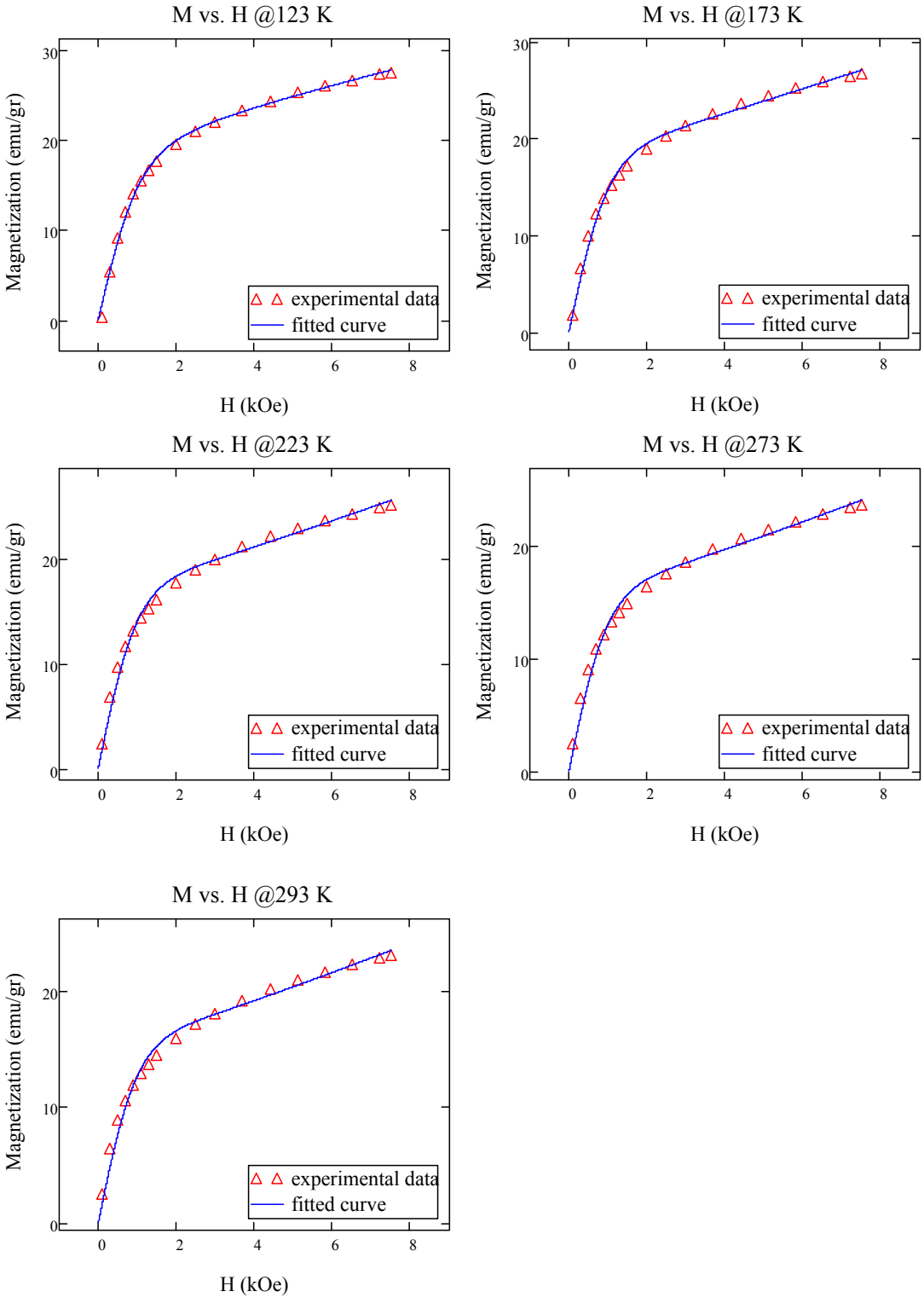

Figure 4.44 Fitted M-H curves of 300 °C heat treated sol-gel sample produced by using diethylene glycol

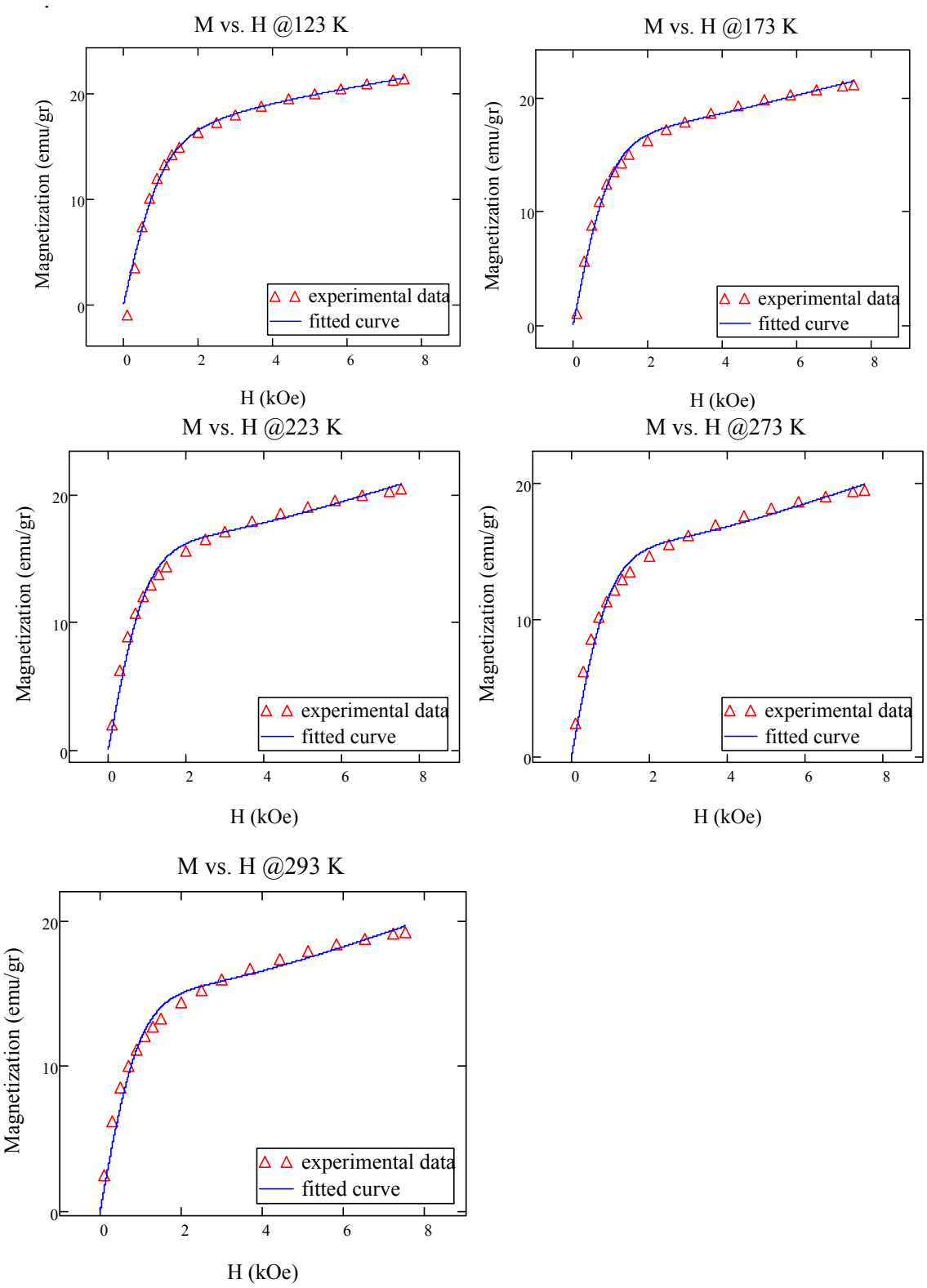

Figure 4.45 Fitted M-H curves of 350 °C heat treated sol-gel sample produced by using diethylene glycol.

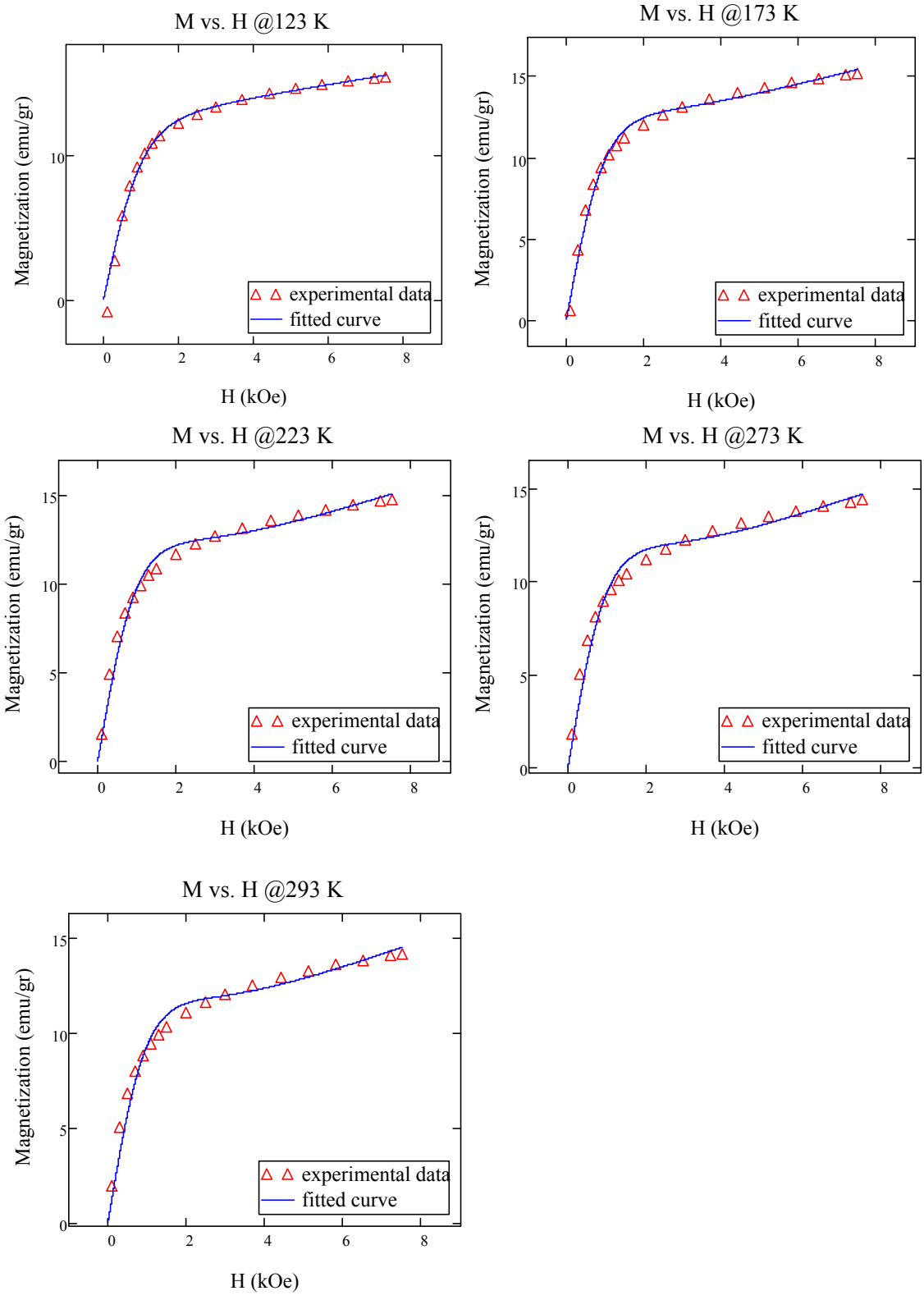

Figure 4.46 Fitted M-H curves of 400 °C heat treated sol-gel sample produced by using diethylene glycol.

Table 4.7 Parameters in Equation 4.5 obtained from the fitting for the samples prepared by using diethylene glycol.

	123 K		173 K		223 K		273 K		293 K	
	C1	**C2**	**C1**	**C2**	**C1**	**C2**	**C1**	**C2**	**C1**	**C2**
OAD300	17.2	11.6	15.1	12.3	13.9	11.9	13.3	10.8	13.1	10.4
OAD350	11.0	11.2	8.4	13.0	7.5	12.9	7.5	12.0	7.4	11.8
OAD400	6.3	9.4	4.4	10.7	3.7	10.9	3.8	10.3	3.7	10.2

Since C1 belongs to the superparamagnetic part and C2 belongs to the paramagnetic part from the Eq.4.5, it can be meaningful to compare the ratios of C1 and C2 with the results obtained from the quantitative analysis of the phases obtained using XRD data of the samples (Table 4.3). Table 4.8 gives these compared results and it can be concluded that results are matching with the amount of the phases present in the samples, because it was thought that maghemite phase provides the superparamagnetic contribution to the magnetic behavior of the sample.

Table 4.8 Comparison of the fitting parameters C1 and C2 with the quantitative analysis of XRD data.

	γ		**123 K**	**173 K**	**223 K**	**273 K**	**293 K**
OAD300	0.77	C1/C1+C2	0.6	0.55	0.53	0.55	0.55
OAD350	0.30	C1/C1+C2	0.49	0.39	0.36	0.37	0.38
OAD400	0.28	C1/C1+C2	0.40	0.29	0.25	0.26	0.26
	α		**123 K**	**173 K**	**223 K**	**273 K**	**293 K**
OAD300	0.23	C2/C1+C2	0.4	0.45	0.47	0.45	0.45
OAD350	0.70	C2/C1+C2	0.51	0.61	0.64	0.63	0.62
OAD400	0.72	C2/C1+C2	0.60	0.71	0.75	0.74	0.74

Finally, Table 4.9 gives the characterization results of the samples produced by ethylene glycol and diethylene glycol route of sol-gel processing.

Table 4.9 General results of all characterization techniques used for the samples produced by ethylene glycol - diethylene glycol route of sol-gel method.
(E: Ethylene glycol, D: Diethylene glycol)

Sample name	Phases	Particle size (nm) (Scherrer Method)	Particle size (nm) (TEM Method)	BET Surface area (m^2/g)	VSM M_S (emu/g), T_B, T_{Morin}
OAE1	γ,α	16.0	-	-	-
OAE2	γ,α	7.8	-	-	-
OAE3	γ,α	8.4	-	-	-
OAE32H	γ (80%), α (20%)	8.4	8.75 ± 0.35	104	28, T_B: 220 K
OAD300	γ (77.5%), α (22.5%)	4.0	5.35 ± 0.27	114.0	27, T_B: 220 K
OAD350	γ (30%), α (70%)	8.0	7.64 ± 1.46	72.9	22, T_B: 300 K
OAD400	γ (28.7%), α (71.3%)	12.1	5.15 ± 0.76	49.9	16, T_B: 300 K
OAD450	γ,α	24.2	-	31.3	-
OAD500	γ,α	24.2	-	22.5	-
OAD700	α	48.5	-	9.5	T Morin: 260-273 K
OAD750	α	34.6	-	5.5	T Morin: 260-273 K

As given in the introduction part of this thesis, γ-Fe_2O_3 maghemite nanoparticles are generally studied for their use in biomedical treatments. Conventional chemotheraphy and hyperthermia treatment of cancer suffers from several drawbacks that reduce therapeutic efficiency and cause undesirable side effects. Hyperthermia involves selective deactivation of cancer cells by heating in the temperature range of 41-47 °C, but conventional hyperthermia techniques suffer from insufficient

temperature rise in the tumor, poor temperature distribution and risk of organ damage to overheating [117].

Iron oxide magnetic nanoparticles can improve cancer therapy by overcoming several limitations of conventional chemotherapy and hyperthermia. These particles release the drug following localization in the tumor, resulting in increased tumor drug concentration with minimal systemic toxicity. If an alternating magnetic field is applied after localization, the iron oxide magnetic cores of the particles generate heat, raising the temperature of the tumor and resulting in hyperthermia [118].

It was found that applied magnetic field strength and frequency as well as particle properties such as particle size and anisotropy constant strongly influence power output; the highest power output is obtained in a relatively narrow particle size range. Optimum sized γ-Fe_2O_3 maghemite particles produce higher power output than optimum sized Fe_3O_4 magnetite particles [117]. The superparamagnetic size limit was determined as 16 nm for spherical iron particles and 28 nm for γ-Fe_2O_3 maghemite particles [45]. Therefore, the maghemite nanoparticles produced by sol-gel processing are feasible to be used in combined hyperthermia and chemotherapy applications.

4.3 Microwave Method

The objective of this part of the study was to synthesize nanoparticles of maghemite (γ-Fe_2O_3) via microwave processing of $Fe(NO3)_3.nH_2O$ followed by low temperature annealing. $Fe(NO_3)_3.nH_2O$ has the ability to effectively absorb microwave radiation, which raises the temperature in the system and initiates the below reaction

$$4Fe(NO_3)_3 \cdot nH_2O = 2Fe_2O_3 + 12NO_2 + 3O_2 + 4nH_2O \qquad \text{Eq. 4.6}$$

The use of low reaction temperatures is essential, because this reduces the probability of the formation of hard agglomerates [119].

XRD was used to characterize the structural phases of nanoparticles. BET measurements were also performed for microwave samples to understand the surface areas of them. TEM study was conducted to examine the morphology and crystal structure of the nanoparticles. VSM (Vibrating Sample Magnetometer) was used in order to characterize the magnetic properties of these particles.

4.3.1 Structural Characterization (XRD)

Table 4.10 shows the approximate particle sizes of the microwave synthesized samples calculated by using Scherrer's equation that were prepared at 850 W microwave power. As can be seen from the table, the particle size generally increases with the increase in the duration of the heat treatment period.

Table 4.10 Approximate particle sizes calculated according to Scherrer's formula for the microwave processed samples produced at 850 W.

	Microwave durations					
	5 min		**10 min**		**15 min**	
	Particle size (nm), Phases	BET (m^2/g)	Particle size (nm), Phases	BET (m^2/g)	Particle size (nm), Phases	BET (m^2/g)
As microwave processed	2.7 (γ)	141.0	6.1 (γ,α)	140.1	6.1 (γ)	159.0
24 h (230 °C)	3.4 (γ,α)	114.9	8.0 (γ,α)	117.0	9.6 (γ,α)	131.4
48 h (230 °C)	4.0 (γ,α)	111.8	8.0 (γ,α)	103.1	12.1 (γ,α)	125.4
72 h (230 °C)	8.0 (γ,α)	116.7	8.0 (γ,α)	127.1	12.1 (γ,α)	-

X-Ray diffraction patterns given in figures 4.47-4.49 were obtained for the same microwave processing time and different furnace heat treatment durations. According to these figures, the sample which is microwave processed for 5 minutes, has only maghemite phase, it contains no hematite phase. The broad peaks are

characteristic of small particles with a mean crystallite size, estimated from the (311) reflection, of 2.7 nm. Further low temperature annealing following microwave processing leads to the coexistence of maghemite and hematite phases as found by XRD. The samples, which were placed in the furnace for different annealing periods showed both maghemite and hematite phases. The amount of hematite phase in these samples increased essentially with the increase in the annealing period as indicated by the increase in the intensities of the α-Fe_2O_3 peaks (Figure 4.47) showing that maghemite particles transformed into more stable hematite particles. Also, with the increase in the annealing time, the peaks are becoming sharper showing the increase in the particle sizes as calculated in Table 4.10. Similar results were obtained for the samples processed for 15 minutes, but hematite peaks were also observed for the sample which was microwave synthesized for 10 minutes without any heat treatment in the furnace (Figure 4.48).

Figure 4.50 shows the XRD patterns of the samples heat treated for 24 h at 230 °C for different microwave durations. As the microwave treatment time increases from 5 to 15 minutes, the increase in the peak intensities of hematite phase and corresponding particle sizes can be observed from the shape of the peaks. Similar results were also observed for the samples heat treated for 48 and 72 h at 230 °C in the Figures 4.51 and 4.52.

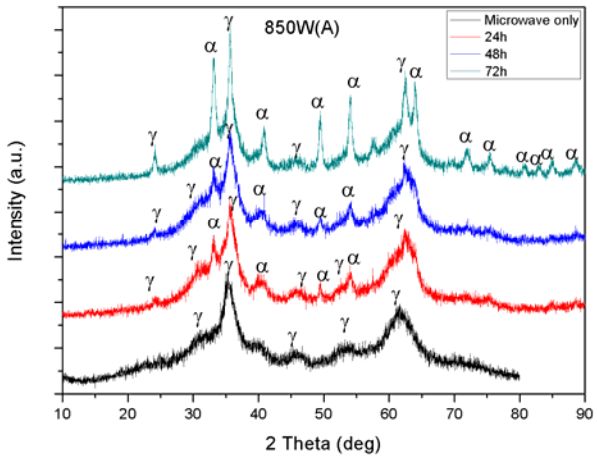

Figure 4.47 XRD patterns of the samples which are microwave synthesized for 5 minutes at 850 W.

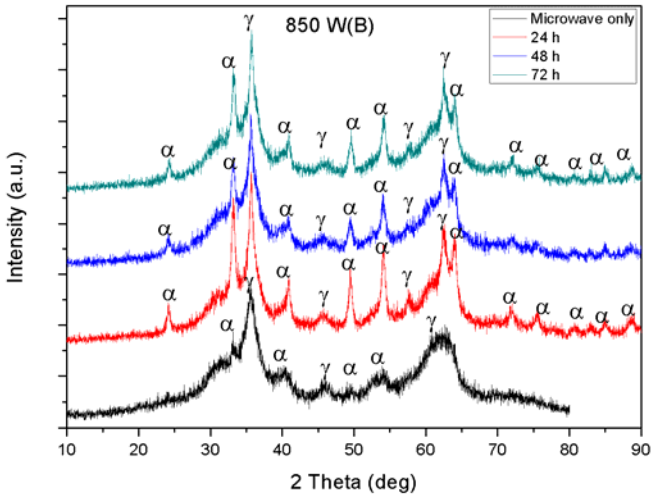

Figure 4.48 XRD patterns of the samples which are microwave synthesized for 10 minutes at 850 W.

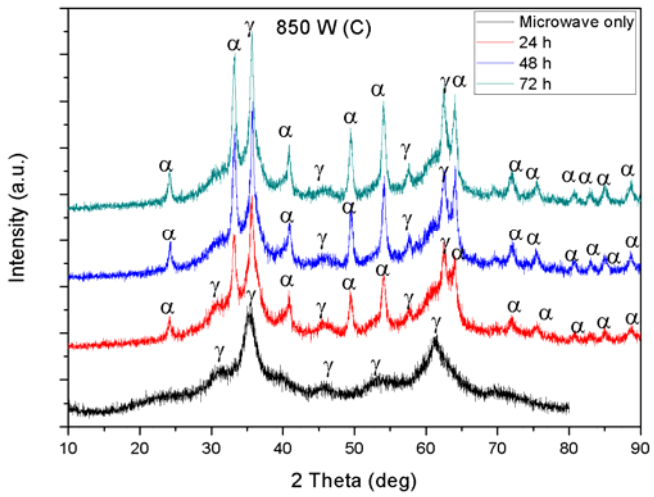

Figure 4.49 XRD patterns of the samples which are microwave synthesized for 15 minutes at 850 W.

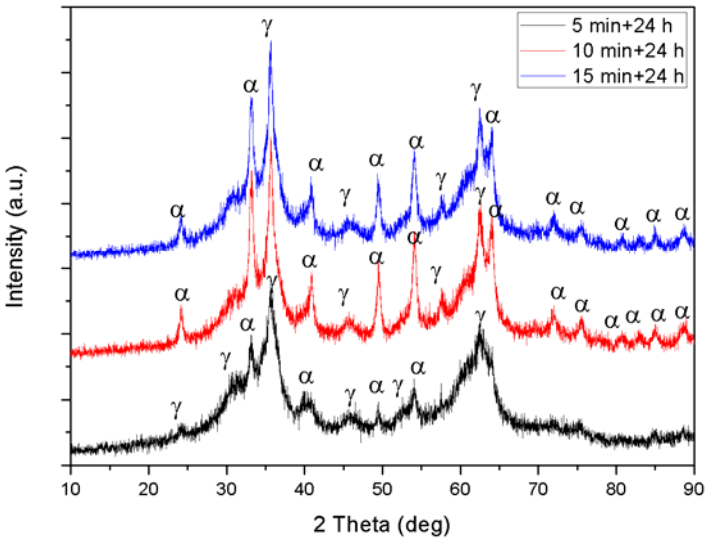

Figure 4.50 XRD patterns of the samples which are microwave synthesized for different periods at 850 W and heat treated for 24 h at 230 °C .

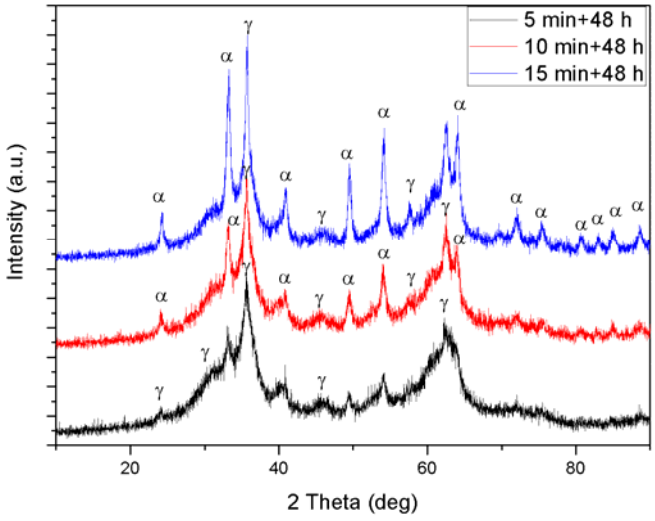

Figure 4.51 XRD patterns of the samples which are microwave synthesized for different periods at 850 W and heat treated for 48 h at 230 °C.

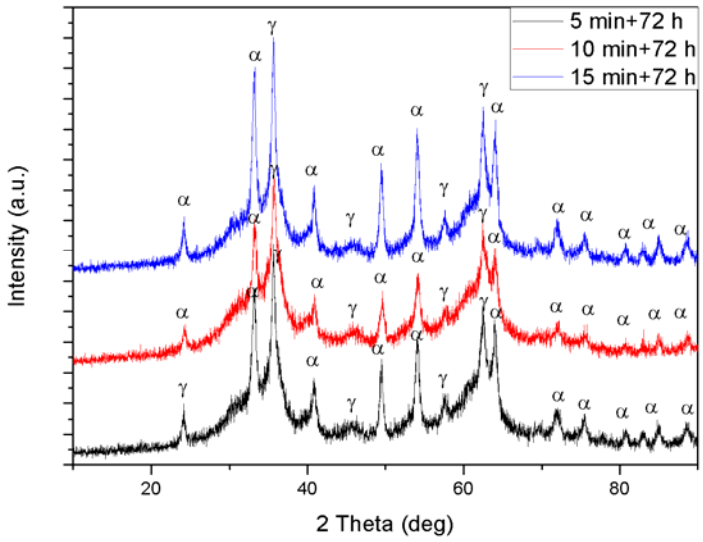

Figure 4.52 XRD patterns of the samples which are microwave synthesized for different periods at 850 W and heat treated for 72 h at 230 °C.

Single point and multi point BET surface area measurements were conducted for the samples which are microwave processed at 850 W for different periods. Multipoint BET measurements yielded surface area values between 100-160 m^2/g as given in Table 4.10. These results show that samples have large surface area and they are nanometer sized particles. Figures 4.53-4.56 are the XRD patterns of the samples which are microwave synthesized at different powers such as 630, 720, 810 and 900 W.

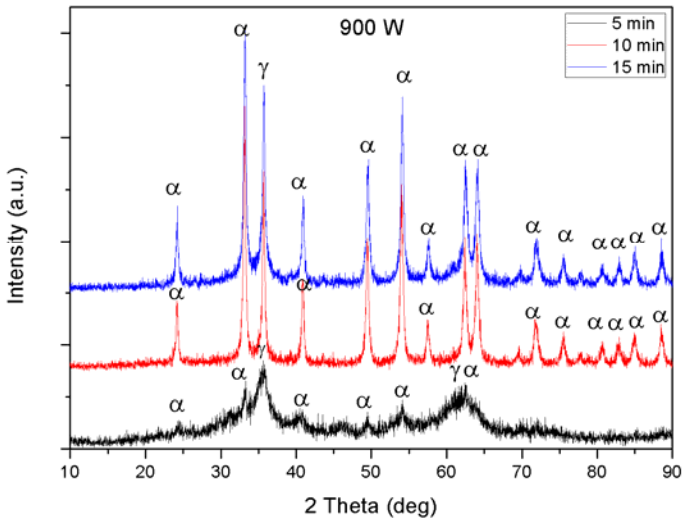

Figure 4.53 XRD patterns of the as microwave processed samples at 900 W.

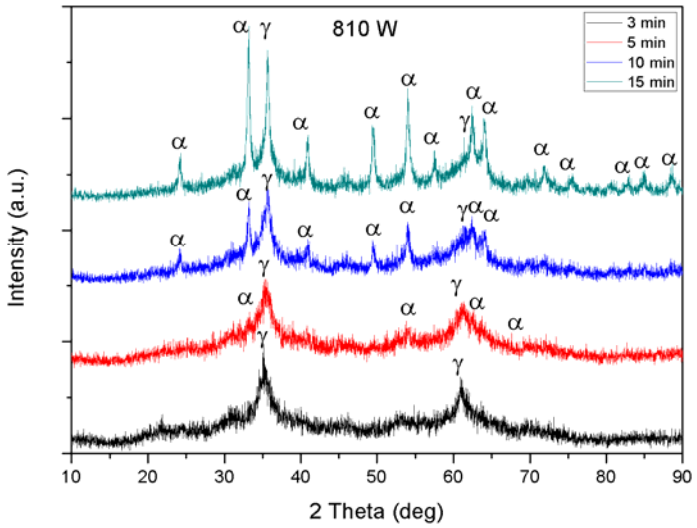

Figure 4.54 XRD patterns of as microwave processed samples at 810 W.

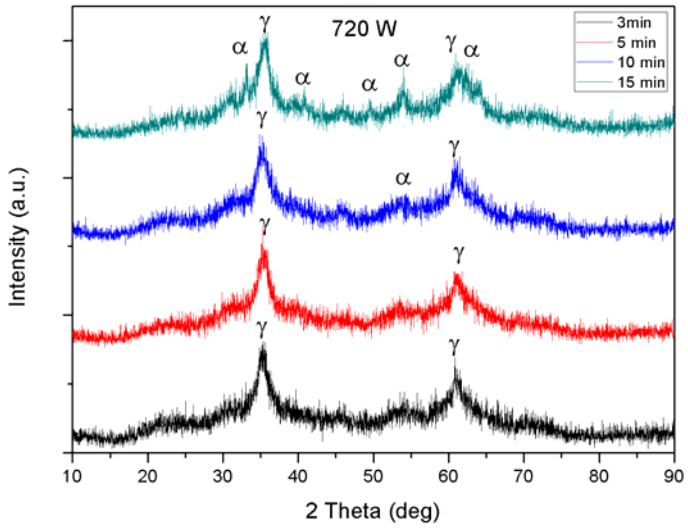

Figure 4.55 XRD patterns of as microwave processed samples at 720 W.

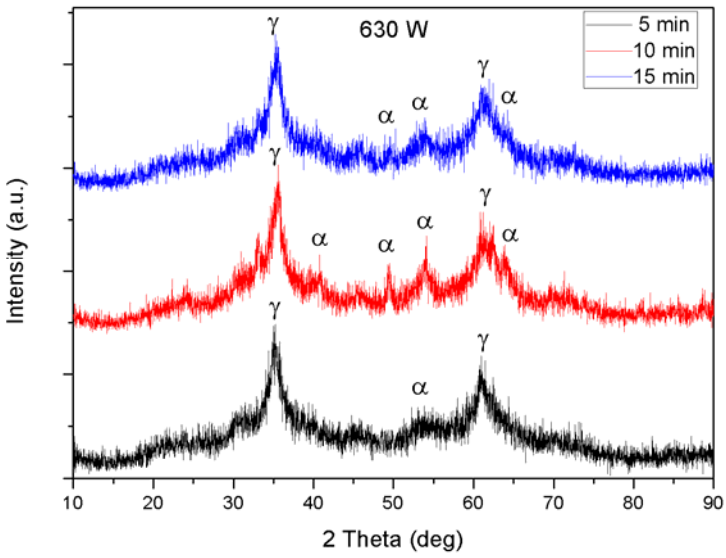

Figure 4.56 XRD patterns of as microwave processed samples at 630 W.

XRD studies showed that some of the samples have only maghemite phase on their diffraction patterns, while the others have both maghemite and hematite phases co-existing together. Low microwave powers and short durations increases the tendency to form maghemite phase. By using Scherrer equation approximate particle sizes were calculated and they are found between 2.6 and 24.6 nm. Larger particles were

found especially at the microwave power of 900 W and long durations as it can be seen from the XRD figures (Figure 4.53).

Multipoint BET measurements were also carried out for these samples which are microwave processed at different power values and surface area values between 95 and 186 m^2/g were determined as given in Table 4.11.

Table 4.11 Approximate particle sizes and BET results of samples which were synthesized by microwave method at different powers.

Sample Name	Microwave Power (W)	Microwave Duration (min)	Particle Size (nm) (Scherrer Method)	BET Surface Area (m^2/g)
Y9005	900	5	4.8	115.0
Y90010		10	24.6	-
Y90015		15	24.2	-
Y8103	810	3	4.8	-
Y8105		5	3.1	138.0
Y81010		10	3.4	-
Y81015		15	16.1	-
Y7203	720	3	2.6	186.0
Y7205		5	3.4	154.0
Y72010		10	3.1	114.0
Y72015		15	3.1	94.4
Y6305	630	5	3.1	169.0
Y63010		10	4.1	-
Y63015		15	4.1	-

Since the conventional microwave ovens close itself in a short time because the electronics and magnetron of the microwave system are affected by microwaves reflected from the walls which heat those parts (electronics and magnetron). That is, the air flow supplied by the conventional fan is not enough to cool the necessary parts of the system. Therefore experiments requiring longer time periods can't be performed in such conventional systems. For this reason, the domestic microwave oven was modified as explained in Section 3.3.

Figure 4.57 is the XRD pattern of some of these samples which were produced by modified microwave system. All samples contain both maghemite and hematite phases existing together in their XRD patterns.

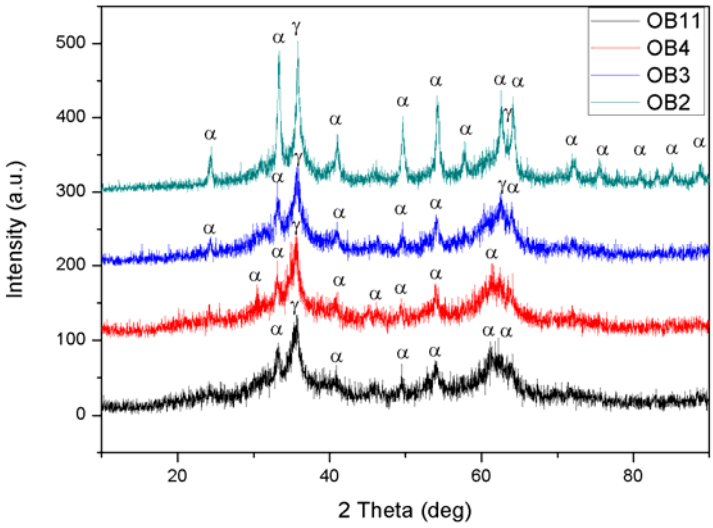

Figure 4.57 XRD patterns of the modified microwave samples.

Table 4.12 gives the preparation conditions and particle sizes of these modified microwave samples. Approximate particle sizes were found between 6.8 to 23.8 nm according to Scherrer's equation.

Table 4.12 Preparation conditions and particle sizes of the samples that were prepared by modified microwave system.

Sample name	**Microwave power (W)**	**Microwave Duration (min)**	**Heat treatment tempereture and time**	**Particle size (nm) (Scherrer Method)**	**BET Surface Area (m^2/g)**
OB2	900	20	200 °C, 24 h	23.8	110.8
OB3	900	20	200 °C, 3 h	7.8	153.7
OB4	900	30	-	6.8	168.2
OB11	810	5	-	7.9	154.8

The experimental procedure in microwave processing seems quite simple but it was difficult to obtain the maghemite phase. Several different microwave powers and durations were applied to prepare the samples. Most of the samples contain maghemite and hematite phases existing together and particle sizes are between 3-30 nm. The main point about this method is the crystallinity of the samples. Short microwave treatment periods yielded maghemite particles, however their crystallinity were not pronounced as compared to sol-gel samples. Some of the samples were well crystalline, but in this case size of the particles became quite large which affects the magnetic properties adversly.

4.3.2 Morphological Characterization (TEM)

Figure 4.58 show the TEM micrographs of the A3 sample which was microwave synthesized at 850 W for 5 minutes and heat treated at 230 °C for 48 h. Figures 4.59 and 4.60 are the TEM micrograph of the A1 sample which was microwave synthesized at 850 W for 5 minutes only, and its size distribution, respectively. As it can be seen from the figures, the sample A1 is composed of nanometer sized particles approximately in the range of 4-6 nanometers indicating narrow size distribution. TEM image indicates that particles larger than 10 nm are only a few percent of all the particles present (Figure 4.60). These figures are in good agreement with the results obtained from Scherrer's equation using XRD spectra of the iron oxide nanoparticles. Figure 4.61 is the HRTEM micrograph of the C1 sample which was microwave synthesized at 850 W for 5 minutes and heat treated at 230 °C for 48 h. This TEM image also indicates that average particle size is about 5 nm and the particles show a narrow size distribution which is an important parameter for biomedical applications.

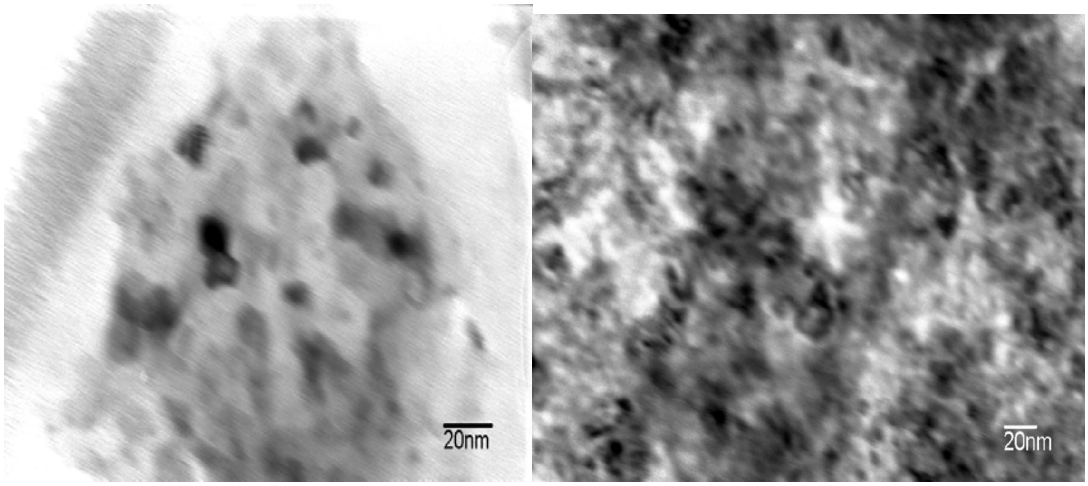

Figure 4.58 TEM micrographs of the sample which was microwave synthesized at 850 W for 5 minutes and heat treated at 230 °C for 48 h.

Figures 4.62 and 4.63 are the TEM micrograph of the sample A1 which was microwave synthesized at 850 W for 5 minutes only and its EDX pattern, respectively. According to EDX analysis mass percentages of Fe and O are ~30 and 70, respectively and from this result it can be concluded that this particle is the Fe_2O_3 phase of the iron oxide sample.

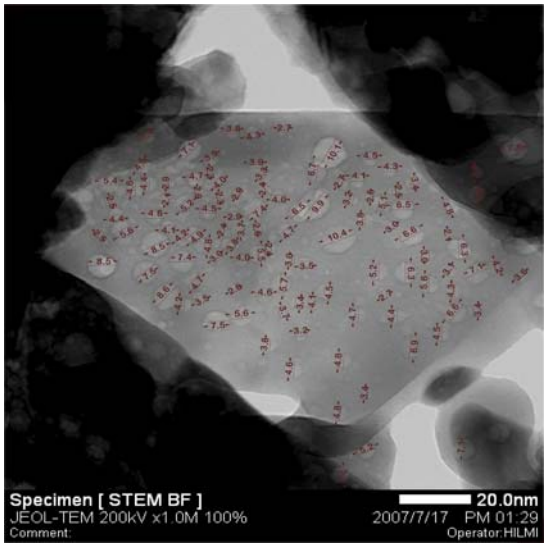

Figure 4.59 TEM micrograph of the sample (A1) which was microwave synthesized at 850 W for 5 minutes only.

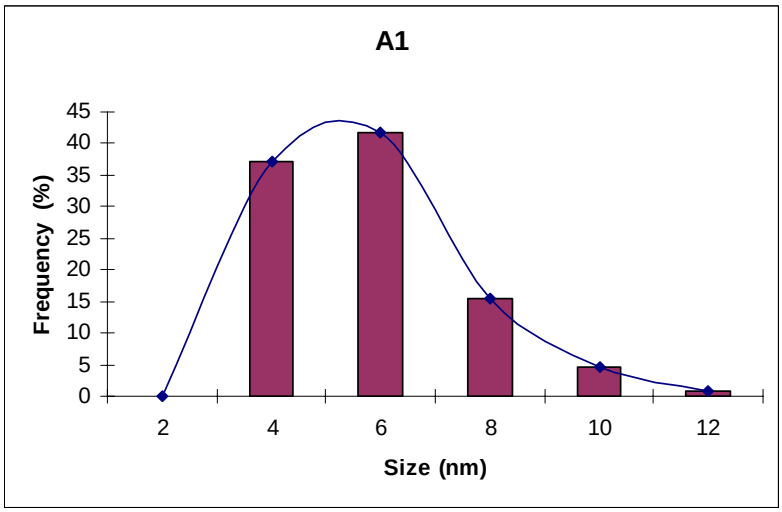

Figure 4.60 Particle size distribution of the sample A1 which was microwave synthesized at 850 W for 5 minutes only.

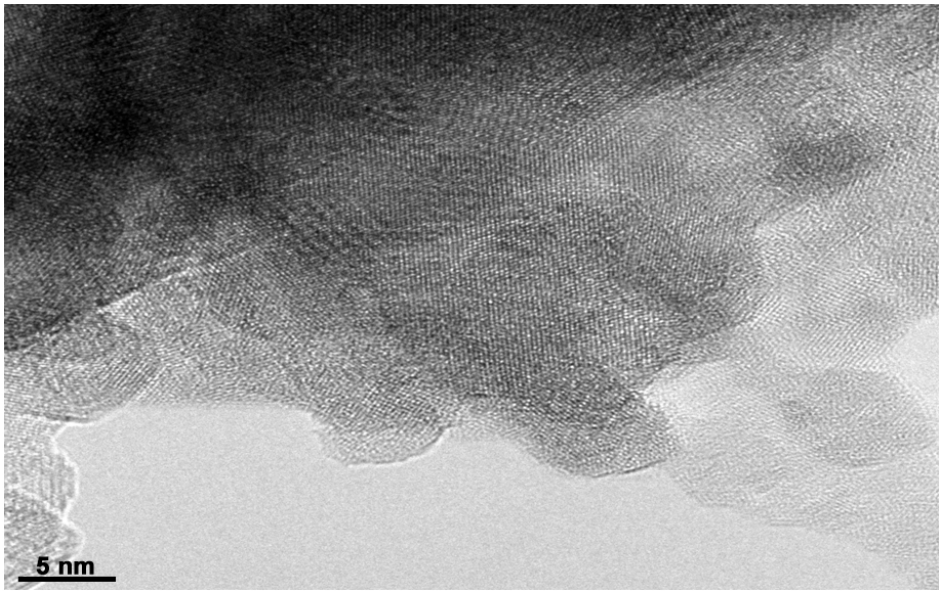

Figure 4.61 HRTEM micrograph of the sample (C1) which was microwave synthesized at 850 W for 15 minutes only.

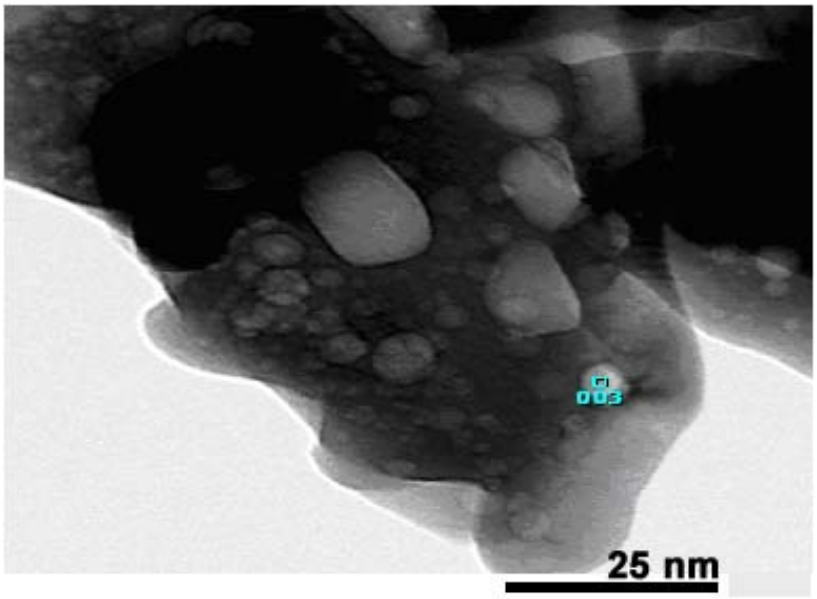

Figure 4.62 TEM micrograph of the sample (A1) which was microwave synthesized at 850 W for 5 minutes only.

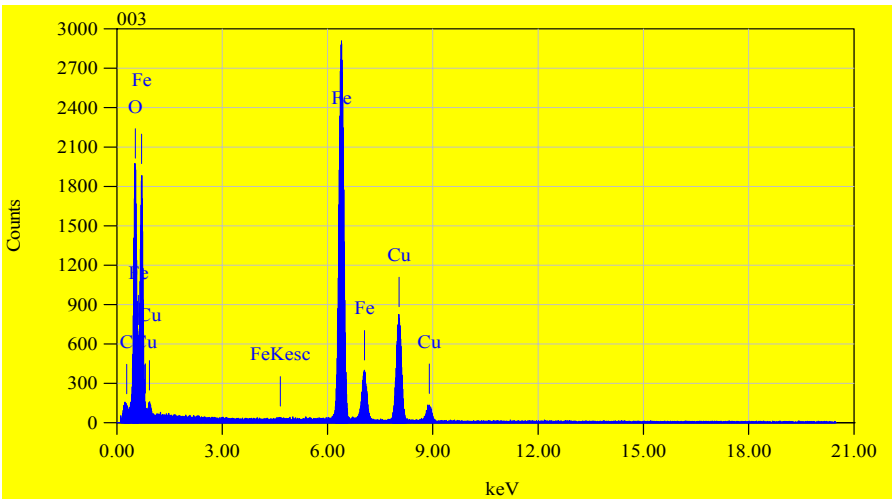

Figure 4.63 EDX pattern of sample A1 which was microwave synthesized at 850 W for 5 minutes only.

Electron diffraction studies were conducted for some of the microwave samples. Figure 4.64 is the TEM micrograph of the A3 sample which was microwave synthesized for 5 minutes at 850 W and heat treated at 230 °C for 48 h and its

diffraction pattern. Table 4.13 shows theoretical interplanar spacing (d) values of maghemite nanoparticles.

The theoretical and measured interplanar spacing values are in good agreement with maghemite, therefore it can be said that the observed ring pattern belongs to the maghemite phase. Ring pattern reveals a fine crystallite size for the investigated sample which supports the particle sizes obtained from XRD patterns.

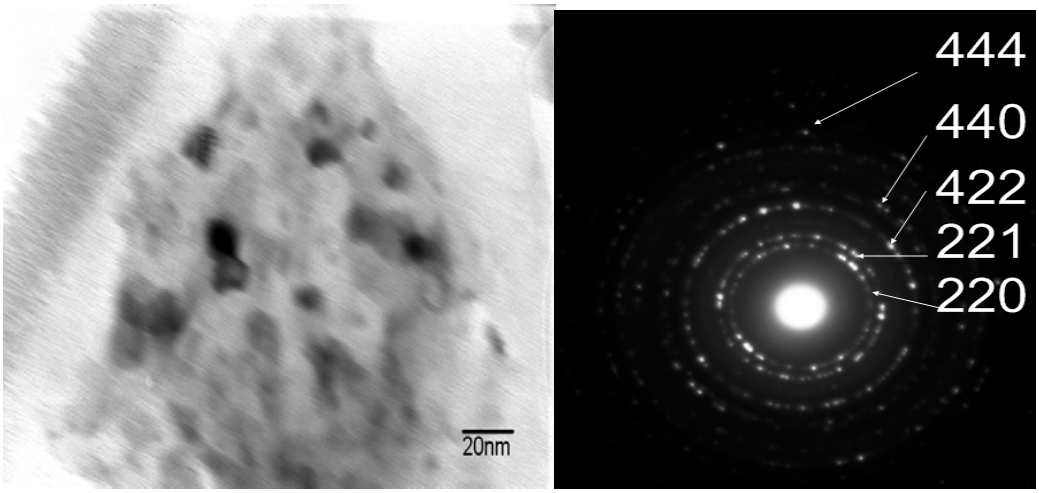

Figure 4.64 TEM micrograph of the sample (A3) which was microwave synthesized at 850 W for 5 minutes and heat treated at 230 °C for 48 h and its diffraction pattern.

Table 4.13 Electron diffraction (ED) results for the maghemite nanoparticles obtained for the sample which was microwave synthesized at 850 W for 5 minutes and heat treated at 230 °C for 48 h (Figure 4.64).

	1	2	3	4	5
Measured ED results - d (Å)	2.92	2.75	1.71	1.46	1.20
Theoretical values - d (Å)	2.95	2.78	1.70	1.47	1.20
Crystalline plane (hkl)	(220)	(221)	(422)	(440)	(444)

TEM study was also performed for the sample which was microwave processed for 3 minutes at 810 W (Figure 4.65). Table 4.14 and 4.15 show the theoretical interplanar spacing (d) values of maghemite nanoparticles of that sample. Calculations were done according to Eq. 4.3 indicating that these values belong to maghemite phase similar to Figure 4.64 and the diffraction patterns also reveal a fine crystallite size.

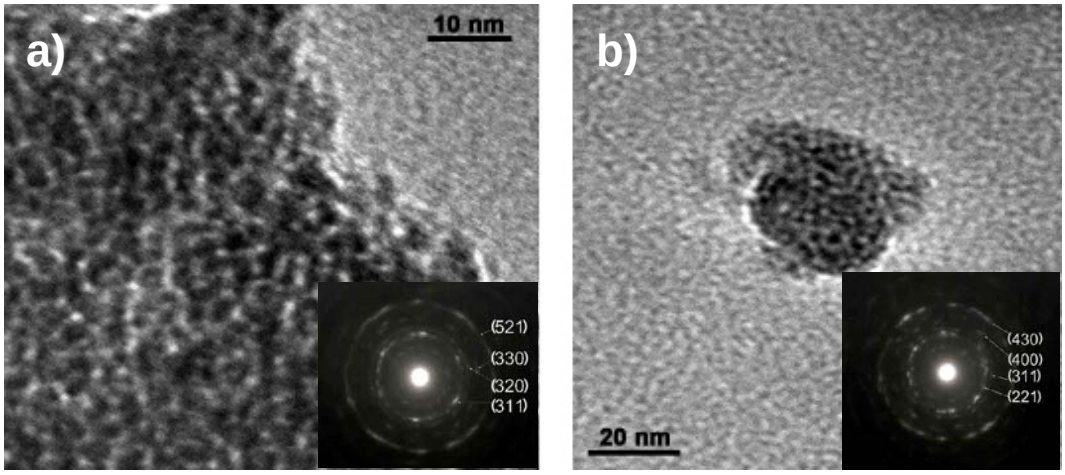

Figure 4.65 a-b. TEM micrographs and diffraction patterns of the sample which was microwave synthesized at 810 W for 3 minutes.

Table 4.14 Electron diffraction (ED) results for the maghemite nanoparticles shown in Figure 4.65.a.

	1	2	3	4
Measured ED results-d(Å)	2.58	2.29	1.95	1.51
Theoretical values-d(Å)	2.51	2.31	1.96	1.52
Crystalline plane (hkl)	(311)	(320)	(330)	(521)

Table 4.15 Electron diffraction (ED) results for the maghemite nanoparticles shown in Figure 4.65.b.

	1	2	3	4
Measured ED results-d(Å)	2.78	2.51	2.09	1.68
Theoretical values-d(Å)	2.78	2.51	2.08	1.67
Crystalline plane (hkl)	(221)	(311)	(400)	(430)

4.3.3 Magnetic Characterization (VSM)

Magnetic measurements for the microwave processed samples were performed at different temperatures from 100 K to 350 K in order to get more information about the magnetic beahvior of these nanoparticles. Figure 4.66 shows M–H curves (Magnetization vs. Applied Magnetic Field) for the samples A1 and A2 at 300 K. Sample A1 is the sample which was microwave synthesized at 850 W for 5 minutes only and sample A2 is the sample microwave synthesized at 850 W for 5 minutes and heat treated at 230 °C for 24 h. Figures 4.67 and 4.68 are M–H curves (Magnetization vs. applied magnetic field) for samples A1 and A2 at different temperatures. The magnetization curves for sample A1 and A2 obtained at 350 K and lower temperatures have no hysteresis loops and coercive fields approach to zero, indicating that these samples A1 and A2 show S-shaped magnetic behavior for all the temperature ranges studied in accordance with their calculated particle sizes (2.7 nm and 3.4 nm) due to the nanoscale dimensions and surface effects of particles. It is well known that superparamagnetism is dependent with the critical size for the single domain structure. As a particle becomes smaller than the critical size, its coercivity decreases and the particle becomes superparamagnetic due to thermal effects [120, 121]. The typical value of the critical size is about 16 nm for Fe [45] and 28 nm for γ-Fe_2O_3 maghemite particles [117]. For sample A2, magnetization curves depicted a slight decrease in saturation magnetization value when compared to pure maghemite

sample A1 (Fig. 4.67), because the sample A2 contained both maghemite and hematite phases. Observed saturation magnetization values (M_S) from the Figures 4.67 and 4.68 for the samples A1 and A2 at 100 K are ~4 and ~3 emu/g, respectively. In the literature different synthesis methods yield different Ms values of ~8, 1, and 2 emu/g for 10–12 nm (mechanical activation) [65], 3–5 nm (microwave irradiation) [72] and 9–10 nm (sol–gel) [88] sized γ-Fe_2O_3 particles, respectively. On the other hand, 2–3 nm sized amorphous iron oxide obtained by microwave heating has much lower M_S value as 0.4 emu/g [122].

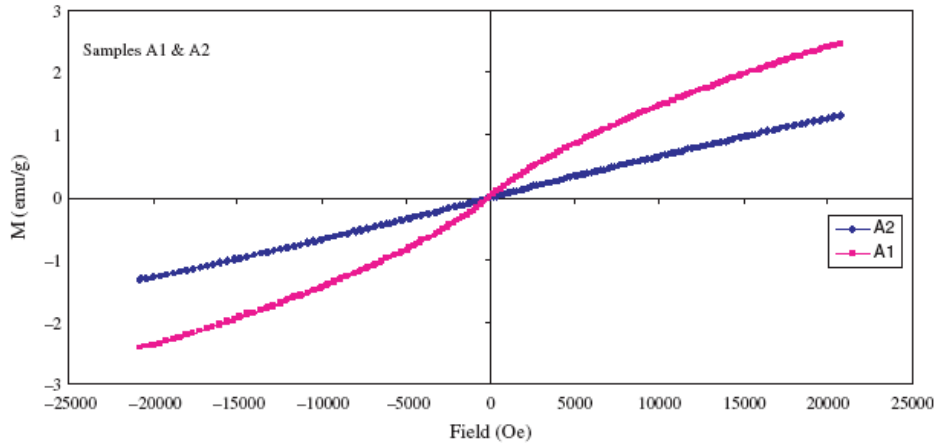

Figure 4.66 M–H curves obtained at 300 K for sample A1 which was microwave synthesized for 5 minutes only and sample A2 which is the sample microwave synthesized for 5 minutes and heat treated at 230 °C for 24 h.

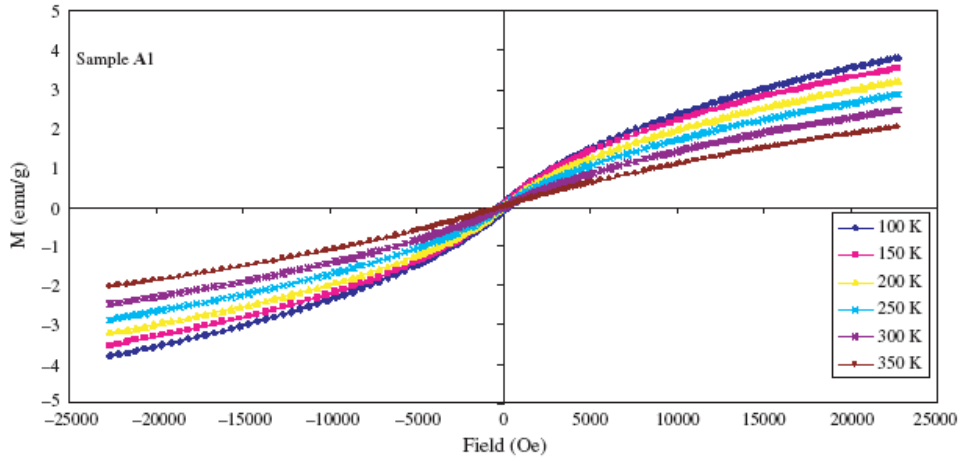

Figure 4.67 M–H curves obtained at different temperatures for sample A1 which is the sample microwave synthesized for 5 minutes only.

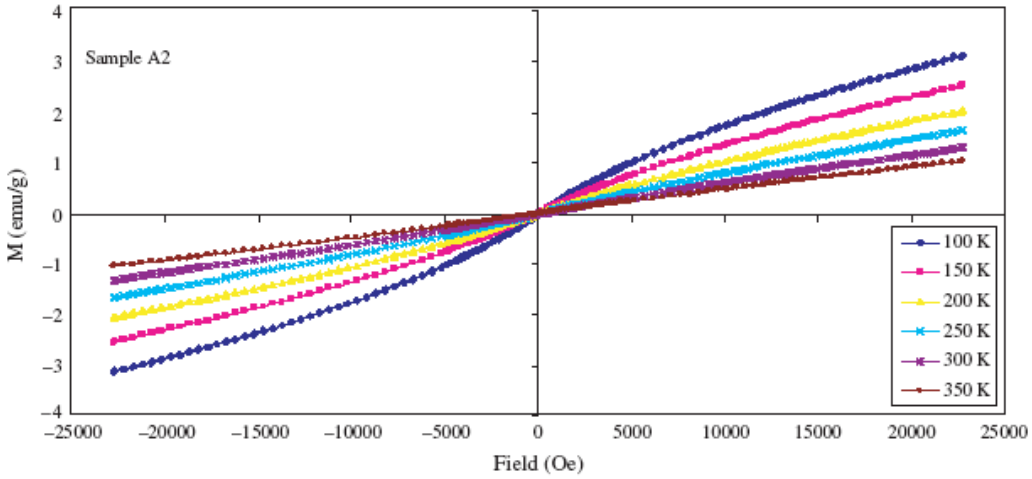

Figure 4.68 M–H curves obtained at different temperatures for sample A2 which is the sample microwave synthesized for 5 minutes and heat treated at 230 °C for 24 h.

Magnetic measurements at different temperatures from 100 K to 298 K were performed for the other samples which are synthesized at microwave powers of 630, 720, 810 and 900 W and figures 4.69-4.79 are the M-H curves, M - H/T curves and FC (Field Cooled) – ZFC (Zero Field Cooled) curves of these samples. Zero-field cooled (ZFC) susceptibilities were measured by cooling the samples in zero magnetic field and then by increasing the temperature in an applied field of 100 Oe, while field-cooled (FC) curves were recorded by cooling the samples in an applied field of 100 Oe. Although they do not exhibit hysteresis loops, they lack to show a perfect S-shaped character in their M-H curves. Their M – H/T curves do not coincide fully on each other. All these magnetic behavior indicate that these particles show higher paramagnetic behavior rather than superparamagnetic behavior. Their M-T curves also did not yield a blocking temperature which is an indication of superparamagnetic range above this temperature. However, all these samples have the particle sizes generally less than 5 nm except longer microwave treated samples (Table 4.11). They are well below the superparamagnetic critical size limit, but their crystallinity was not pronounced as in the case of sol-gel processed samples, resulting such behavior of magnetic character.

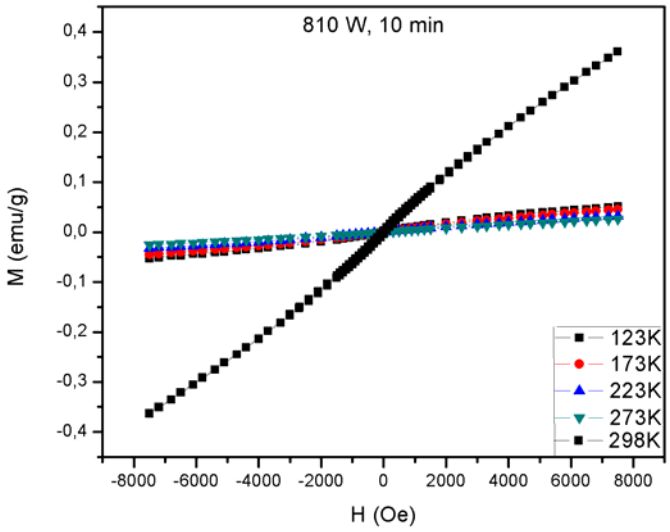

Figure 4.69 M–H curves obtained at different temperatures for the sample which was microwave synthesized at 810 W for 10 minutes.

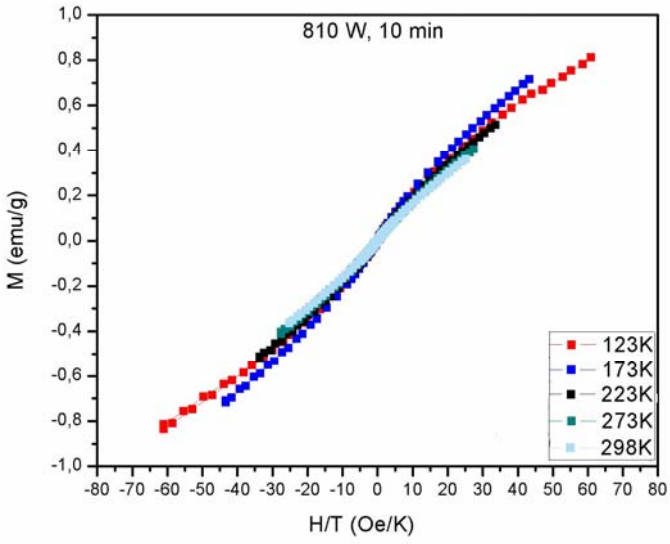

Figure 4.70 M - H/T curves obtained at different temperatures for the sample which was microwave synthesized at 810 W for 10 minutes.

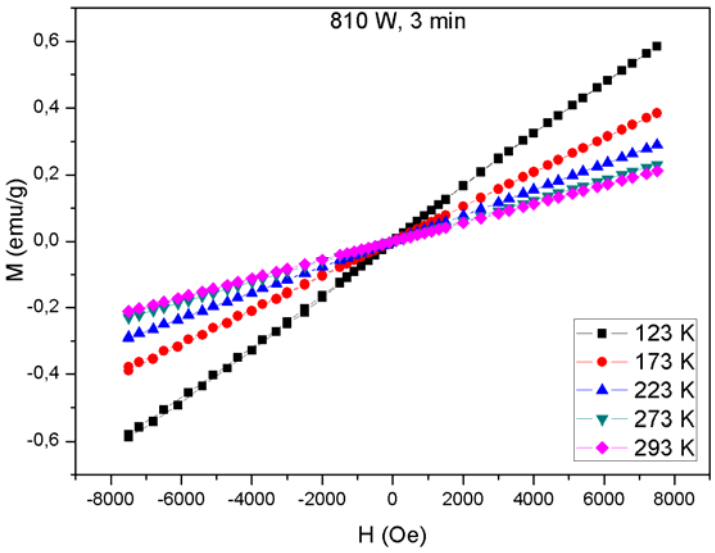

Figure 4.71 M–H curves obtained at different temperatures for the sample which was microwave synthesized at 810 W for 3 minutes.

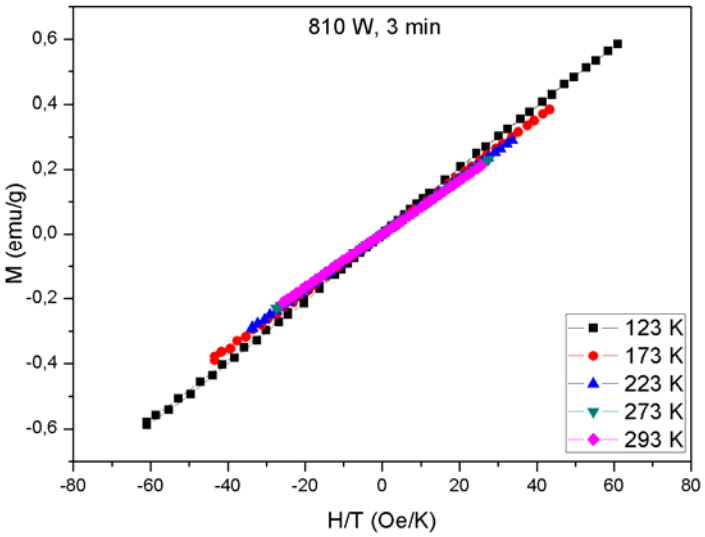

Figure 4.72 M - H/T curves obtained at different temperatures for the sample which was microwave synthesized at 810 W for 3 minutes.

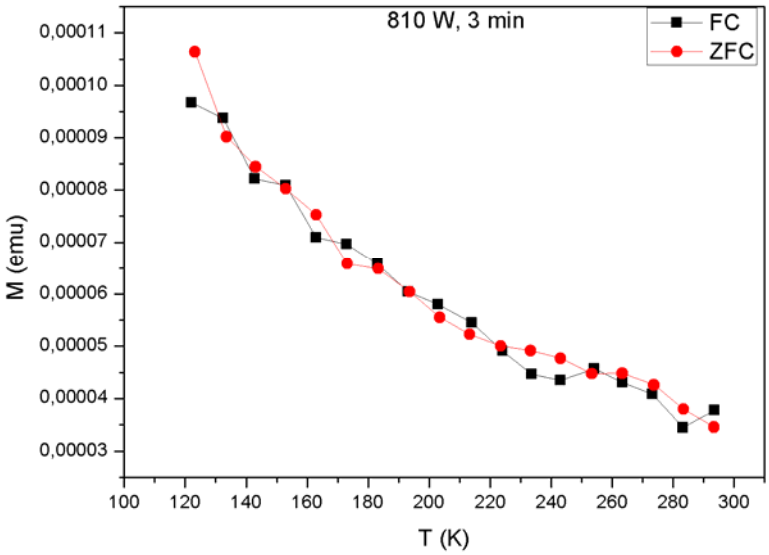

Figure 4.73 M-T curves for the sample which was microwave synthesized at 810 W for 3 minutes using zero field cooling and field cooling procedures at the applied field of 100 Oe.

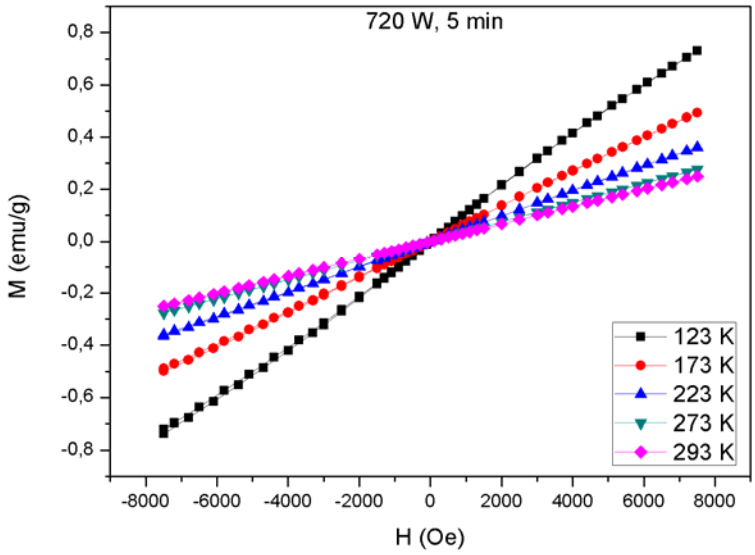

Figure 4.74 M–H curves obtained at different temperatures for the sample which was microwave synthesized at 720 W for 5 minutes.

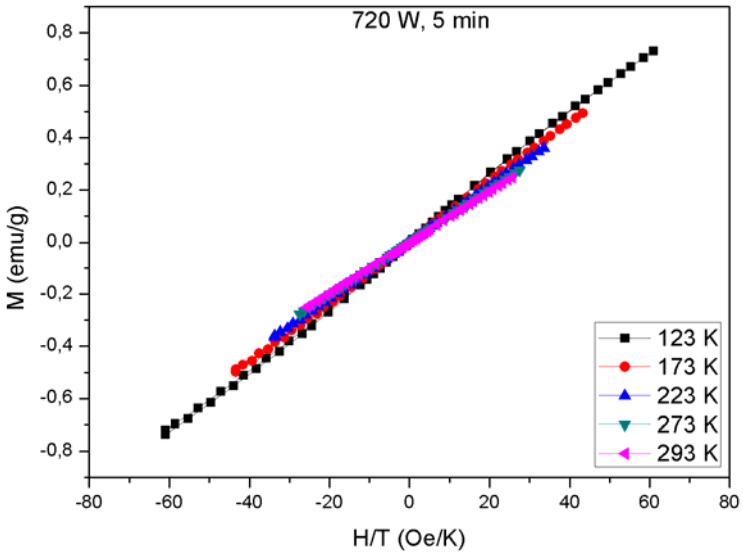

Figure 4.75 M - H/T curves obtained at different temperatures for the sample which was microwave synthesized at 720 W for 5 minutes.

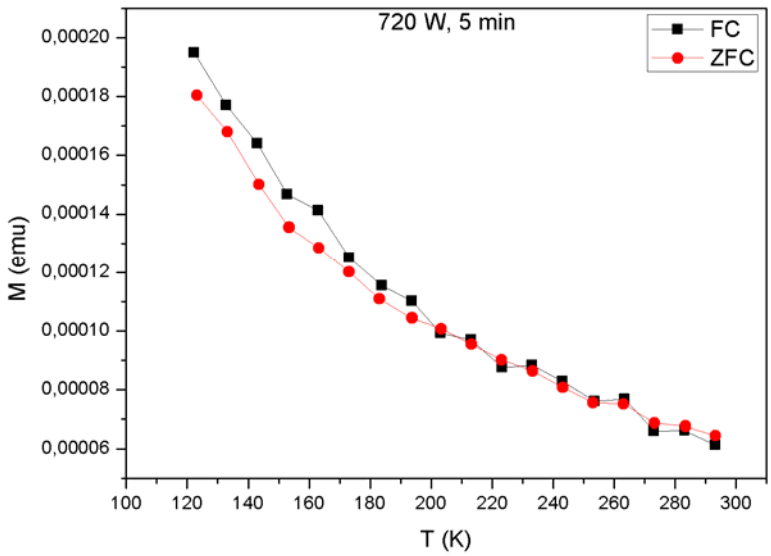

Figure 4.76 M-T curves for the sample which was microwave synthesized at 720 W for 5 minutes using zero field cooling and field cooling procedures at the applied field of 100 Oe.

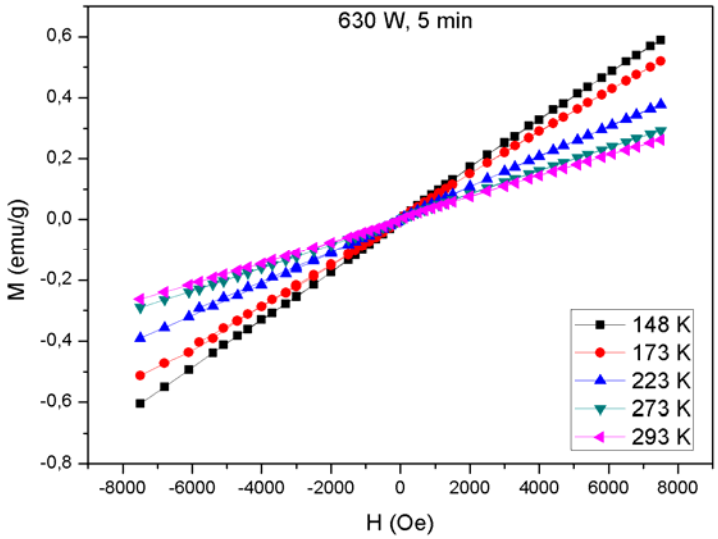

Figure 4.77 M–H curves obtained at different temperatures for the sample which was microwave synthesized at 630 W for 5 minutes.

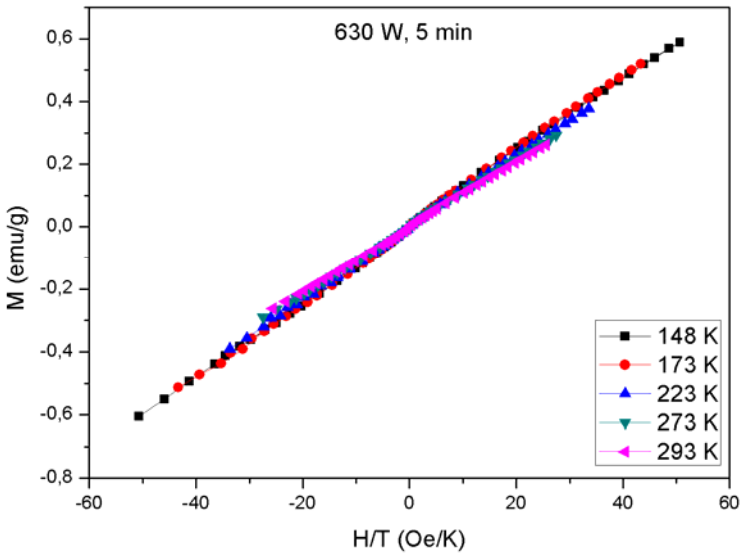

Figure 4.78 M - H/T curves obtained at different temperatures for the sample which was microwave synthesized at 630 W for 5 minutes.

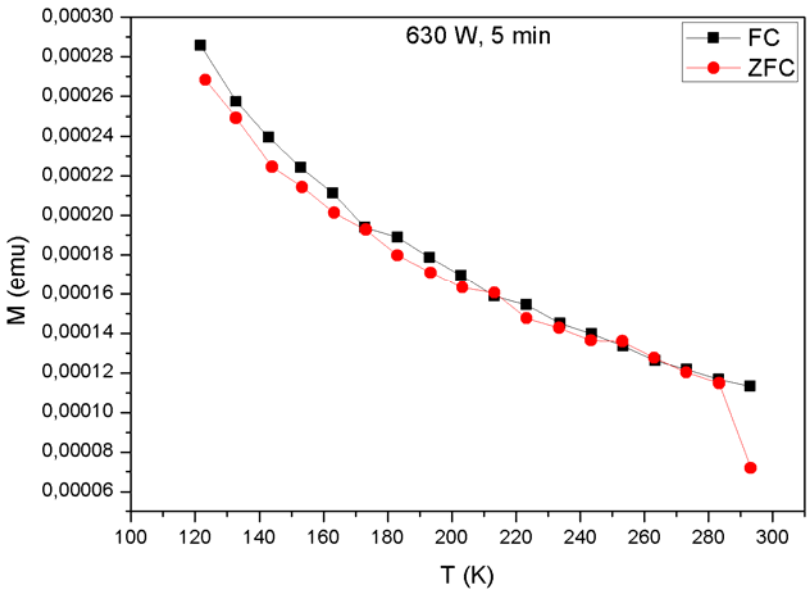

Figure 4.79 M-T curves for the sample which was microwave synthesized at 630 W for 5 minutes using zero field cooling and field cooling procedures at the applied field of 100 Oe.

Microwave oven was modified to increase its effectiveness for longer treatments to overcome the difficulty of lacking perfect crystallinity and different series of samples were prepared by using different combinations of microwave powers and durations that yielded a change in magnetization results as given Figures 4.80-4.87, which are the M-H curves and M - H/T curves of the samples produced by modified microwave oven.

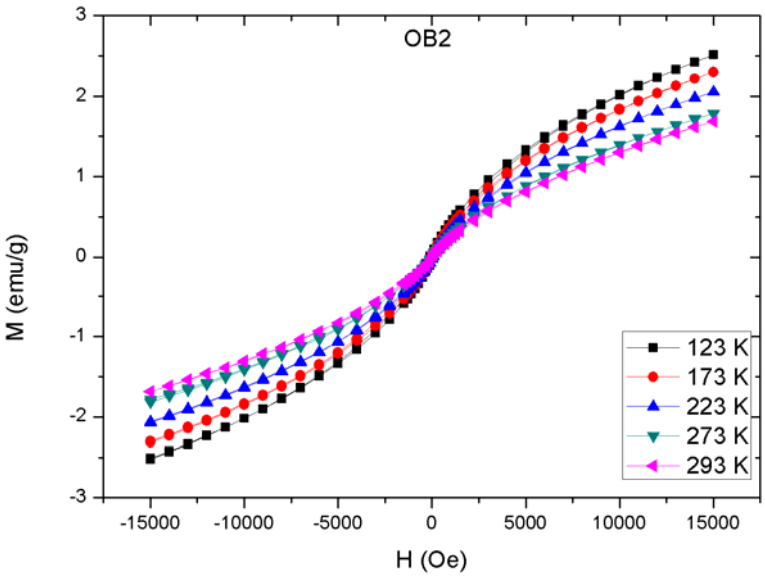

Figure 4.80 M–H curves obtained at different temperatures for sample which was microwave processed in the modified oven at 900 W for 20 min and heat treated in the furnace at 200 °C for 24h.

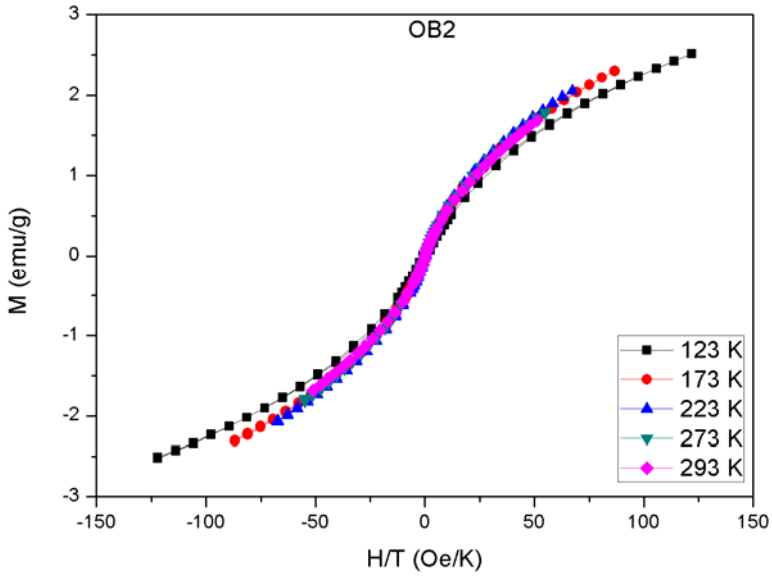

Figure 4.81 M-H/T curves obtained at different temperatures for sample which was microwave processed in the modified oven at 900 W for 20 min and heat treated in the furnace at 200 °C for 24h.

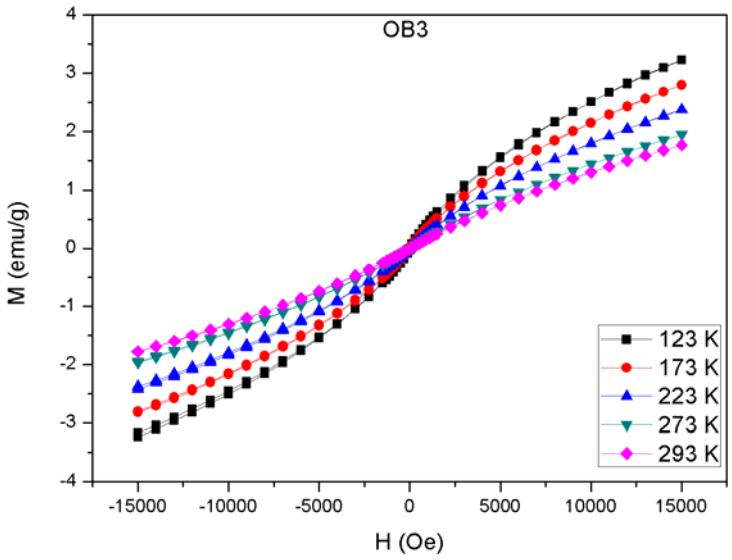

Figure 4.82 M–H curves obtained at different temperatures for sample which was microwave processed in the modified oven at 900 W for 20 min and heat treated in the furnace at 200 °C for 3h.

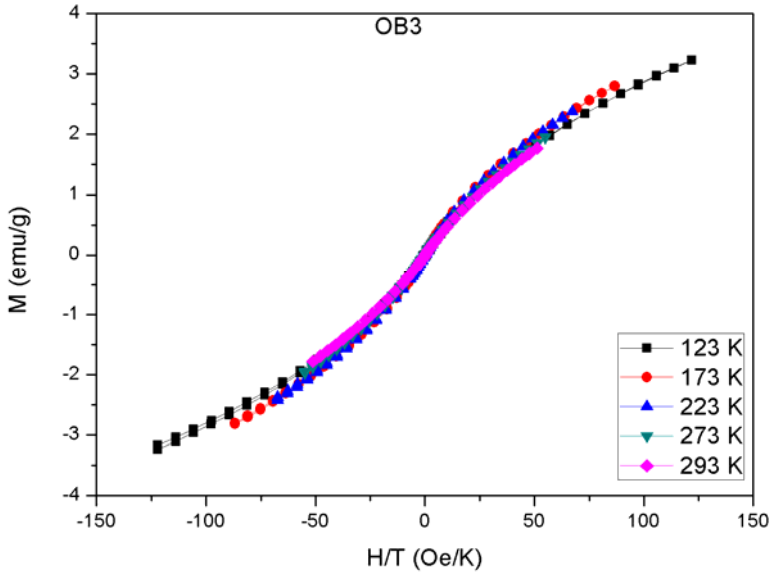

Figure 4.83 M-H/T curves obtained at different temperatures for sample which was microwave processed in the modified oven at 900 W for 20 min and heat treated in the furnace at 200 °C for 3h.

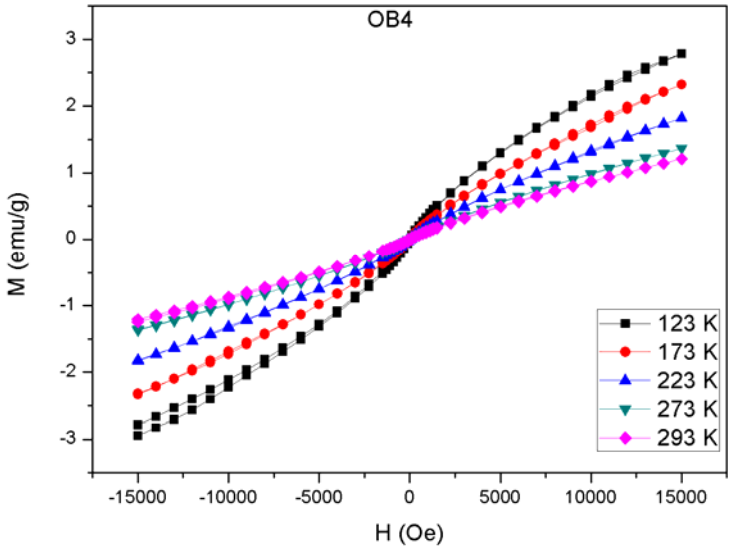

Figure 4.84 M–H curves obtained at different temperatures for sample which was microwave processed in the modified oven at 900 W for 30 min.

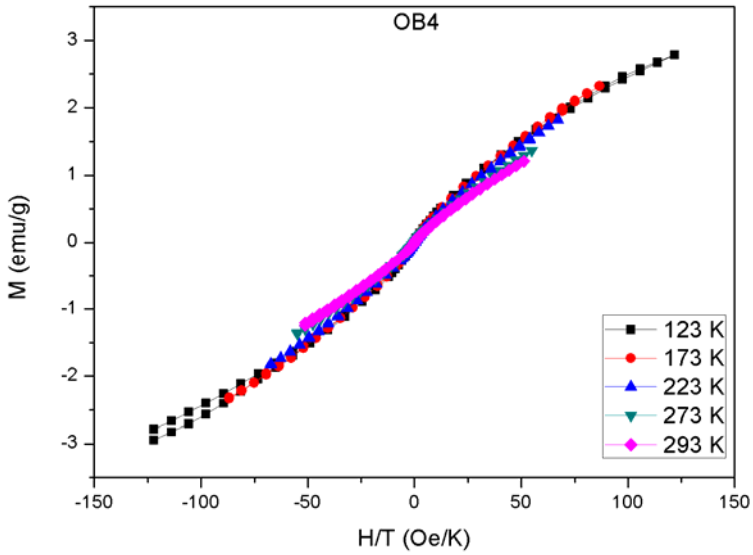

Figure 4.85 M-H/T curves obtained at different temperatures for sample which was microwave processed in the modified oven at 900 W for 30 min.

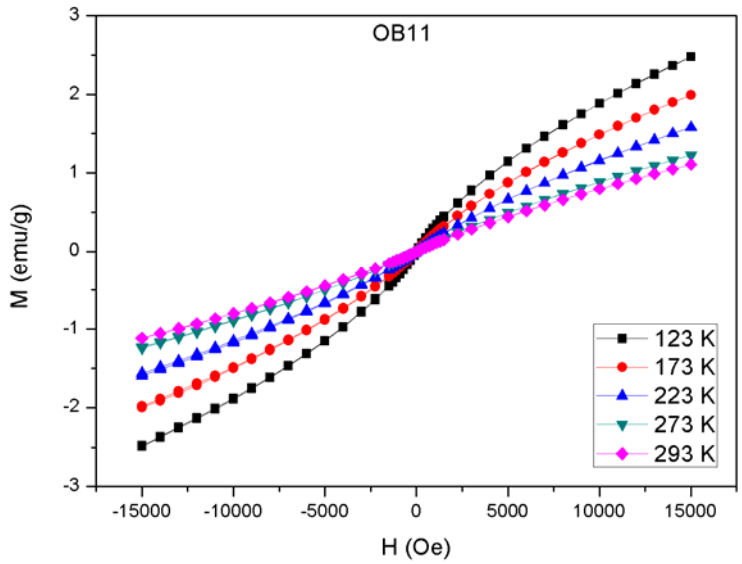

Figure 4.86 M–H curves obtained at different temperatures for sample which was microwave processed in the modified oven at 810 W for 5 min.

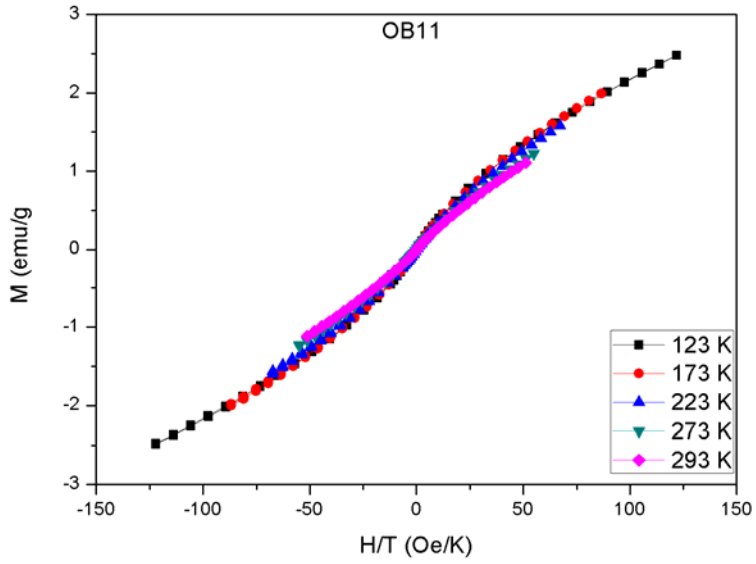

Figure 4.87 M-H/T curves obtained at different temperatures for sample which was microwave processed in the modified oven at 810 W for 5 min.

By looking at the magnetization results it was observed that the magnetic behaviors of lastly prepared modified microwave samples are different from than that of the previous microwave samples; they are not paramagnetic, their M-H curves have the S-shape but their saturation magnetization values are smaller with the value of about 3 emu/g when compared to sol-gel samples (highest value 28 emu/g in Table 4.6). These magnetic characteristics indicate that the crystallinity becomes better in the modified microwave processing, but still most of the samples contain both maghemite and hematite phases together (Figure 4.57). Longer microwave treatment periods cause an increase both in the particle size and the amount of hematite, which affects the magnetic properties adversely.

CHAPTER 5

SUMMARY

In this study main aim is to produce maghemite nanoparticles that exhibit superparamagnetic behavior which are generally intended for use in biomedical applications, especially in magnetic resonance imaging (MRI) as contrast agents and for drug delivery in chemotheraphy and hyperthermia treatment of cancer. When these nanoparticles are superparamagnetic, there will be no residual magnetization in the human body after MRI applications. Particles have to be composed of smaller sized nanoparticles for superparamagnetic behavior. In the literature the critical value of superparamagnetism is about 10 nm for the maghemite nanoparticles.

It is difficult to produce maghemite phase since its stability doesn't exist when the particle size becomes larger. Maghemite phase turns into hematite phase that is thermodynamically stable when the particle size increases. There are various different techniques that are used for the production of this material. Some of them are sol-gel, homogeneous precipitation, mechanical processing and microwave methods. Usually maghemite nanoparticles are stabilized by using polymeric, glass or ceramic matrix. Generally for metal or metal oxide nanoparticles, sol-gel matrices are used since they have many advantages over other methods.

In this thesis, firstly sol-gel method was employed by using tetraethoxysilane (TEOS) to produce maghemite nanoparticles. Different metal salts were used and the nitrate salts yielded better results. Approximate particle sizes of these samples lie between 12.0-23.4 nm. Samples that heat treated at 400 °C contain maghemite and hematite phases together, on the other hand in the samples that heat treated at 900

°C, a different phase, fayalite, was observed together with the hematite phase. Probably it is due to the reaction with the matrix. From the magnetization measurements saturation magnetization values are obtained between 4 -12 emu/g. The saturation magnetization values are below the reported value for bulk γ-Fe_2O_3 (74 emu/g), but these values are in fairly good agreement with the values measured in γ-Fe_2O_3 particles of similar size given in the literature. Surface and finite size effects have been reported as being responsible for the decrease in the magnetic properties of nanoparticles.

Another sol-gel method was used in order to obtain maghemite phase with desired magnetic properties. In the literature sol gel derived maghemite nanoparticles are prepared by using TEOS generally. Ethylene glycol was used as starting material as different from the classical sol-gel method. In this case there is no hydrolysis and condensation reaction. Instead of ethylene glycol, diethylene glycol was also used for some of the samples. The aim of using this material is to decrease the particle size. Samples were heated at different temperatures up to 700 °C and they contained both maghemite and hematite phases and showed superparamagnetic behavior.

The particle sizes were generally below 10 nm, although there were some particles greater than 10 nm and having larger particle sizes for the case of ethylene glycol-diethylene glycol route of sol-gel processing. However, all TEM images indicate that these particles are spherical and show 3-dimensional assemblies demonstrating the uniformity of the nanoparticles. Electron diffraction, X-ray diffraction, and high resolution transmission electron microscope (HRTEM) images of the nanoparticles showed the highly crystalline nature of the γ-Fe_2O_3 structures. From the electron diffraction study, it is observed that interplanar spacing (d) values of the ethylene glycol sample matched with the maghemite phase. Also quantitative analysis were applied to these samples.

M-H (M: Magnetization, H: Applied Magnetic Field) curves of the samples exhibited no hysteresis at all the temperature ranges. M_s (saturation magnetization) value was found as 28 emu/g for the ethylene glycol sample heat trated at 300 ^{0}C as

the highest magnetization value due to having the highest amount of maghemite phase in this sample with respect to the other samples with the value of 80 %. M_s values were found as approximately 27, 22 and 16 emu/g for the diethylene glycol samples heat treated at 300, 350 and 400 °C, respectively. The saturation magnetization values of these samples processed by diethylene glycol are also quite high when compared with the results of the sol-gel processed samples from the literature such as 8 emu/g as the maximum value of saturation magnetization (M_s).

Two key qualities remain for a superparamagnetic system: 1) lack of hysteresis and 2) data of different temperatures superimpose onto a universal curve of M versus H/T. From the results for sol-gel processed samples, it can be concluded that the samples that were heat treated at 300, 350 and 400 °C, show superparamagnetic behaviour.

VSM results of the samples heat treated at 500, 700 and 750 °C showed different magnetic properties than the other samples due to containing mainly hematite phase. The diethylene glycol samples heat treated at 500, 700 and 750 °C exhibited Morin temperatures in the range 260-273 K and this variation is attributed to the variation in the particle sizes and they yield M-H curves with a paramagnetic slope at lower temperatures (123, 173 and 223 K), on the other hand at 273 and 293 K the same samples showed a hysteretic behaviour according to magnetic measurements. This transition in magnetic behavior is attributed to Morin transition in the hematite phase

Observed experimental results show that the magnetizations of nanoparticles produced in this study originate from two contributions;

- one due to the superparamagnetic particles and
- the other due to the blocked particles.

Superparamagnetic part can be described by Langevin function $L(x) = \coth(x) - \frac{1}{x}$ from a minimum particle size up to a critical size, and the blocked part can be described by hyperbolic tangent function (tanh(x)) from the critical size up to a maximum particle size. This distribution was also proved by the TEM micrographs.

Best fit was obtained when it is assumed that there is a size distribution of particles. According to this assumption smaller particles behave as superparamagnetic and described by Langevin function, on the other hand larger blocked particles described by tangent hyperbolic function.

Also the ratios of the fitting parameters for the Langevin function and the tangent hyperbolic function at different temperatures are matching with the amount of the phases present in the samples, because it was thought that maghemite phase provides the superparamagnetic contribution to the magnetic behavior of the sample.

In this study blocking temperatures, where the whole sample becomes superparamagnetic above this temperature and the particles are free to align with the field during the measurement period, were found as approximately 220 K, 300 K and 300 K for the samples heat treated at 300, 350 and 400 °C, respectively using M-T curves (M: Magnetization, T: Temperature). T_B was found approximately as 265 K for the ethylene glycol sample of sol-gel processing. These results show that these samples behave superparamagnetically at the room temperature. Since the aim of the study is to produce maghemite nanoparticles that can be used in biomedical applications at room temperature, the results obtained seem to be quite satisfactory.

It is considered that ethylene glycol-diethylene glycol route of sol-gel method was better than the conventional one, because the preparation period was easier than that of the TEOS route, also results are satisfactory from the magnetization point of view.

It was found in the literature that applied magnetic field strength and frequency as well as particle properties such as particle size and anisotropy constant strongly influence power output for chemotheraphy and hyperthermia treatment of cancer; the highest power output is obtained in a relatively narrow particle size range. The particle sizes obtained in this study are generaly less than the superparamagnetic size limit which was determined as 28 nm for γ-Fe_2O_3 maghemite particles [45]. Therefore, the maghemite nanoparticles produced by ethylene glycol-diethylene

glycol route of sol-gel processing are feasible to be used in combined hyperthermia and chemotherapy applications.

Another method to prepare the maghemite nanoparticles is the microwave method. In the literature it is reported that microwave radiation has many advantages and little work has been reported on the maghemite material. So by using this technique it was aimed to obtained small sized superparamagnetic maghemite nanoparticles. The experimental procedure seems quite simple but it was difficult to obtain the maghemite phase due to inhomogeneity of the power distribution in the domestic microwave oven used in this study. Several different microwave powers and durations were applied to prepare the samples. Most of the samples contain maghemite and hematite phases together and particle sizes are between 3 – 30 nm. The TEM images of microwave processed samples also indicate that average particle size is about 5 nm and the particles show a narrow size distribution which is an important parameter for biomedical applications.

It was considered that microwave radiation is not effective enough for the preparation of the samples, so the domestic oven was modified and different series of samples were prepared by using different combinations of microwave power and durations. This time magnetization results were changed. But saturation magnetization values of these microwave samples were lower than that of the sol-gel samples. Sol-gel samples have the saturation values about 28 emu/g, whereas microwave samples have this value about 3 emu/g. The main point about this method is the crystallinity of the samples. Short microwave treatment periods yielded maghemite particles, however their crystallinity were not pronounced as compared to sol-gel samples. Some of the samples were well crystalline, but in this case size of the particles became quite large which affects the magnetic properties adversely.

Although both techniques are quite facile, sol-gel method in which ethylene glycol and diethylene glycol are the starting materials is more advantageous than the microwave method due to magnetic characterization results which are the main parameter for the biomedical applications.

CHAPTER 6

CONCLUSIONS AND FURTHER SUGGESTIONS

- Firstly sol-gel method was employed by using tetraethoxysilane (TEOS) to produce maghemite nanoparticles. Different metal salts were used and the nitrate salts yielded better results.

- The saturation magnetization values of the first sol-gel method are below the reported value for bulk γ-Fe_2O_3 (74 emu/g), but these values are in fairly good agreement with the values measured in γ-Fe_2O_3 particles of similar size given in the literature. Surface and finite size effects have been reported as being responsible for the decrease in the magnetic properties of nanoparticles.

- In the second sol-gel route ethylene glycol and diethylene glycol were used as the starting materials. The particle sizes for the case of ethylene glycol-diethylene glycol route of sol-gel processing were generally below 10 nm and samples have good crystallinity.

- The saturation magnetization values of the samples processed by ethylene glycol-diethylene glycol route are quite high when compared with the results of the sol-gel processed samples from the literature.

- It is considered that ethylene glycol-diethylene glycol route of sol-gel method was better than the conventional one, because the preparation period was easier than that of the TEOS route, also results are satisfactory from the magnetization point of view.

- The maghemite nanoparticles produced by ethylene glycol-diethylene glycol route of sol-gel processing are feasible to be used in combined hyperthermia and chemotherapy applications.

- Another method to prepare the maghemite nanoparticles is the microwave method. The experimental procedure seems quite simple but it was difficult to obtain the maghemite phase due to inhomogeneity of the power distribution in the domestic microwave oven used in this study.

- The main point about microwave method is the crystallinity of the samples. Short microwave treatment periods yielded maghemite particles, however their crystallinity were not pronounced as compared to sol-gel samples.

- Although both techniques are quite facile, sol-gel method in which ethylene glycol and diethylene glycol are the starting materials is more advantageous than the microwave method due to magnetic characterization results which are the main parameter for the biomedical applications.

- However, more work is required to understand the formation mechanisms and characterization results of these magnetic nanoparticles; namely systematic TEM study is required for the complete statistical distribution of these nanoparticles and VSM work down to liquid helium temperatures is required for full magnetic characterization especially for the determination of blocking temperatures.

REFERENCES

1. R. Kelsall, I. Hamley, M. Geoghegan, Nanoscale Science and Technology, John Wiley & Sons, UK, 2005.
2. G. Cao, Nanostructures & Nanomaterials, Imperial College Press, London, 2004
3. C. P. Poole Jr., F. J. Owens, Introduction to Nanotechnology, John Wiley & Sons, New Jersey, 2003.
4. S. P. Gubin, Magnetic Nanoparticles, Wiley-VCH Verlag GmbH&Co. KGaA, Weinheim, 2009.
5. J. E. Macdonald, Synthesis and Application of Iron containing Nanoparticles, PhD. Thesis, University of Alberta, Canada, 2008.
6. C. Savii, M. Popovici, C. Enache, J. Subrt, Solid State Ionics, 151, 219, 2002.
7. A. Millan, F. Palacio, A. Falqui, E. Snoeck , Acta Materialia,55, 2201, 2007.
8. D. C. Culita, G. Marinescu, L Patron, O. Carp, Materials Chemistry and Physics , 111, 381, 2008
9. S. Asua, S. Zhao, H. Y. Wu , L. Song, O. Tegus, Journal of Alloys and Compounds, 472, L24, 2008.
10. S. Solinas, G. Piccaluga, M. P. Morales, C. J. Serna, Acta Materialia, 49, 2805, 2001
11. Y. K. Sun, M. Ma, Y. Zhang, N. Gu, Colloids and Surfaces A: Physicochem. Eng. Aspects, 245, 15, 2004.
12. C. Cannas, G. Concas, D. Gatteschi, A. Falqui, Phys. Chem., Chem. Phys., 3, 832, 2001.
13. S. Lefebure, E. Dubois, V. Cabuil, J. Mater . Res. 13, 2975, 1998.
14. A. S. Edelstein, R. C. Cammarata, Nanomaterials: Synthesis, Properties and Applications, Institute of Physics Publishing, Bristol, 1996.
15. P. Hollister, J. W. Weener, C. R. Vas, T. Harper, Nanoparticles Technology White Papers, 3, Cientifica Ltd., 2003.

16. A. I. Gusev, A. A. Rempel, Nanocrystalline Materials, Cambridge International Publishing, 2004.
17. R. M. Cornell and U. Schwertmann, The Iron Oxides: Structure, Properties, Reactions, Occurences and Uses. 2nd ed.: WILEY-VCH GmbH & Co. KGaA, Weinheim, 2003.
18. G. Kletetschka et al., Physics of the Earth and Plenetary Interiors, 119,259, 2000.
19. Mineralogy Database, http:// www.webmineral.com/ last accessed on 23. 07.2010
20. R. E. Vandernberghe, E. Van San, E. De Grave, Czechoslovak Journal of Physics, 51, 663, 2001.
21. T. P. Raming, A. J. A. Winnubst, C. M. V. Kats, A. P. Philipse, Journal of Colloid and Interface Science, 249,346, 2002.
22. G. Kim, K. H. Han, C. H. Lee, J. Y. Jeong, Journal of the Korean Physical Society, 38, 798, 2001.
23. E. L. Williamson, R. Venturini, R. A. Graham, B. Morosin, Pyhsical Review B, 34, 1899, 1986.
24. E. V. San, E. D. Grave, R. E. Vanderberghe, Journal of Magnetism and Magnetic Materials, 269, 54, 2004.
25. A. S. Teja, P. Y. Koh, Prog. Crys. Growth Charac. of Mater., 55, 22, 2009.
26. W. B. Mi, J. J. Shen, E.Y. Jiang, H. L. Bai, Acta Materialia 55, 1919, 2007.
27. G. Zhang, C. Fan, L. Pan, F. Wang, P. Wu, H. Qiu, Y. Gu, Y. Zhang, Journal of Magnetism and Magnetic Materials, 293, 737, 2005.
28. L. An, Z. Li, W.Li, Y. Nie, Z.Chen, Y. Wang, B. Yang, Journal of Magnetism and Magnetic Materials, 303,127, 2006.
29. Z. Mohammadi, In Stu Synthesis of Iron Oxide within Polvinlyamine Nanoparticles, M. S. Thesis, University of Tehran, 2008.
30. U. Schwertmann and R.M. Cornell, Iron Oxides in the Laboratory: Preparation and Characterization, Weinheim, New York, VCH, 1991.
31. E. Parton, G. Borghs, R. De Palma, Biomedical applications using magnetic nanoparticles,http://www.solidstate.com/display_article/302118/5/ARTCL/none/none/Biomedical-applications-using-magnetic nanoparticles/ last accessed on 23.07.2010

32. K.Gupta, S. Wells, IEEE Transactions on Nanobioscience, 3, 66, 2004.
33. F. H. Chen, Q. Gao, J. Z. Ni, Nanotechnology 19, 165103, 2008.
34. P. Tartaj, M. P. Morales, S. V. Verdaguer, T. G. Carreno, C. J. Serna, Synthesis, Properties and Biomedical Applications of Magnetic Nanoparticles, Handbook of Magnetic Materials, 16, Madrid, Spain, 2006.
35. G. S. Alvarez, Synthesis, Characterization and Applications of Iron Oxide Nanoparticles, PhD Thesis, University of Stockholm, 2004.
36. M. P. Morales, O. B. Miguel, R. P. Alejo, J. R. Cabello, Journal of Magnetism and Magnetic Materials, 266,102, 2003.
37. J. H. Kim, C. H. Lee, S. K. Lee, Bull. Korean Chem. Soc., 30, 1305, 2009.
38. O. B. Miguel, M. P. Morales, P. Tartaj, Biomaterials 26, 5695, 2005.
39. R. K. Singh, A. Srinivasan, G. P. Kothiyal, J. Mater Sci: Mater Med,20, S147, 2009.
40. D. L. Zhao, X. W. Zeng, Q. S. Xia, J. T. Tang, Journal of Alloys and Compounds, 469, 215, 2009.
41. Q. Song, Size and Shape Controlled Synthesis and Superparamagnetic Properties of Spinel Ferrites Nanocrystals, Georgia Institute of Technology, USA, 2005.
42. N. Poudyal, Synthesis and Characterization of Magnetic Nanoparticles, The University of Texas at Arlington, USA, 2005.
43. S. O. Kasap, Principles of Electronic Materials and Devices, McGraw Hill, New York, 2002.
44. A.E. Eken, Characterization of magnetite thin films produced by sol-gel processing, M. S. Thesis, Middle East Technical University, Turkey, 2008.
45. K. J. Klabunde, Nanoscale Materials in Chemistry, John Wiley&Sons, Inc., Publication, 2001.
46. W.D. Callister, Materials Science and Engineering an Introduction, John Wiley and Sons, New York, 2000.
47. P. Tartaj, M. P. Morales, S. V. Verdaguer, T. G. Carreno, C. J. Serna, J. Phys. D: Appl. Phys. 36, R182, 2003.
48. C. J. J. Den Quden, R. W. Thompson, J. Colloid Interface Sci., 143, 77, 1991.
49. N. Feltin, M. P. Pleni, Langmuir, 13, 3927, 1997.

50. G. Viau, F. Ravel, O. Acher, F. F. Vicent, F. Fievel, J. Appl. Phys., 76, 6570, 1994.

531. F. Fievet, J. P. Lagier, B. Blin, B. Beaudoin, M. Figlarz, Solid State Ionics, 32, 198, 1989.

52. J. Rockenberger, E. C. Scher, A. P. Alivisatos, J. Am. Ceram. Soc., 121, 11595, 1999.

53. T. Hyeon, S. S. Lee, J. Park, Y. Chung, H. B. Na, J. Am. Chem. Soc., 123, 12798, 2001

54. S. Shen, H. Zeng, J. Am. Chem. Soc, 123, 8204, 2002.

55. T. C. Gonzalez, M. P. Morales, M. Gracia, C. J. Serna, Mater. Lett, 18, 151, 1993.

56. S. V. Verdaguer, M. P. Morales, C. J. Serna, Mater. Lett., 35, 227, 1998.

57. F. Caruso, M. Spasova, A. Susha, M. Giersig, R. A. Caruso, Chem. Mater., 13, 109, 2001.

58. F. Caruso, Adv. Mater., 13, 11, 2001.

59. S. Sakka, Handbook of Sol-Gel Science and Technology; Processing, Characterization and Applications. Applications of Sol-Gel Technology. Vol. 3: Kluwer Academic Publishers, New York, Boston, Dordrecht, London, Moscow, 2005.

60. L. C. Klein, J. A. Pope, S. Sakka, J. L. Woolfrey, Sol-Gel Processing of Advanced Materials, Ceramic Transactions Vol:81, Published by American Ceramic Society, Westerwille, Ohio, 1996.

61. J. A. Pope, S. Sakka, L. C. Klein, Sol-Gel Science and Technology, Ceramic Transactions Vol:55, Published by American Ceramic Society, Westerwille, Ohio, 1994.

62. S. Lee, J. Jeong, Journal of Magnetism and Magnetic Materials , 282, 147, 2004.

63. B. Martinez, A. Roig, X. Obradors, E. Mollins, A. Rouanet and C. Monty, J. Appl. Phys., 79, 2580, 1996.

64. R. Janot, Journal of Alloys and Compounds, 333, 302, 2002.

65. J. Xue, Zhaohui Zhou, J. Am. Ceram. Soc., 85, 807, 2002.

66. T. Hyeon, S. Lee, J. Am. Ceram. Soc., 123, 12798, 2001.

67. C. Albornoz, E. Sileo, Physica B, 354, 149, 2004.

68. F. A. Kulikov, A. S. Vanetsev, Inorganic Materials, 30 , 1074, 2003.
69. V. Sreeja, P. A. Joy, Materials Research Bulletin, 42, 1570, 2007.
70. W. W. Wang, Y. J. Zu, M. L. Ruan, Journal of Nanoparticle Research, 9, 419, 2007.
71. R. Y. Hong, T. T. Pan, H. Z. Li, Journal of Magnetism and Magnetic Materials, 303, 60, 2006.
72. X. Liao, J. Zhu, W. Zhong, and H. Chen, Mater. Lett., 50, 341, 2001.
73. A. Khaleel, Chem. Eur. J. 2004, 10, 925-932
74. J. Yang, M. Li, Materials Research Bulletin, 40, 1968, 2005.
75. S. Bakardjieva, Solid State Sciences 7, 367, 2005.
76. J. Jolivet, E. Tronc, C. R. Chimie 5, 659, 2002.
77. Y. Kang, S. Risbud, Chem Mater., 8, 2209, 1996.
78. M. D. Mukadam, S. M. Yusuf, Journal of Magnetism and Magnetic Materials, 272, 1401, 2004.
79. S. Tao, X. Liu, Sensors and Actıators B, 61, 33, 1999.
80. G. Ennas, G. Marongiu, J. Mater Res., 14, 1570, 1999.
81. S. Kanzaki, T. Inada, Journal of Power Sources, 146, 323, 2005.
82. C. Cannas, G. Concas, Z. Naturforsch, 57a, 154, 2002.
83. B. Clapsaddle, A. Gash, Journal of Non-Crystalline Solids, 331, 190, 2003.
84. G. Ennas, A. Musinu , G. Piccaluga and D. Zedda, Chem. Mater., 10, 495, 1998.
85. I. K. Battisha, H. H. Afify, Journal of Magnetism and Magnetic Materials, 292, 440, 2005.
86. C. T. Hseih, W. L. Huang, Journal of Physics and Chemistry of Solids, 63, 733, 2002.
87. G. M. Da Costa, E. De Grave, Journal of Solid State Chemistry, 113, 405, 1994.
88. C. Caizer, C. Savii, and M. Popovici, Mater. Sci. Eng., B97, 129, 2003.
89. R. F. Ziolo, E. P. Giannelis, B. A. Weinstein, M. P. O'Horo, B. N. Ganguly, V. Mehrotra, M. W. Russel and D. R. Huffman, Science**,** 257, 219, 1992.
90. F. del Monte, M. P. Morales, D. Levy, A. Fernandez, M. Ocana, A. Roig, E. Molins, K. O'Grady and C. J. Serna, Langmuir, 13, 3627, 1997.
91. D. Vollath, D. V. Szabo, R. D. Taylor, and J. O. Willis, J. Mater. Res.,12, 2175, 1997.

92. M. T. De Meuse, and C. L. Ryan, Advances in Polymer Technology, 12, 197, 1993.
93. H. P. Klug and L. E. Alexander, X-Ray Diffraction Procedure, Wiley & Sons, New York, 1954.
94. S. Brunauer, P. H. Emmet, E. Teller, Contribution from the Bureu of Chemistry and Soils and George Washington University, 309, 1938.
95. S. Foner, IEEE Trans. Magn., 17, 3358, 1981.
96. S. Foner, J. Appl. Phys., 79, 4740, 1996.
97. A. Niazi, P. Poddar, A. K. Rastogi, Current Science, 79, 99, 2000.
98. C. M. Flynn, Chem. Rev., 84, 31, 1984.
99. S. Music, A. Vertes, G. W. Simmons, I. Czako-Nagy and H. Leidheiser, J. Colloid Interface Sci., 85, 256, 1982.
100. M. P. Morales, T. Gonzalez-Carreno and C. J. Serna, J. Mater. Res., 7, 2538, 1992.
101. P. J. Murphy, A. M. Posner and J. P. Quirk, J. Colloid Interface Sci., 56, 312, 1976.
102. S. Solinas, G. Piccaluga, M. P. Morales and C. J. Serna, Acta mater., 49, 2805, 2001.
103. A. E. Berkowitz, W. J. Schuele and P. J. Flanders, J. Appl. Phys., 39, 1261, 1968.
104. Z. Jing, S. Wu, Journal of Solid State Chemistry, 177, 1213, 2004.
105. Z. D. Qing, W. S. Jun, S. H. Shan, W. X. Li, J. Sol-Gel Techn., 41, 157, 2007.
106. B. D. Cullity, Elements of X-Ray Diffraction, Addison Wesley Publishing Company, Inc., 1967.
107. T. Belin, N. Millot, N. Bovet, M. Gailhanou, Journal of Solid State Chemistry, 180, 2377, 2007.
108. D. K. Kim, Y. Zhang, W. Voit, K. V. Rao, M. Muhammed, Journal of Magnetism and Magnetic Materials, 225, 30, 2001.
109. G. N. Rao, Y. D. Yao, J. W. Chen, IEEE Transactions on Magnetics, 41, 3409, 2005.
110. S. Hariharan, J. Gass, Rev. Adv. Mater. Sci., 10, 398, 2005.
111. S. R. Shinde, S. B. Ogale, J. S. Higgins, H. Zheng, Physical Review Letters, 92,

166601, 2004.
112. J. K. Vassiliou, V. Mehrotra, M. W. Russell, E. P. Giannelis, J. Appl. Phys., 73, 5109, 1993.
113. J. G. Kim, K. H. Han, C. H. Lee, J. Y. Jeong, Journal of the Korean Physical Society, 38, 798, 2001.
114. S. T. Lin, Physical Review, 6 , 116, 1959.
115. D. Craik, Magnetism Principles and Applications, John Wiley & Sons, England, 1995.
116. J. M. Soares, J. H. de Araujo, F. A. O. Cabral, Journal of Non-Crystalline Solids, 354, 4883, 2008.
117. S. Purushotham, R. V. Ramanujan, Journal of Applied Physcs, 107, 114701, 2010.
118. R. E. Rosensweig, Journal of Magnetism and Magnetic Materials, 252, 370, 2002.
119. O. Acarbas, M. Ozenbas, Journal of Nanoscience and Nanotechnology, 8, 655, 2008.
120. J. Jeong, S. Lee, J. Kim, and S. Shin, Phys. Stat. Sol. (b), 241, 1593, 2004.
121. S. Ko, J. Soh, and Y. Kim, IEEE Transactions on Magnetics, 41, 3304, 2005.
122. O. Palchik, I. Felner, G. Kataby, and A. Gedanken, J. Mater. Res., 15, 2176, 2000.

APPENDIX A

CORRELATION COEEFFICIENTS OF THE MAGNETIZATION DATA

Table A.1 Correlation coefficients of the magnetization data of the diethylene glycol route of sol-gel processing.

	123 K		173 K		223 K		273 K		293 K	
Model	**1**	**2**	**1**	**2**	**1**	**2**	**1**	**2**	**1**	**2**
OAD300	0.995	0.998	0.992	0.998	0.990	0.996	0.989	0.996	0.988	0.996
OAD350	0.994	0.996	0.992	0.997	0.990	0.995	0.988	0.994	0.987	0.994
OAD400	0.992	0.995	0.990	0.995	0.987	0.993	0.985	0.992	0.985	0.992

CURRICULUM VITAE

PERSONAL INFORMATION

Surname, Name: BALTACI ACARBAŞ, Özge
Nationality: Turkish (TC)
Date and Place of Birth: 02 August 1979, Eskişehir, TURKEY
Marrital Status: Married
e-mail: oacarbas@hotmail.com

EDUCATION

Ph.D	Metallurgical and Materials Engineering Middle East Technical University, Ankara, TURKEY	2010
BS	Materials Science and Engineering Anadolu University, Eskişehir, TURKEY	2003
High School	Yunusemre High School, Eskişehir, TURKEY	1997

WORK EXPERIENCE

Research Assistant (2003-2010)
Metallurgical and Materials Engineering
Middle East Technical University, Ankara, TURKEY

PUBLICATIONS

A. Thesis

1. Özge Acarbaş Baltacı, Ph. D. Thesis, METU, September 2010.
   Production and Characterizaton of Maghemite Nanoparticles

B. Journal Articles

1. O. Acarbas, M. Ozenbas, "Preparation of Iron Oxide Nanoparticles by Microwave Synthesis and Their Characterization", Journal of Nanoscience and Nanotechnology, 8, 655, 2008.
2. Ö. Acarbaş , E. Suvaci, A. Doğan, "Preparation of nanosized tin oxide(SnO_2) powder by homogeneous precipitation", Ceramics International, 33, 537, 2007.
3. Ö. Acarbaş, E. Suvaci, A. Doğan, "Synthesis of Nanosized Tin Oxide (SnO_2) Particles via Homogeneous Precipitation", Key Engineering Materials, 264, 1205, 2004.

C. Articles in Conference Proceedings

1. Ö. Acarbaş, M. Volkan, S. Atalay, M. Özenbaş, "Production and Characterization of Magnetic Nanoparticles", 12th International Metallurgy and Materials Congress Bildiriler Kitabı, İstanbul.
Editors: U. Ertem, C. H. Gür, G. Orhan, B. Özkal, H. Savaş, M. Ürgen, pp.212-219, 2005.
2. Ö. Acarbaş, M. Özenbaş, "Production and Characterization of Iron Oxide Nanoparticles by Microwave Synthesis", 13th International Metallurgy and Materials Congress Bildiriler Kitabı, İstanbul.
Editors: U. Ertem, C. H. Gür, C. Kaynak, H. Savaş, T. Öztürk, pp.824-831, 2006.

3. Ö. Acarbaş, M. Özenbaş, "Production and Characterization of Iron Oxide Nanoparticles", 14th International Metallurgy and Materials Congress Bildiriler Kitabı, İstanbul.
Editors: C. Arslan, U. Ertem, C. H. Gür, S. Gürmen, G. Orhan, H. Savaş, pp.741-750, 2008.

D. Conference & Meeting Presentations

1. Ö. Acarbaş, M. Özenbaş, "Production and Characterization of Iron Oxide Nanoparticles by Microwave Synthesis", International Workshop on Nanostructured Materials NANOMAT 2006, Abstract Book, pp.145, 2006.
2. Ö. Acarbaş, M. Özenbaş, "Production and Characterization of Iron Oxide Nanoparticles by Mechanical Methods", International Workshop on Nanostructured Materials NANOMAT 2006, Abstract Book, pp.136, 2006.
3. Ö. Acarbaş, M. Özenbaş, "Preparation of Iron Oxide Nanoparticles by Microwave Synthesis and Their Characterization", Third Seeheim Conference on Magnetism, Abstract Book, Almanya, pp.51, 2007.
4. Ö. Acarbaş, M. Özenbaş, "Preparation of Iron Oxide Nanoparticles by Microwave Synthesis and Their Characterization", Materials Research Society, Spring 2008 Meeting, San Francisco, USA, Abstract Book, pp.I12.6, 2008.
5. Ö. Acarbaş Baltacı, M. Özenbaş, "Superparamagnetic Maghemite Nanoparticles for Diverse Biomedical Applications: Effective Parameters on Their Characteristics", Materials Research Society 2009 Fall Meeting, Boston, USA, Abstract Book, pp.410, 2009.
6. Ö. Acarbaş Baltacı, M. Özenbaş, "Synthesis and Characterization of Maghemite Nanoparticles", 2nd TU Darmstadt- METU Joint Workshop on Nanotechnology, Germany, 2009.
7. Ö. Acarbaş Baltacı, M. Özenbaş, "Production and Characterization of Magnetic Nanoparticles", 5. Ulusal Nanobilim ve Nanoteknoloji Konferansı, Abstract Book, Eskişehir, pp.8, 2009.